DESIGN SYNTHESIS OF
LCC HVDC CONTROL SYSTEMS

LEON CHETTY

IN FULFILLMENT OF DOCTOR OF PHILOSOPHY DEGREE

FACULTY OF ENGINEERING

UNIVERSITY OF KWAZULU NATAL

September 2011

SUPERVISOR: PROFESSOR N.M. IJUMBA

As the candidate's Supervisor I agree to the submission of this thesis.

Signed:

Professor N.M. Ijumba

September, 2011

DECLARATION

I, Leon Chetty, declare that

(i)   The research reported in this thesis, except where otherwise indicated, is my original work.

(ii)   This thesis has not been submitted for any degree or examination at any other university.

(iii)   This thesis does not contain other persons' data, pictures, graphs or other information, unless specifically acknowledged as being sourced from other persons.

(iv)   This thesis does not contain other persons' writing, unless specifically acknowledged as being sourced from other researchers. Where other written sources have been quoted, then:

    a) their words have been re-written but the general information attributed to them has been referenced;

    b) where their exact words have been used, their writing has been placed inside quotation marks, and referenced.

(v)   Where I have reproduced a publication of which I am author, co-author or editor, I have indicated in detail which part of the publication was actually written by myself alone and have fully referenced such publications.

(vi)   This thesis does not contain text, graphics or tables copied and pasted from the Internet, unless specifically acknowledged, and the source being detailed in the thesis and in the References sections.

Signed:

Leon Chetty

September, 2011

Acknowledgements

My deepest gratitude to my Lord and Saviour Jesus Christ for the grace that He has bestowed upon me.

I would like to thank Prof. Nelson Ijumba, my supervisor, for giving me the opportunity to explore the interesting field of power engineering, and for his guidance and support during the research.

Financial support provided by Eskom and THRIP is gratefully acknowledged.

I would like to thank Collin Reddy and Logan Pillay for the support that the have provided through the early part of my career and for the immense opportunities that they have created for me. These opportunities have facilitated gaining the necessary experience to complete this PhD project.

I would like to thank my mother for her love and support.

Most of all, I am grateful to my wife, Leola, and my son, Liam, for their love, patience, encouragement and support during the preparation of this thesis.

Leon Chetty
September, 2011

Abstract

From the early days of HVDC system applications, the importance of mathematical modelling of the dynamics of Line Commutated Converter (LCC) HVDC systems has been appreciated. There are essentially two methodologies used to develop mathematical models of dynamic systems. One methodology is to define the properties of the system by the "laws of nature" and other well-established relationships. Basic techniques of this methodology involve describing the system's processes using differential equations. This methodology is called "Deductive Modelling".

The other methodology used to derive mathematical models of a dynamic system is based on experimentation. Input and output signals from the original system are recorded to infer a mathematical model of the system. This methodology is known as "Inductive Modelling".

A review of the current state of the art of modelling LCC HVDC systems indicates that majority of the techniques utilized to develop mathematical models of LCC HVDC systems have used the "Deductive Modelling" approach. This methodology requires accurate knowledge of the ac systems and the dc system and involves complicated mathematics. In practice, it is nearly impossible to obtain accurate knowledge of the ac systems connected to LCC HVDC systems.

The main aim of this thesis is to present an "Inductive Modelling" methodology to calculate the plant transfer functions of LCC HVDC systems. Due to the uncertain nature of the effective short circuit ratio of rectifier and inverter converter stations, generic ranges of parametric uncertainties of the developed plant transfer functions were determined. Based on the determined range of HVDC plant parametric uncertainty, Quantitative Feedback Theory (QFT) methodology was used to design the parameters of the LCC HVDC control system. The stability of the start-up and step responses for varying ac system conditions validated the "Inductive Modelling" technique and the QFT design methodology.

The thesis presents the following, which are considered to be scientific advancements and contributions to the body of knowledge:

- Novel LCC HVDC Step Response (HSR) equations were developed using an "Inductive Modeling" technique.
- The range of parametric variations of the LCC HSR equations were determined for various rectifier and inverter ac system effective short circuit ratios.
- The LCC HSR equations were used to develop the LCC HVDC plant transfer functions for various rectifier and inverter effective short circuit ratios.
- The LCC HVDC plant transfer functions were utilized to design an LCC HVDC control system for varying ac system conditions using Quantitative Feedback Theory (QFT) methodology.

The main contributions of this thesis relate to LCC HVDC systems. This thesis does not attempt to advance control theory however this thesis does apply existing classical control theory to LCC HVDC control systems.

Index Terms: Line Commutated Converter, HVDC, inductive modelling, power system, transient analysis

Contents

Chapter 1

Introduction

1.1 Background

Line Current Commutated (LCC) HVDC systems are dynamic systems that have natural oscillatory modes [1-3]. The natural oscillatory modes of LCC HVDC systems are the result of the interactions between the dc network and the ac networks. [3-8]. The importance of developing mathematical models of LCC HVDC systems to study these oscillatory modes has been appreciated from the early days of LCC HVDC system applications. [1-17].

There are essentially two methodologies used to develop mathematical models of dynamic systems. One methodology is to define the properties of the system by the "laws of nature" and other well established relationships [18]. Basic techniques of this methodology involve describing the system processes using differential equations. This methodology is called "Deductive Modeling" [19].

The other methodology used to determine mathematical models of a dynamic system is based on experimentation [18]. Input and output signals from the original system are recorded to infer a mathematical model of the system. This methodology is known as "Inductive Modeling" [19]. Inductive models may be described by a system's response, $H(s)$, to an impulse or a frequency response function $H(j\omega)$ [20]. These functions are obtained by application of either periodic input signals or non-periodic input signals to the dynamic system. Periodic input signals are utilized in such a manner that the dynamic system is operating in steady state with the output oscillating with the same frequency as the input signal with all transients having decayed. Models determined from periodic input and output signals are usually the frequency response type $H(j\omega)$. Frequency response models are naturally non-parametric models.

A review of the current state of the art of modelling LCC-HVDC systems indicates that the majority of the techniques utilized to develop mathematical models of LCC-

HVDC systems have used the "Deductive Modelling" approach. This methodology requires accurate knowledge of the ac systems and the dc systems and involves complicated mathematics. In practice, it is nearly impossible to obtain accurate knowledge of the ac systems connected to LCC-HVDC systems. Also the limited time constraints imposed on HVDC control practitioners, the ac system uncertainties and the complicated mathematics have prevented the widespread practical use of the "Deductive Modelling" methodology to derive the plant transfer functions of LCC-HVDC systems.

1.2 Aim and Outline of Thesis

The main aim of this thesis is to present an "Inductive Modelling" method to calculate the plant transfer functions of LCC HVDC systems. Due to the uncertain nature of the effective short circuit ratio of rectifier and inverter converter stations, ranges of parametric uncertainties of the developed plant transfer functions were determined. Based on the determined range of HVDC plant parametric uncertainty, Quantitative Feedback Theory (QFT) method was used to design the parameters of the LCC HVDC control system. The stability of the start-up and step responses for varying ac system conditions validated the "Inductive Modelling" technique and the QFT design method.

1.3 Main Contributions of Thesis

The thesis presents the following, which are considered to be scientific advancements and contributions to the body of knowledge:
- Novel LCC HVDC Step Response (HSR) equations were developed using an "Inductive Modelling" technique.
- The range of parametric variations of the LCC HSR equations were determined for various rectifier and inverter ac system effective short circuit ratios.
- The LCC HSR equations were used to develop the LCC HVDC plant transfer functions for various rectifier and inverter effective short circuit ratios.
- The LCC HVDC plant transfer functions were utilized to design an LCC HVDC control system for varying ac system conditions using a Quantitative Feedback Theory (QFT) method.

Chapter 2

LCC HVDC Control System

2.1 Introduction

From the early days of HVDC system applications, the importance of the HVDC control system has been appreciated [10-17]. Eriksson et. al. [10] acknowledged that many of the operational properties of the HVDC transmission system are determined by the control system.

Due to the importance of HVDC control systems, this chapter present a mathematical overview of the LCC HVDC control system and also illustrates an implementation of an LCC HVDC control system.

The next section describes the fundamental topologies of LCC HVDC systems and the related components of LCC HVDC systems. Thereafter a mathematical discussion of converter operation is presented, followed by description of the LCC HVDC control system. This chapter concludes by illustrating an implementation of the LCC HVDC control system.

2.2 LCC HVDC System Configuration and Components

Over the past six decades, traditional applications of LCC HVDC transmission technology has centred around point-to-point transfer of dc power. The commonly used LCC HVDC systems, can be broadly classified into the following categories:

- Monopolar links
- Bipolar links

In the monopolar link, Fig 2.1, two converter stations are joined by a single conductor and earth (or the sea) is used as the return conductor.
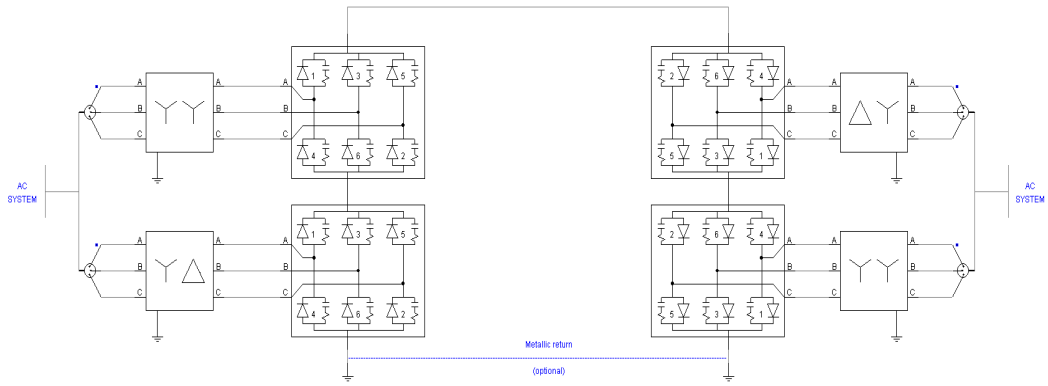
Figure 2.1: LCC HVDC Monopolar Link

The most common configuration is the bipolar link, shown in Fig 2.2, which consists of two monopolar systems, one at positive polarity and one at negative polarity with respect to ground.
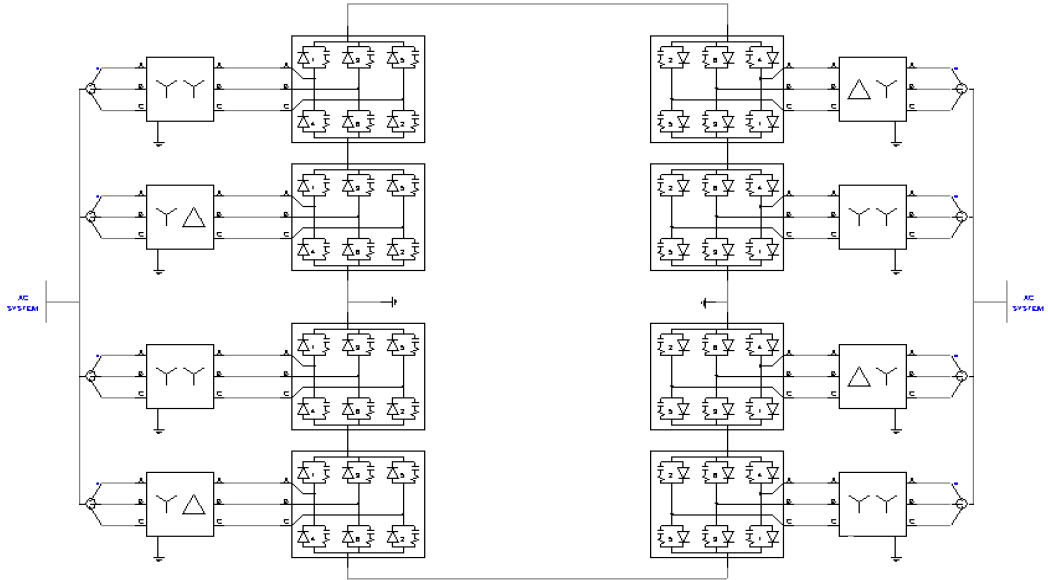
Figure 2.2: LCC HVDC Bipolar Link

Each monopolar system can operate on its own, with ground return [28]. In essence, the monopolar HVDC link is the elementary HVDC configuration; therefore, all LCC HVDC control system discussions to follow are with reference to the monopolar HVDC links.

The main components associated with an LCC HVDC system are shown in Fig. 2.3, using a monopolar system as an example.
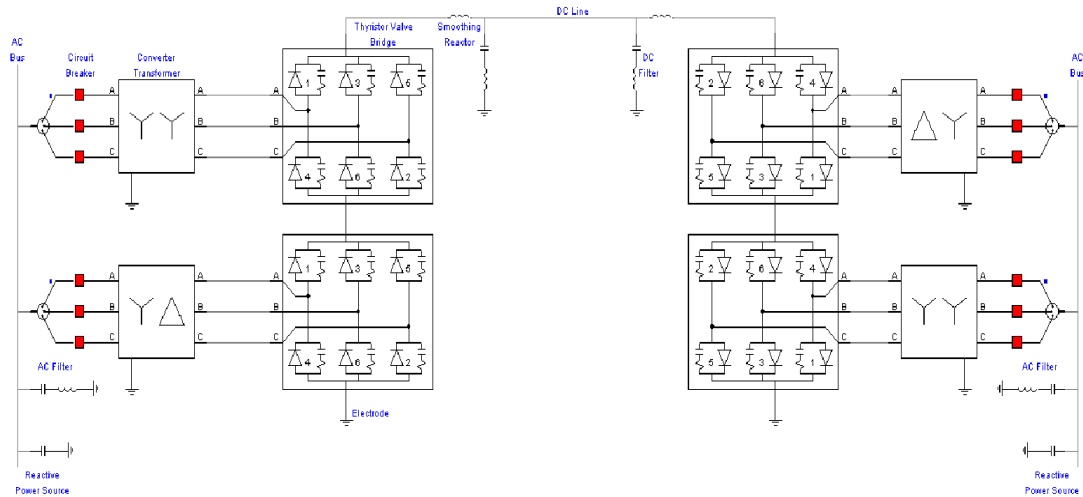
Figure 2.3: A schematic of an LCC HVDC monopolar system

The following is a brief description of each component:

Converters:

These devices perform ac to dc and dc to ac conversions, and consist of thyristor valve bridges and converter transformers. The thyristor bridges are connected in a 6-pulse or 12-pulse arrangement. The converter transformers provide ungrounded three-phase voltage source of appropriate level to the thyristor bridge. With the valve side of the transformer ungrounded, the dc system will be able to establish its own reference to ground, usually by grounding the positive or negative end of the thyristor bridge [28].

Smoothing Reactors:

These are large reactors connected in series with each pole of each converter station.

Harmonic Filters:

Converters generate harmonic voltages and currents on both the ac and dc sides. Therefore filters are required for both the ac and dc sides.

Reactive Power Supplies:

Converters inherently absorb reactive power [28]. Therefore, reactive power sources are required near the converters. Shunt capacitors are common sources of reactive

power. The capacitance associated with the ac filters also provide part of the reactive power required.

Electrodes:

Most dc links are designed to use earth as a neutral conductor for periods of time.

Dc Lines:

These may be overhead lines or cables.

AC Circuit Breakers:

Circuit breakers are used on the ac side, to clear faults in the transformer and for taking the dc link out service,

2.3 Converter Theory

The basic module of an LCC HVDC converter is the three-phase full wave bridge circuit shown in Fig. 2.4. This circuit is known as the Graetz bridge [29]. The ac system side windings of the converter transformer are star-connected with grounded neutral; the valve side windings are delta-connected or star-connected with ungrounded neutral.
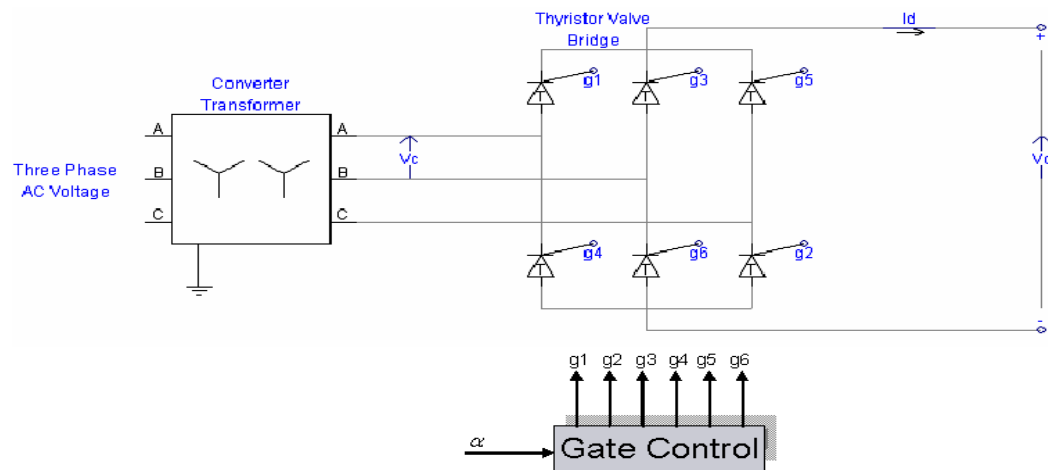
Figure 2.4: Three-phase full wave bridge circuit

Fig. 2.5 illustrates the thyristor valve operation. The gate control is used to delay the ignition of the thyristors. The "delay angle" or "firing angle" is denoted by α; it

corresponds to time delay of α/ω seconds, where ω is defined as the ac system angular frequency. The effect of the firing angle is to reduce the average "ideal no-load" direct voltage by the factor $\cos\alpha$. The average "ideal no-load" direct voltage is given by [29]:

$$V_{do} = \frac{3\sqrt{2}}{\pi} V_c \qquad (2.3.1)$$

where V_c is the phase-to-phase rms commutating voltage referred to the valve side of the converter transformer

As a result of the inductance L_c, which is the combination of the inductance of the ac system and inductance the converter transformers, the phase currents cannot change instantly. Therefore the transfer of current from one thyrsitor valve to another requires short periods of time called commutation time. The corresponding commutation angle is denoted by μ. During each commutation period, the current in the outgoing valve reduces from I_d to 0.
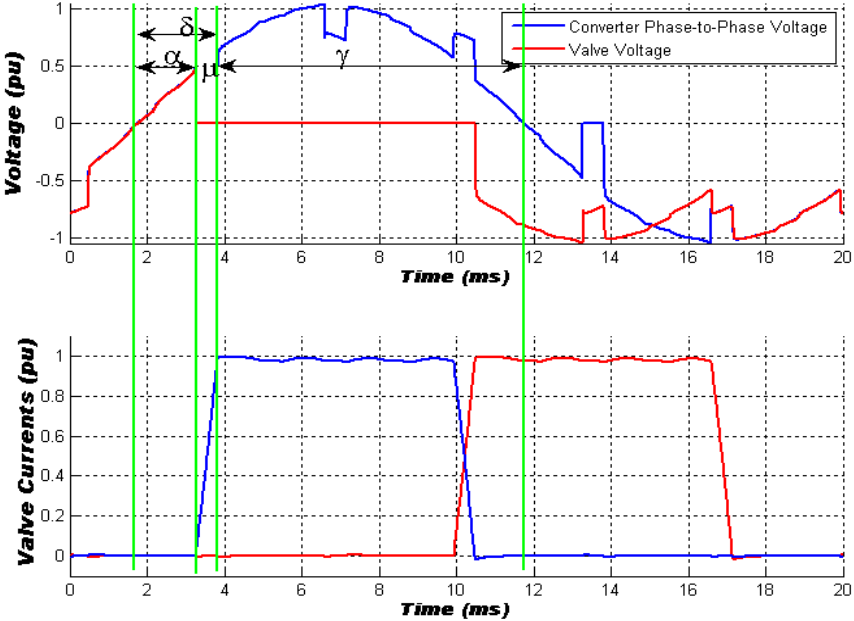
Figure 2.5: Thyristor Valve Operation

14

The commutation begins when $\omega t = \alpha$ and ends when $\omega t = \alpha + \mu = \delta$, where δ is the extinction angle. With commutation overlap and firing delay, the direct voltage for a rectifying converter is given by [28]:

$$V_d = V_{do}.\cos\alpha - R_c.I_d \tag{2.3.2}$$

where $\qquad R_c = \dfrac{3}{\pi}.\omega.L_c \tag{2.3.3}$

R_c is called the "equivalent" commutating resistance.

The inverter operation of the converter is described in terms of α and δ. These quantities are defined in same way as for the rectifier operation except having values between 90° and 180°. However, the common practice is to use firing advance angle β and extinction advance angle γ for describing inverter performance.

$$\beta = \pi - \alpha \tag{2.3.4}$$
$$\gamma = \pi - \delta \tag{2.3.5}$$

The direct voltage for an inverting converter is given by [28]:

$$V_d = V_{do}.\cos\gamma - R_c.I_d \tag{2.3.6}$$

This section presented a mathematical overview of the converter's operation. The next section will describe how the converter operations at the rectifier station and at the inverter station are coordinated to facilitate the transmission of dc power.

2.4 Control of LCC HVDC Systems

Consider the LCC HVDC link shown in Fig. 2.6. It represents a monopolar link or one pole of a bipolar link. The direct current flowing from the rectifier to the inverter is given by [28]:

$$I_d = \frac{V_{dor}.\cos\alpha_r - V_{doi}.\cos\gamma_i}{R_{cr} + R_L - R_{ci}} \qquad\qquad (2.4.1)$$
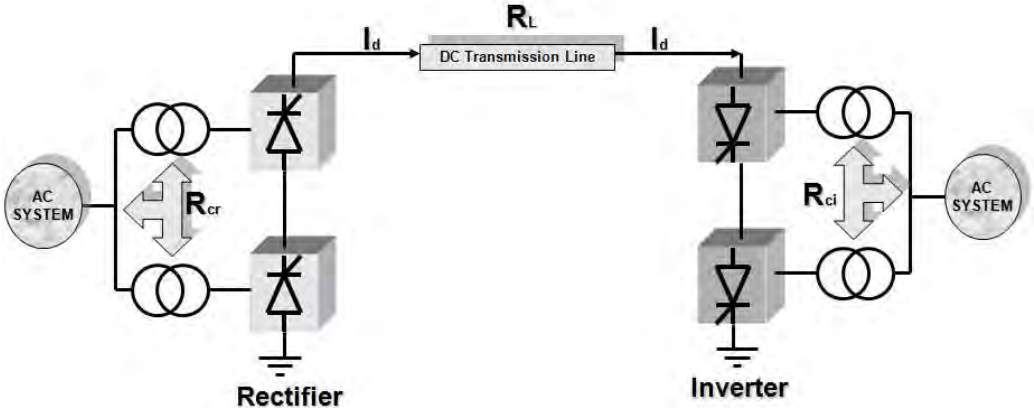
Figure 2.6: LCC HVDC Scheme

By controlling the internal voltages ($V_{dor}.\cos\alpha_r$) and ($V_{doi}.\cos\gamma_i$), the direct voltage and the current (or power) can be controlled. This is accomplished continuously via the control system and the gate control of the valve firing angle. An important requirement for the satisfactory operation of the LCC HVDC link is the prevention of large direct current fluctuations by rapidly controlling the converters' internal voltages by manipulating the rectifier and inverter firing angles. In effect, the adjustment of the rectifier and inverter firing angles are utilized to improve the small signal stability of the HVDC control system.

To satisfy the fundamental requirements, the responsibilities for dc voltage control and dc current control are kept distinct and are assigned to separate converter stations. Under normal operation, the rectifier maintains constant dc current control (CC), and the inverter maintains constant direct voltage control (VC) by operating with constant extinction angle (CEA) [28]. The basis for the control philosophy is illustrated in Fig. 2.7.
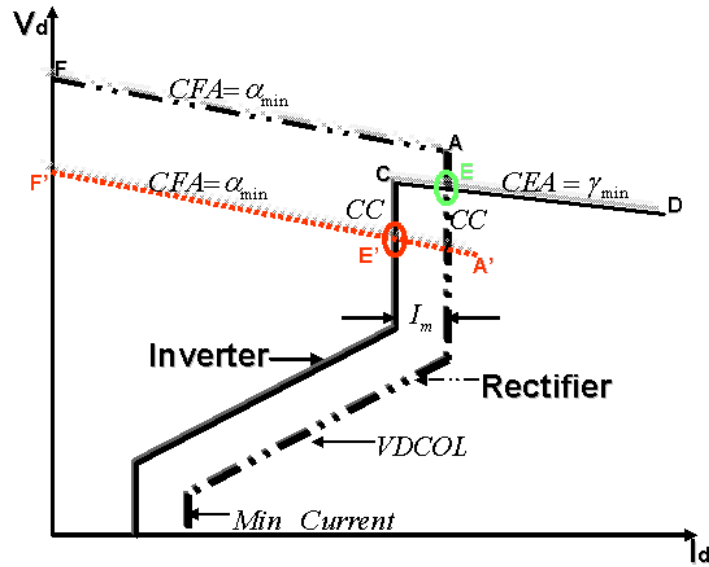
Figure 2.7: Steady-state V-I Control Characteristics

Under normal operating conditions (represented by the intersection point E) the rectifier controls the direct current and the inverter controls the direct voltage. With a reduced rectifier voltage, the operating condition is represented by the intersection point E'. The inverter takes over the direct current control and the rectifier establishes the direct voltage. Under low voltage conditions, it is not be desirable or possible to maintain rated direct current or power [28]. The problems associated with operation under low voltage conditions may be prevented by using a "voltage dependent current order limit" (VDCOL) [28]. This limit reduces the maximum allowable direct current when the voltage drops below a predetermined value [28]. The VDCOL characteristic is a function of the dc voltage.

This section described how the converter operations at the rectifier station and at the inverter station are theoretically coordinated to facilitate the transmission of dc power. The next section will present a practical implementation of the LCC HVDC control system.

2.5 LCC HVDC Control System Implementation

Fig. 2.8 illustrates the scheme for practically implementing the LCC HVDC control system. It should be noted that the rectifier and inverter have the same control system structure.
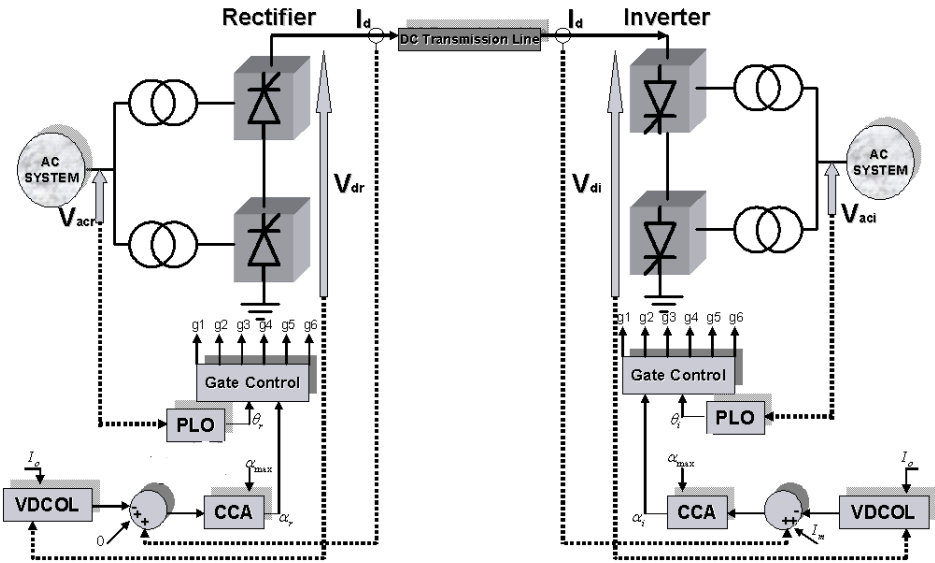
Figure 2.8: LCC HVDC Control System

The next sections discuss in detail the implementation of the following LCC HVDC control system functions:

- Voltage Dependent Current Order Limiter (VDCOL)
- Current Control Amplifier (CCA)
- Phase Locked Oscillator (PLO)
- Gate Control

Voltage Dependent Current Order Limiter (VDCOL)

The VDCOL function will strive to reduce the dc current order for reduced measured dc voltage. The static characteristics of the VDCOL function are displayed in Fig 2.9 and implementation of this function is illustrated in Fig. 2.10.
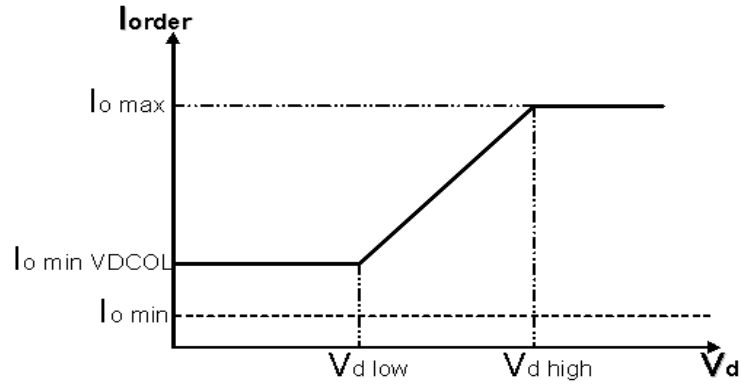
Figure 2.9: Static characteristics of VDCOL [30]
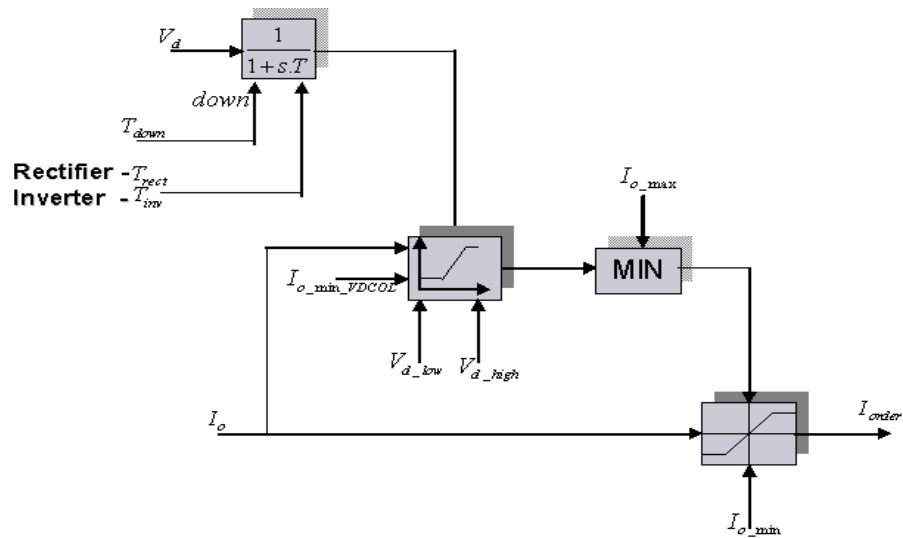
Figure 2.10: VDCOL Implementation [30]

In the implementation of the VDCOL function, the measured direct voltage is passed through a first-order time lag filter. The time lag for increasing and decreasing voltage conditions are different [28]. While the voltage is going down, fast VDCOL action is required; hence the time lag is small [28]. If the same short periods of time are used during the voltage recovery, it may lead to oscillations and possibly instability [28]. To prevent this, the large time lag is used when the direct voltage is recovering [28]. The rectifier time constant is lower than the inverter time constant to maintain current margin [28]. With reference to Fig. 2.9, if V_d becomes lower than V_{d_low}, the reduction of the maximum limitation will stop and the limitation level

will be kept at $I_{o\_min\_VDCOL}$. The minimum limitation I_{o_min} of the current order prevents discontinuous conduction of the current during conduction intervals.

Phase Locked Oscillator (PLO)[22]

The phase locked oscillator (PLO) is based on the Phase Vector technique. This technique exploits trigonometric multiplication identities to form an error signal, which speeds up or slow down the PLO in order to match the phase. The output signal θ is a ramp synchronized to the Phase A commutating bus L-G voltage. The block diagram of the PLO is shown below:
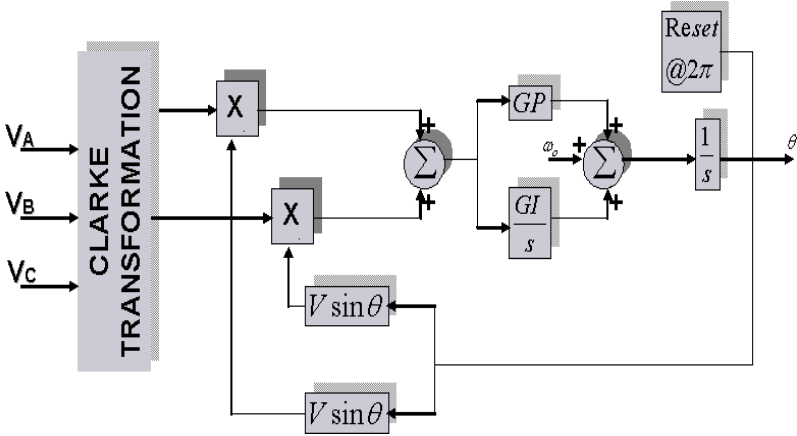
Fig. 2.12: Phase Locked Oscillator (PLO) Implementation

Current Control Amplifier (CCA)

Both the rectifier and the inverter have a CCA function as illustrated in Fig. 2.8. The main function of the current control amplifier is to improve the dynamic operation of current control loop. The main requirements of the current control loop are:

- Fast enough step response
- Insignificant current error at steady-state
- Stable current control

The CCA has a proportional part ($k_i.k_p$) and an integrating part ($\frac{k_i}{s.T_i}$), as illustrated in Fig. 2.13. The CCA also has a summing junction, in which the difference between the current order, the current response and current margin is formed. The subsequent firing angle order is determined by the following equation:

$$\alpha_{order} = -\left[k_i.k_p + \frac{k_i}{s.T_i}\right](I_{order} - I_m - I_d) \qquad (2.5.1)$$

The current controller's proportional gain and integral time constant parameters should be designed to achieve the best stability performance.
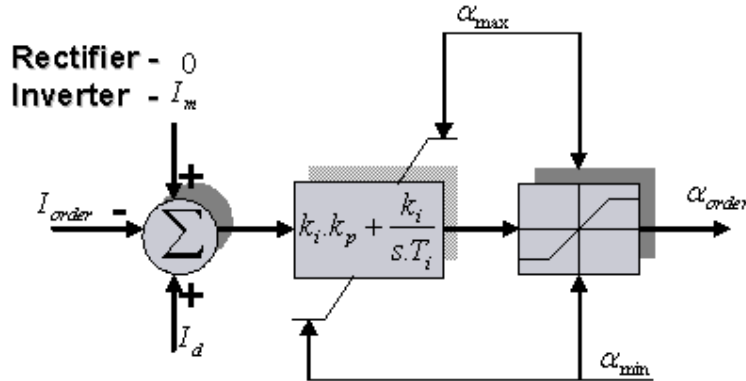
Figure 2.13: Current Control Amplifier Implementation [30]

<u>*Gate Control*</u>

The gate control compares the firing order α_{order} to the phase locked ramp signal θ and produces the gate firing pulses.

2.6 Conclusions

In this chapter, an overview of the LCC HVDC control system was described. The different fundamental topologies of LCC HVDC transmission systems were illustrated. From the illustrations, it is evident that only monopolar LCC HVDC systems need to be investigated for control system studies. A mathematical analysis of the converter operation and the associated LCC HVDC control system were also presented. This chapter concluded by illustrating the practical implementation of the LCC HVDC control system. The next chapters describe how the parameters of LCC HVDC control system are methodically derived to improve the small signal stability of an LCC HVDC system.

Houpis et. al. [31] states that a small signal stability control problem can be divided into the following steps:

- Performance specifications are established.

- An inductive modelling technique is applied in order to obtain the plant model transfer functions.

- A control theory design approach should be used to design the control parameters.

- Perform a simulation of the system to verify the performance of the design.

The next chapter presents an "Inductive Modelling" technique, which can be used to obtain the LCC HVDC plant model. Chapter 4 then further investigates the parameter variations of the derived LCC HVDC plant models. Chapter 5 subsequently presents a Quantitative Feedback Theory (QFT) design of the LCC HVDC control system parameters. The transient analysis of the designed LCC HVDC control system is investigated in Chapter 6.

Chapter 3

LCC HVDC System Modelling

3.1 Introduction

Line Current Commutated (LCC) HVDC systems are dynamic systems that have natural oscillatory modes [1-3]. The natural oscillatory modes of LCC HVDC systems are the result of the interactions between the dc network and the ac networks. [3-8]. The importance of developing mathematical models of LCC HVDC systems to study these oscillatory modes has been appreciated from the early days of LCC HVDC system applications. [1-17].

There are essentially two methodologies used to develop mathematical models of dynamic systems. One methodology is to define the properties of the system by the "laws of nature" and other well established relationships [18]. Basic techniques of this methodology involve describing the system processes using differential equations. This methodology is called "Deductive Modeling" [19].

The other methodology used to determine mathematical models of a dynamic system is based on experimentation [18]. Input and output signals from the original system are recorded to infer a mathematical model of the system. This methodology is known as "Inductive Modeling" [19]. Inductive models may be described by a system's response $H(s)$, to an impulse or a frequency response function $H(j\omega)$ [20]. These functions are obtained by application of either periodic input signals or non-periodic input signals to the dynamic system. Periodic input signals are utilized in such a manner that the dynamic system is operating in steady state with the output oscillating with the same frequency as the input signal with all transients having decayed. Models determined from periodic input and output signals are usually the frequency response type $H(j\omega)$. Frequency response models are naturally non-parametric models.

With regard to the non-periodic input signal, the dynamic system is operated until steady state operation, corresponding to zero initial conditions and then the dynamic

system is perturbed by the input signal. The step function is the most commonly used non-periodic input signal and the output step response facilitates the impulse response $H(s)$. Step response models can be parametric in nature.

This chapter presents the state of the art of methodologies utilized to derive mathematical models of LCC HVDC systems. The analysis is presented with reference to the mathematical modeling framework depicted in Fig. 3.1.
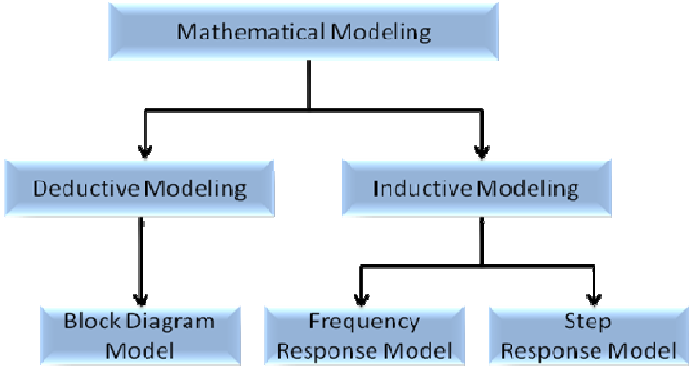
Figure 3.1: Mathematical Modeling Framework

Traditionally classic HVDC systems have been treated as "linear time invariant systems" [4-17]. Based on this premise, Persson [9] developed a meshed block diagram, illustrated in Figure 3.2, to calculate the current control loop plant transfer function. The transfer functions of each block in the meshed system were derived using the state variable approach. The transfer functions describing the ac and dc interactions were derived using describing function analysis. Persson [9] called these transfer functions "conversion functions". Toledo et. al. recently applied space vectors to the Persson's classic technique [17]. Space vector analysis was illustrated to be a form of describing function analysis.

Based on the assumption that the classic HVDC system is linear with regard to small variations in the firing angle, Freris et al. [11] developed a block diagram, illustrated in Figure 3.3, to calculate the transfer function of the rectifier current control loop.
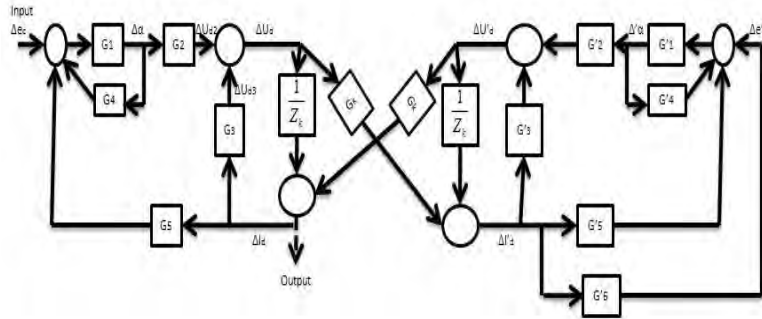
Figure 3.2: Block diagram of HVDC transmission system according to Persson [9]

Continuous wave modulation and Fourier analysis were used to determine the transfer functions of each block in the meshed block diagram. The continuous wave modulation technique was used as a method of developing the describing functions to account for the ac/dc interactions.
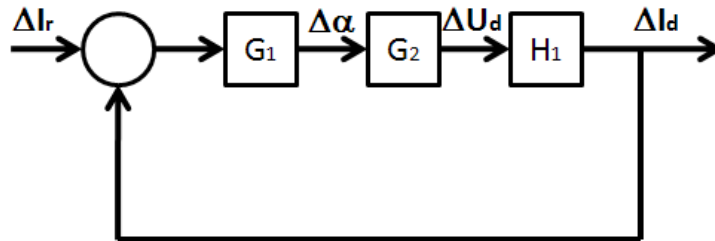
Figure 3.3: Block diagram of HVDC system according to Freris et. al. [11]

From the linear time invariant system foundation, Wood et al. [4] performed Fourier analysis on the dc voltage and ac current waveforms of the converter. From these analyses, transfer functions were obtained for the dc voltage and ac currents with respect to the phase voltages and dc currents. These transfer functions accommodated variations in the firing angle and the commutation period. The subsequent transfer functions facilitated the predictions of voltage waveform distortion on the dc side of the converter, and the prediction of current waveform distortion on the ac side of the converter. Using the transfer functions derived in [4], Wood et al. [5] developed an expression for the converter dc side frequency dependent impedance.   This expression was developed using the state-variable approach. Using the state-variable approach and the frequency dependent impedance of the converter, Wood et al [6] derived the transfer function for the current control loop.

Jovcic et al. [13], assumed that classic HVDC systems are linear time invariant systems and developed the plant transfer function of the current control loop using a state-variable approach and the block diagram illustrated in Figure 3.4. The state variables were chosen to be the instantaneous values of currents in the inductors and voltages across the capacitors. In order to represent the ac system dynamics together with the dc system dynamics in the same frequency frame, the effect of the frequency conversion through the AC-DC converter was accommodated using Park's transformation. The developed system model was linearized around the normal operating point, and all states were represented as dq components of the corresponding variables. The phase locked oscillator [22] was incorporated into the system model.
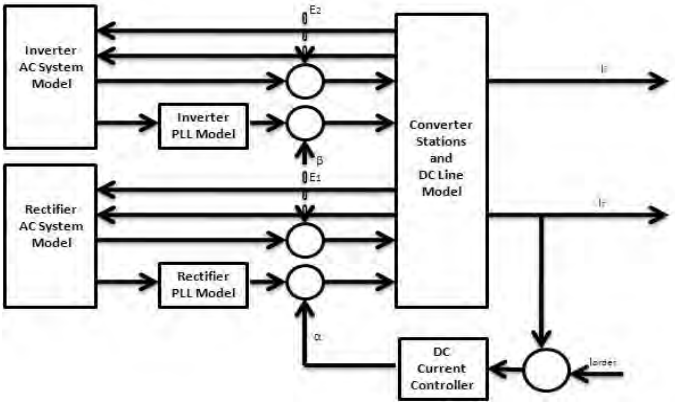
Figure 3.4: Block diagram of HVDC system according to Jovcic et. al. [13]

A review of the above state of the art of modeling LCC HVDC systems clearly indicates that majority of the techniques utilized to develop mathematical models of LCC HVDC systems have used the "Deductive Modeling" methodology. This methodology requires accurate knowledge of the ac systems and the dc systems and involves complicated mathematics.

In practice, it is nearly impossible to obtain accurate knowledge of the ac systems connected to classic HVDC systems. Also the limited time constraints imposed on HVDC control practitioners, the ac system uncertainties and the complicated mathematics have prevented the widespread practical use of the "Deductive Modeling" methodology to derive the plant transfer functions of classic HVDC

systems. Therefore the objective of this study was to utilize an "Inductive Modeling" method to derive mathematical models of the classic HVDC systems.

"Inductive Modeling" is the art of building mathematical models of dynamic systems based on observed data from the systems [19]. A key concept in utilizing the inductive modeling technique is the definition of the dynamic system upon which experimentation can be conducted. Manitoba HVDC Research Centre commissioned a study to examine the validity of digitally defining the LCC HVDC system [23-24]. To examine the validity of digitally defining the LCC HVDC system, the Nelson River HVDC system was defined and simulated using the PSCAD/EMTDC program. PSCAD/EMTDC is a Fortran program and was used to represent and solve the linear and non-linear differential equations of electromagnetic systems in the time domain. A comparison was conducted between the actual real-time system responses and the digitally derived responses. The results of the study illustrated that the digitally derived responses correlated excellently with the real system responses. The study concluded that the PSCAD/EMTDC program is a valid option for digitally defining a LCC HVDC system [23-24].

Based on this premise, Jiang et. al [7] modelled the LCC HVDC system using PSCAD/EMTDC, and developed a frequency response model of the LCC HVDC system. A current source was used to inject a spectrum of frequency components into an operating LCC HVDC system. The resulting harmonic voltages were observed. The frequency response model that was developed for the LCC HVDC system was non-parametric. It is possible however to develop the plant transfer function by the fitting of measured frequency domain responses with rational function approximations [25]. Todd et. al. [12] demonstrated the application of a rational function approximation of the closed loop frequency response of a simplified CIGRE Benchmark HVDC test system.

In this thesis, a simple method is presented to develop a parametric step response model (i.e. an inductive model) of an LCC HVDC system. In this study, the LCC HVDC system is defined and experimented upon using the PSCAD/EMTDC program.

3.2 Jacobian Linearization of LCC HVDC Nonlinear Operation

3.2.1 Jacobian Linearization Theory [32]

Consider a nonlinear system defined by the following differential equation:

$$\overset{o}{x} = f(x) + g(x)u \qquad\qquad (3.2.1)$$

$$y = h(x) \qquad\qquad (3.2.2)$$

where x is the state variable vector

u is the input vector

y is the output vector

The Jocabian linearization of the above nonlinear system at a stable operating point (u_o, x_o, y_o) is defined as

$$\overset{o}{x} = \left[\frac{\partial f(x_o)}{\partial x} + \frac{\partial g(x_o)}{\partial x} u_o \right](x - x_o) + g(x_o)(u - u_o) \qquad\qquad (3.2.3)$$

$$y - y_o = \frac{\partial h(x_o)}{\partial x}(x - x_o) \qquad\qquad (3.2.4)$$

Equations (3.2.3) and (3.2.3) can be written in standard linear state space representation as:

$$\overset{o}{x} = Ax + Bu \qquad\qquad (3.2.5)$$

$$y = Cx \qquad\qquad (3.2.6)$$

where A, B, C are constant matrices

The model described by equations (3.2.5) and (3.2.6) is a linear approximation of the original nonlinear system, described by equations (3.2.1) and (3.2.2), around the stable operating point (u_o, x_o, y_o). A linear control strategy based on the linearized model can therefore be used to stabilize the system for a small region around the stable operating point.

3.2.2 LCC HVDC System Application

Section 2.4 illustrated that there are 2 definitive modes of operation of the LCC HVDC system. These definitive operational modes are explicitly described as:

1. Rectifier in Current Control and the Inverter in Voltage Control
2. Rectifier in Voltage Control and the Inverter in Current Control

This implies that the each of the converter stations has two controlling states namely:

1. DC Current Control, where the dc current is defined by:

$$I_d = \frac{V_{dor}.\cos\alpha_r - V_{doi}.\cos\gamma_i}{R_{cr} + R_L - R_{ci}} \qquad (3.2.7)$$

2. DC Voltage Control, where the dc voltage is defined by:

$$V_d = V_{do}.\cos\alpha - R_c.I_d \qquad (3.2.8)$$

Rectifier in DC Current Control Mode

When rectifier is in dc current control mode, the inverter is in constant dc voltage control mode this implies that equation (3.2.7) can be written as:

$$I_d = k_1.\cos\alpha_r - k_2 \qquad (3.2.9)$$

where

$$k_1 = \frac{V_{dor}}{R_{cr} + R_L + R_{ci}} \qquad (3.2.10)$$

$$k_2 = \frac{V_{doi}.\cos\gamma_i}{R_{cr} + R_L + R_{ci}} \qquad (3.2.11)$$

The derivative of equation (3.2.9), assuming that the ac line voltage is not affected significantly by the change in α_r results in:

$$\frac{\Delta I_d}{\Delta\alpha_r} = -k_1.\sin\alpha_{ro} = \quad \text{constant} \qquad (3.2.12)$$

where α_{ro} is the initial rectifier firing angle

Therefore for small changes in α_r, the rectifier's current control loop can be linearized around a stable (or equilibrium) operating point. This is defined as the "Jacobian Linearization" of the original nonlinear current control loop.

Rectifier in DC Voltage Control Mode

When rectifier is in dc voltage control mode, the inverter is in constant dc current control mode this implies that equation (3.2.8) can be written as:

$$V_{dr} = k_3 . \cos \alpha_r - k_4 \qquad (3.2.13)$$

where
$$k_3 = V_{dor} \qquad (3.2.14)$$

$$k_4 = R_{cr} . I_d \qquad (3.2.15)$$

The derivative of equation (3.2.13), assuming that the ac line voltage is not affected significantly by the change in α_r results in:

$$\frac{\Delta V_{dr}}{\Delta \alpha_r} = -k_3 . \sin \alpha_{ro} = \text{constant} \qquad (3.2.16)$$

where α_{ro} is the initial rectifier firing angle

Therefore for small changes in α_r, the rectifier's voltage control loop can be linearized around a stable (or equilibrium) operating point. This is defined as the "Jacobian Linearization" of the original nonlinear voltage control loop.

Inverter in DC Current Control Mode

When the inverter is in dc current control mode, the rectifier is in constant dc voltage control mode this implies that equation (3.2.7) can be written as:

$$I_d = k_5 - k_6 . \cos \gamma_i \qquad (3.2.17)$$

where
$$k_5 = \frac{V_{dor} . \cos \alpha_r}{R_{cr} + R_L + R_{ci}} \qquad (3.2.18)$$

$$k_6 = \frac{V_{doi}}{R_{cr} + R_L + R_{ci}} \qquad (3.2.19)$$

The derivative of equation (3.2.17), assuming that the ac line voltage is not affected significantly by the change in α_i results in:

$$\frac{\Delta I_d}{\Delta \alpha_i} = -k_6 . \sin \gamma_{io} = \text{constant} \qquad (3.2.20)$$

where γ_{io} is the initial inverter extinction angle

Therefore, for small changes in α_i, the inverter's current control loop can be linearized around a stable (or equilibrium) operating point.

Inverter in DC Voltage Control Mode

When inverter is in dc voltage control mode, the rectifier is in constant dc current control mode this implies that equation (3.2.8) can be written as:

$$V_{di} = k_7.\cos\alpha_i - k_8 \qquad (3.2.21)$$

where
$$k_7 = V_{doi} \qquad (3.2.22)$$

$$k_8 = R_{ci}.I_d \qquad (3.2.23)$$

The derivative of equation (3.2.21), assuming that the ac line voltage is not affected significantly by the change in α_i results in:

$$\frac{\Delta V_{di}}{\Delta\alpha_i} = -k_7.\sin\alpha_{io} = \text{constant} \qquad (3.2.24)$$

where α_{io} is the initial inverter firing angle

Therefore for small changes in α_i, the inverter's voltage control loop can be linearized around a stable (or equilibrium) operating point.

3.3 Inductive Modeling of LCC HVDC System

Using PSCAD/EMTDC, the LCC HVDC system's linear and nonlinear differential equations were defined. The normal steady-state operating point of the LCC HVDC system is defined as the stable (or equilibrium) point of operation and according to equations (3.2.12), (3.2.16), (3.2.20) and (3.2.24), the LCC HVDC system can be considered linearized around the normal steady-state operating point. Therefore LCC HVDC system can be considered as "linear time invariant system" around a stable operating point.

The impulse response of a "linear time invariant system" is determined by first determining the step response and then exploiting the fact that the impulse response is obtained by differentiating the step response. The Laplace transform of the impulse response is defined as the transfer function of the "linear time-invariant system". The

plant transfer function can be explicitly obtained by determining the ratio of the Laplace transform of the step response to the Laplace transform of the step input [35].

This implies that the small signal plant transfer function of an LCC HVDC system can be obtained by determining the ratio of the Laplace transform of the small signal step response of the LCC HVDC system to the Laplace transform of the step input of the rectifier firing angle or inverter firing angle.

3.3.1 Current Control Plant Transfer Function Derivation

PSCAD/EMTDC was used to obtain the dc current step response of a LCC HVDC system. To derive the current control plant transfer function, the feed-forward controlled LCC HVDC system shown in Fig. 3.1 below was modelled in PSCAD/EMTDC.
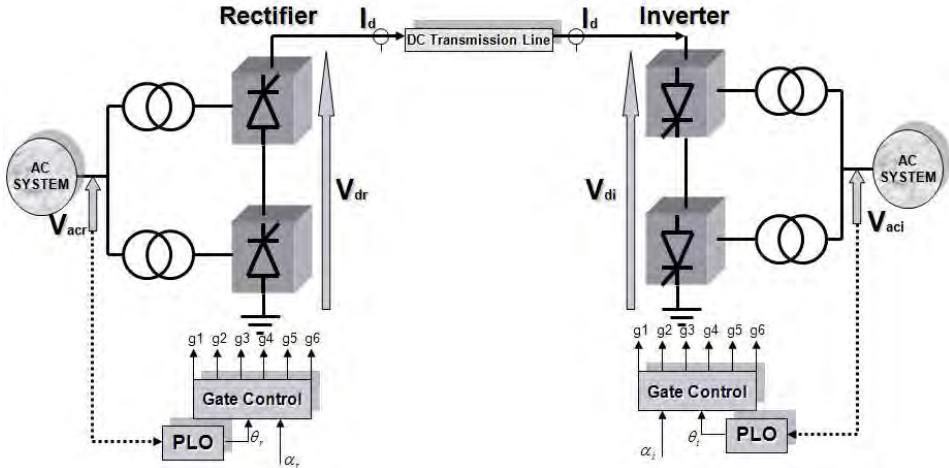
Figure 3.1: Simulated Feed-Forward Controlled LCC HVDC System

The following points should be noted about the model:

- The converter was simulated so as to represent its actual nonlinear behaviour.
- The influence of phase-locked oscillator was simulated.
- The details of each of these components were discussed in Section 2.5
- The rectifier's ac system's effective short circuit ratio with reference to the transmitted dc power was chosen to be 8.

- The inverter's ac system's effective short circuit ratio with reference to the transmitted dc power was chosen to be 8.

The next section will describe, in detail, the processes used to develop the rectifier and inverter current control plant transfer functions.

Rectifier Current Control Plant Transfer Function

The process used to calculate the rectifier current control plant transfer function is as follows:

1. Model the LCC HVDC system, shown in Fig. 3.1, in PSCAD/EMTDC.
2. Simulate the LCC HVDC system so that it reaches steady-state, capture a snap-shot at this point.
3. Maintain the inverter firing angle constant.
4. Apply a 5° step increase in the rectifier firing angle α_r and measure the dc current response I_{dr}.
5. Approximate the step response I_{dr}, with characteristic time domain functions.
6. Calculate the Laplace transform, $I_{dr}(s)$ of the characterized step response.
7. Calculate the Laplace transform, $\alpha_r(s)$ of the step input.
8. Calculate the Rectifier Current Control plant transfer function $P_{cr}(s) = \dfrac{I_{dr}(s)}{\alpha_r(s)}$

The above described process was executed, and the measured time domain current response is illustrated Fig. 3.2.
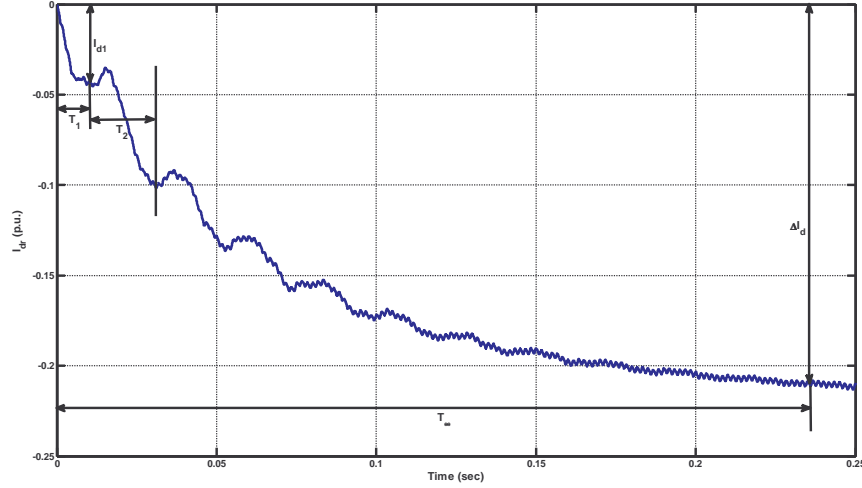
Figure 3.2: Measured Rectifier DC Current Response

The measured current response was approximated using the time domain function illustrated in equation (3.3.1):

$$I_{dr}(t) = \begin{cases} 1.1 m(\Delta I_d - I_{d1})(1 - e^{-bt}) & 0 < t < T_o \\ 1.1 m(\Delta I_d - I_{d1})(1 - e^{-bt}) + I_{d1}(n - p.c.e^{-a.t} + k.c.e^{-a.t}.(\sin(wt) - m.\cos(wt)) & t \geq T_o \end{cases} \quad (3.3.1)$$

where I_{d1} is the first peak of the oscillating component of the dc current (p.u.)

ΔI_d Defined as final value of the dc current (p.u.) from nominalised zero

     reference

$a = \dfrac{r}{T_1}$ T_1 is defined as the time (sec) of the first peak of the dc current (p.u.).

     r is a constant

$w = \dfrac{2\pi}{T_2}$ T_2 is defined as the first period (sec) of the oscillating component of

     the dc current.

c   is constant ($0 < c \leq 1$); chosen to be 0.25

T_∞ Defined as time to reach final value (sec.)

$$b = \frac{\log\left(\dfrac{1}{11}\right) - \log\left(1 - \dfrac{10.I_{d1}(1 - e^{-1})}{11.\Delta I_d}\right)}{-T_\infty}$$

T_o Time delay (sec) illustrated and defined in Figure (3.3). This time

delay is introduced to avoid the formation of very high order models.
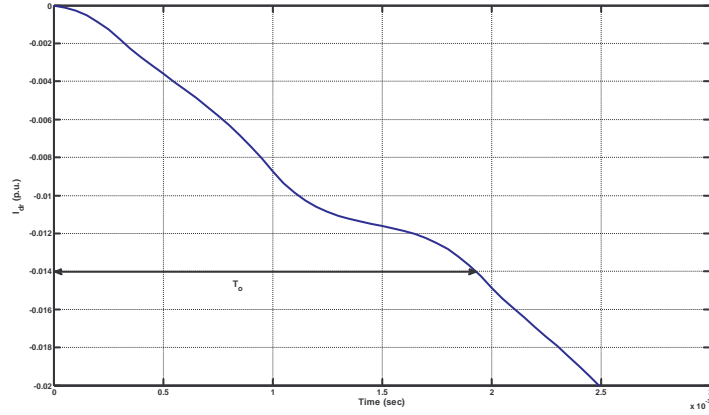
Figure 3.3: Time Delay Definition

For rectifier effective short circuit ratios greater than 2.6:

$$m = 0$$

$$n = \frac{\Delta I_d}{I_{d1}}$$

$$p = \frac{\Delta I_d}{c.I_{d1}}$$

$$0 < r < 1$$

$$k = \frac{\Delta I^2{}_d}{I_{d1}}$$

For rectifier effective short circuit ratios less than 2.6:

$$m = 1$$

$$n = 1$$

$$r = 1$$

$$q = 1$$

$$k = 1$$

In this thesis, when the rectifier is in current control, only scenarios where rectifier effective short circuit ratios are greater than 2.6 will be investigated. Therefore equation (3.3.1) simplifies to:

$$I_{dr}(t) = \begin{cases} 0 & t < T_o \\ \Delta I_d \left(1 - e^{-at} + c|\Delta I_d|.e^{-at}.\sin(wt)\right) & t \geq T_o \end{cases} \qquad (3.3.2)$$

Equation (3.3.1) and subsequently equation (3.3.2) is called the ***Current HVDC Step Response (HSR)*** equation and was simulated using MATLAB and the characteristic time domain response is illustrated in Figure 3.4, together with the associated error when compared to the original signal.

Figure 3.4 clearly illustrates that the ***Current HVDC Step Response (HSR)*** equation adequately approximates the dc current response to a step change in the rectifier's firing angle since the resultant error does not exceed 2.5%.
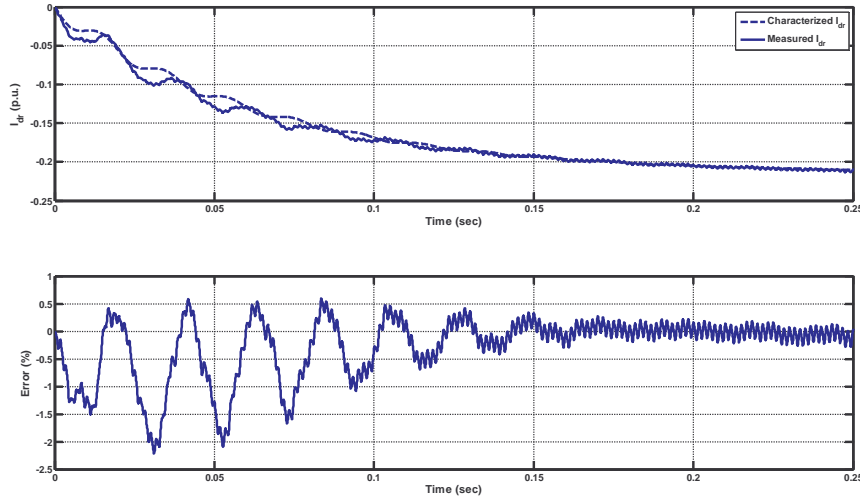
Figure 3.4: Characterized Rectifier DC Current Response

The Laplace transform of the characterized dc current response was calculated as:

$$I_{dr}(s) = \Delta I_d.e^{-s.T_o}\left(\frac{s^3 + (3a-1)s^2 + (3a^2 - 2a + w^2 + c|\Delta I_d|w)s + (a^3 - a^2 + aw^2 - w^2 + c|\Delta I_d|aw)}{s(s+a)(s^2 + 2as + a^2 + w^2)}\right)$$

(3.3.2)

The Laplace transform of the firing angle step input was calculated as:

$$\alpha_r(s) = \frac{\Delta\alpha}{s} \qquad (3.3.3)$$

Therefore the rectifier current control plant transfer function was calculated as:

$$P_{cr}(s)=\frac{\Delta I_d}{\Delta \alpha}.e^{-s.T_o}\left(\frac{s^3+(3a-1)s^2+(3a^2-2a+w^2+c|\Delta I_d|w)s+(a^3-a^2+aw^2-w^2+c|\Delta I_d|aw)}{(s+a)(s^2+2as+a^2+w^2)}\right)$$

(3.3.4)

Please note that Appendix 1 presents a case for the rectifier short circuit ratio being 2.5.

Inverter Current Control Plant Transfer Function

The process used to calculate the inverter current control plant transfer function is as follows:

1. Model the LCC HVDC system, shown in Fig. 3.1, in PSCAD/EMTDC.
2. Simulate the LCC HVDC system so that it reaches steady-state, capture a snap-shot at this point.
3. Maintain the rectifier firing angle constant.
4. Apply a 5° step decrease in the inverter firing angle α_i and measure the dc current response I_{di}.
5. Approximate the step response I_{di}, with characteristic time domain functions.
6. Calculate the Laplace transform, $I_{di}(s)$ of the characterized step response.
7. Calculate the Laplace transform, $\alpha_i(s)$ of the step input.
8. Calculate the Inverter Current Control plant transfer function $P_{ci}(s)=\frac{I_{di}(s)}{\alpha_i(s)}$

The above described process was executed, and the measured time domain current response is illustrated Fig. 3.5.
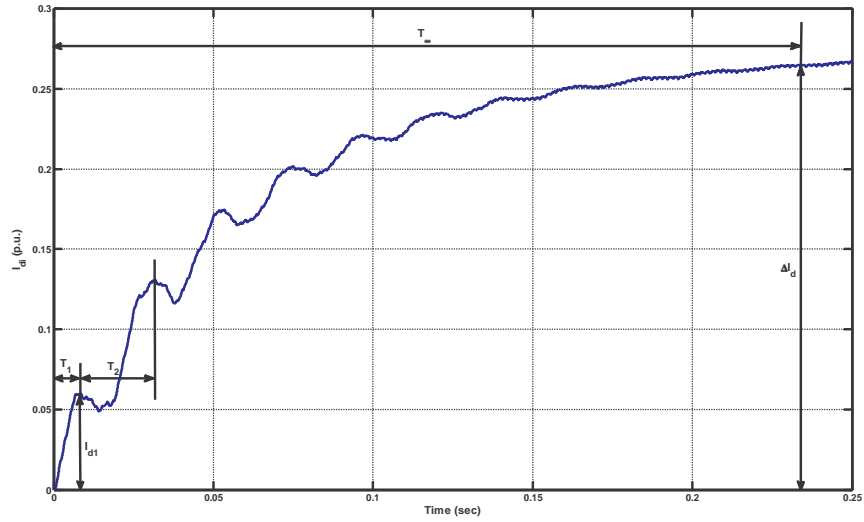
Figure 3.5: Measured Inverter DC Current Response

The measured current response was approximated using the *Current HSR* equation as described in equation (3.3.5):

$$I_{di}(t) = \begin{cases} 0 & t < T_o \\ \Delta I_d \left(1 - e^{-at} + c|\Delta I_d|.e^{-at}.\sin(wt)\right) & t \geq T_o \end{cases} \qquad (3.3.5)$$

The *Current HSR* equation was again simulated using MATLAB and characteristic time domain response is illustrated in Figure 3.6, together with the associated error when compared to the original signal.
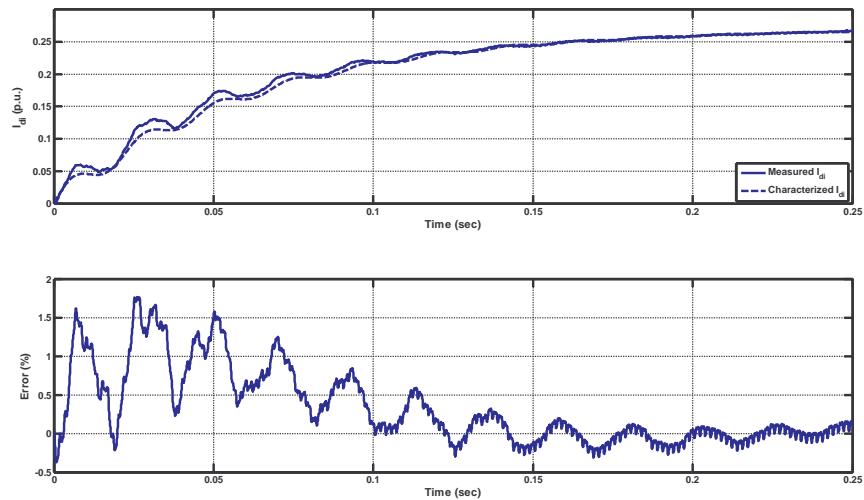
Figure 3.6: Characterized DC Current Response

Figure 3.6 clearly illustrates that the ***Current HSR*** equation adequately approximates the dc current response to a step change in the inverter's firing angle since the resultant error does not exceed 2.0%.

The Laplace transform of the characterized dc current response was calculated as:

$$I_{di}(s) = \Delta I_d \cdot e^{-s.T_o}\left(\frac{s^3 + (3a-1)s^2 + (3a^2 - 2a + w^2 + c|\Delta I_d|w)s + (a^3 - a^2 + aw^2 - w^2 + c|\Delta I_d|aw)}{s(s+a)(s^2 + 2as + a^2 + w^2)}\right)$$

(3.3.6)

The Laplace transform of the firing angle step input was calculated as:

$$\alpha_i(s) = \frac{\Delta \alpha}{s}$$

(3.3.7)

Therefore the inverter current control plant transfer function was calculated as:

$$P_{ci}(s) = \frac{\Delta I_d}{\Delta \alpha} \cdot e^{-s.T_o}\left(\frac{s^3 + (3a-1)s^2 + (3a^2 - 2a + w^2 + c|\Delta I_d|w)s + (a^3 - a^2 + aw^2 - w^2 + c|\Delta I_d|aw)}{(s+a)(s^2 + 2as + a^2 + w^2)}\right)$$

(3.3.8)

3.3.2 Voltage Control Plant Transfer Function Derivation

The development of the voltage control plant transfer function was slightly more challenging than the development of the current control plant transfer function since the dc current needed to be constant.

To achieve constant dc current when the rectifier is controlling the dc voltage, the inverter must be modelled as a constant current load, as shown in Fig. 3.7. To achieve constant dc current when the inverter is controlling the dc voltage, the rectifier must be modelled as a constant current source, as shown in Fig. 3.8.
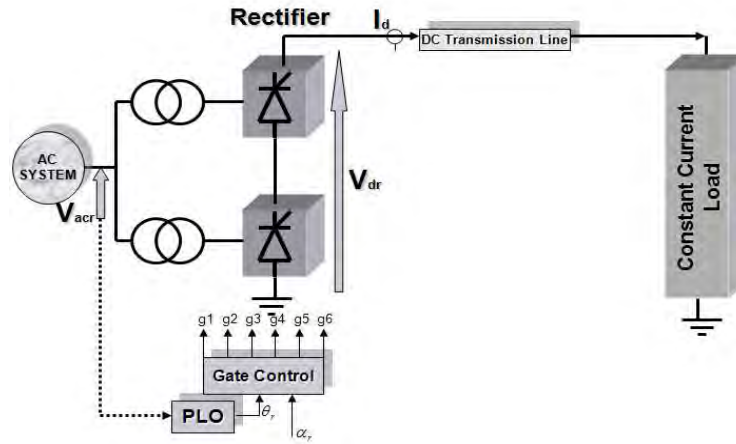
Figure 3.7: LCC HVDC System with Constant Current Load
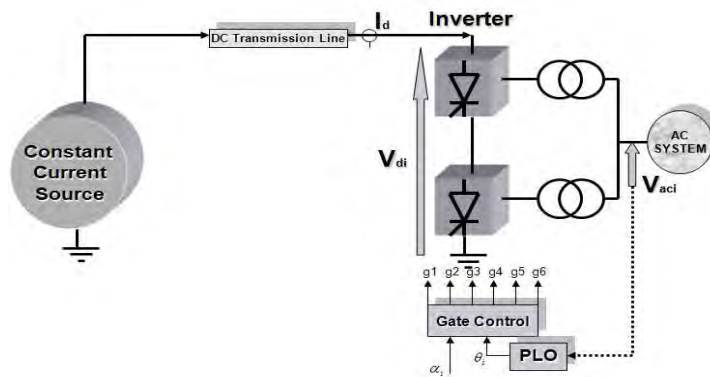
Figure 3.8: LCC HVDC System with Constant Current Source

These systems were modelled in PSCAD/EMTDC. The following points should be noted about the models:

- The converter was simulated so as to represent its actual nonlinear behaviour.
- The influence of phase-locked oscillator was simulated.
- The details of each of these components were discussed in Section 2.5
- The rectifier's ac system's effective short circuit ratio with reference to the transmitted dc power was chosen to be 8.
- The inverter's ac system's effective short circuit ratio with reference to the transmitted dc power was chosen to be 8.

Rectifier Voltage Control Plant Transfer Function

The process used to calculate the rectifier voltage control plant transfer function is as follows:

1. Model the LCC HVDC system, shown in Fig. 3.7, in PSCAD/EMTDC.

2. Simulate the LCC HVDC system so that it reaches steady-state.

3. Apply a 5° step increase in the rectifier firing angle α_r and measure the dc voltage response V_{dr}.

4. Approximate the step response V_{dr}, with characteristic time domain functions.

5. Calculate the Laplace transform, $V_{dr}(s)$ of the characterized step response.

6. Calculate the Laplace transform, $\alpha_r(s)$ of the step input.

7. Calculate the Rectifier Voltage Control plant transfer function

$$P_{vr}(s) = \frac{V_{dr}(s)}{\alpha_r(s)}$$

The above described process was executed, and the measured time domain voltage response is illustrated Fig. 3.9.
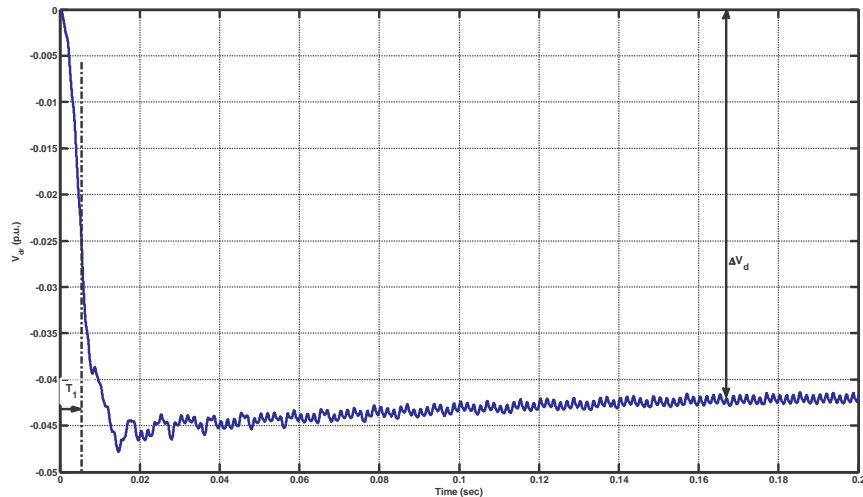
Figure 3.9: Measured DC Voltage Response

The measured voltage response was approximated using the following time domain function:

$$V_{dr}(t) = \Delta V_d \left(1 - e^{-at}\right)$$
(3.3.9)

where ΔV_d is the steady state change in the dc current (p.u.)

$a = \dfrac{1}{T_1}$ T_1 is defined as the time (sec) it takes the decaying waveform

to reach e^{-1} of its final value.

This function was simulated using MATLAB and characteristic time domain response is illustrated in Figure 3.10, together with the associated error when compared to the original signal.
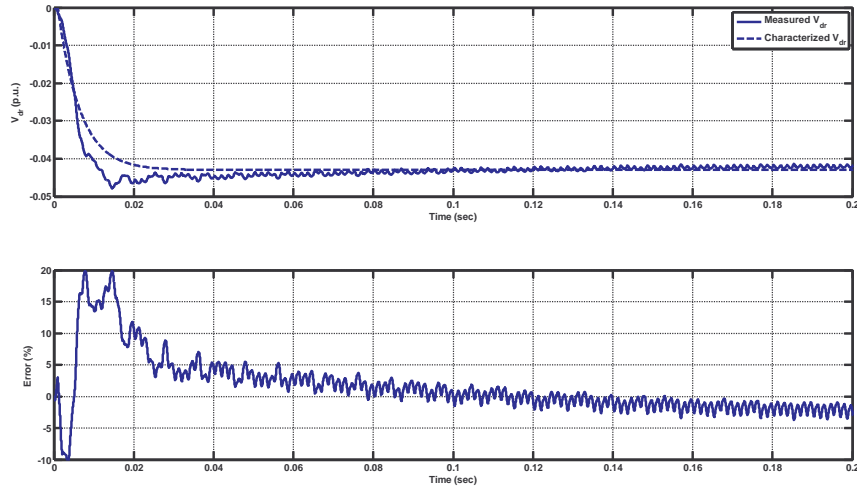
Figure 3.10: Characterized DC Voltage Response

Figure 3.10 clearly illustrates that equation (3.3.9) adequately approximates the dc voltage response to a step change in the rectifier's firing angle. Although there are moderate errors, in the characterized signal, these errors are high frequency signals (>100Hz). According to Jovic et. al. [13], for studies involving most of the HVDC phenomena, a frequency range less than 100Hz on the dc side is of interest. This claim was also supported by the results presented in [10 - 12]. A visual analysis of the error signal highlights the fact that the error is comprised of mainly high frequency signals. The largest error components are high frequency signals that have a large damping coefficient since these signals are damped out within 20msec.The remaining error is comprised of high frequency signals whose total combined magnitude is less than 5%.

The Laplace transform of the characterized dc voltage response was calculated as:

$$V_{dr}(s) = \frac{\Delta V_d}{s(s+a)} \qquad (3.3.10)$$

The Laplace transform of the firing angle step input was calculated as:

$$\alpha_r(s) = \frac{\Delta \alpha}{s} \qquad (3.3.11)$$

Therefore the rectifier voltage control plant transfer function was calculated as:

$$P_{vr}(s) = \frac{\Delta V_d}{\Delta \alpha} \frac{1}{s+a} \qquad (3.3.12)$$

Inverter Voltage Control Plant Transfer Function

The process used to calculate the inverter voltage control plant transfer function is as follows:

1. Model the LCC HVDC system, shown in Fig. 3.8, in PSCAD/EMTDC.

2. Simulate the LCC HVDC system so that it reaches steady-state.

3. Apply a 5° step decrease in the inverter firing angle α_i and measure the dc voltage response V_{di}.

4. Approximate the step response V_{di}, with characteristic time domain functions.

5. Calculate the Laplace transform, $V_{di}(s)$ of the characterized step response.

6. Calculate the Laplace transform, $\alpha_i(s)$ of the step input.

7. Calculate the Rectifier Voltage Control plant transfer function $P_{vi}(s) = \dfrac{V_{di}(s)}{\alpha_i(s)}$

The above described process was executed, and the measured time domain voltage response is illustrated Fig. 3.11.
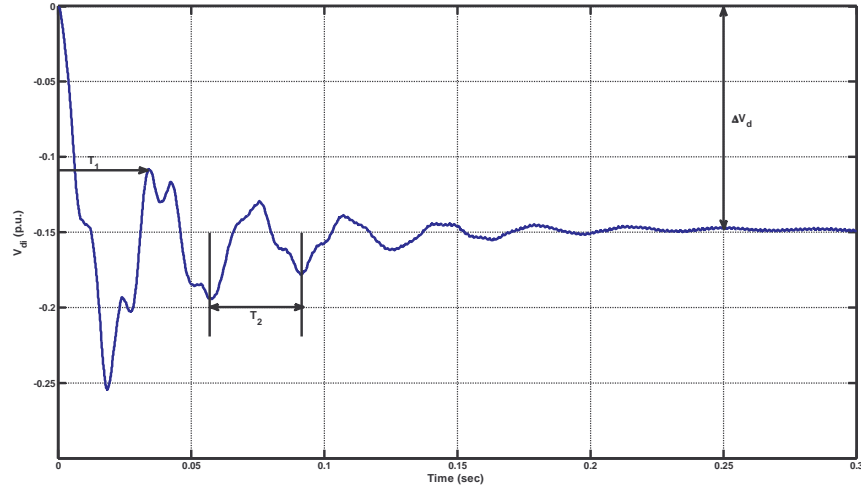
Figure 3.11: Measured DC Voltage Response

The measured voltage response was approximated using the following time domain function:

$$V_{di}(t) = \Delta V_d.(1 - e^{-at}.\cos(wt)) \tag{3.3.13}$$

where ΔV_d is the steady-state change in the dc voltage (p.u.)

$a = \dfrac{1}{T_1}$ T_1 is defined as the time (sec) it takes the decaying waveform to reach within e^{-1} of its final value.

$w = \dfrac{2\pi}{T_2}$ T_2 is defined as the period (sec) of the superimposed ac waveform.

This function is called the **Voltage HSR** equation and was simulated using MATLAB and characteristic time domain response is illustrated in Fig. 3.12, together with the associated error when compared to the original signal.
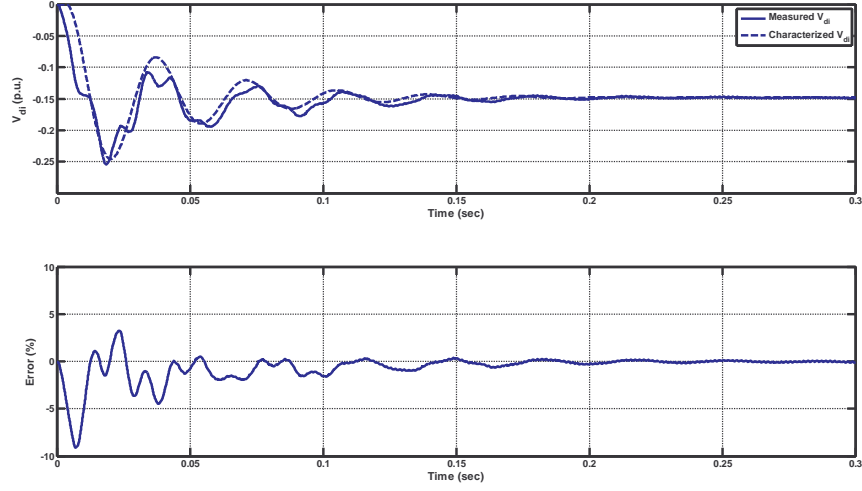
Figure 3.12: Characterized DC Voltage Response

Figure 3.12 clearly illustrates that **_Voltage HSR_** equation adequately approximates the dc voltage response to a step change in the inverter's firing angle. Although there are moderate errors, in the characterized signal, these errors are high frequency signals (>100Hz). A visual analysis of the error signal illuminates the fact that the error is comprised of mainly high frequency signals. The large error components are damped out relatively quickly and the remaining error is comprised of high frequency signals whose total combined magnitude is less than 5%.

The Laplace transform of the characterized dc voltage response was calculated as:

$$V_{di}(s) = \frac{w.\Delta V_d}{s\left[(s+a)^2 + w^2\right]} \qquad (3.3.14)$$

The Laplace transform of the firing angle step input was calculated as:

$$\alpha_i(s) = \frac{\Delta\alpha}{s} \qquad (3.3.15)$$

Therefore the inverter voltage control plant transfer function was calculated as:

$$P_{vi}(s) = \frac{\Delta V_d}{\Delta\alpha} \frac{w}{(s+a)^2 + w^2} \qquad (3.3.16)$$

45

3.4 Sensitivity to Thevenin's Equivalent Circuit Representation

In this chapter the HSR equations were developed. For the development of HSR equations, the Thevenin's equivalent ac network impedance was represented using a pure inductance. This implies that the network resistance is assumed to be zero and the "damping angle" was taken as 90°. Kundur [28] states that while local resistive loads do not have a significant effect on the ESCR, these resistive loads do improve the damping of the system thereby improving the dynamic performance of the control system. However, Hingorani et. al. [33] suggested that although in many studies, the ac system impedance is represented by its equivalent inductance at power frequency, it is important to simulate ac network impedance correctly at various frequencies due to distortions of ac voltages at the converter.

To investigate effect of the ac network representation on the HSR equations, two types of Thevenin equivalent representations were investigated for effective short circuit ratio of 8. These Thevenin equivalent circuits are illustrated in Fig. 3.14.
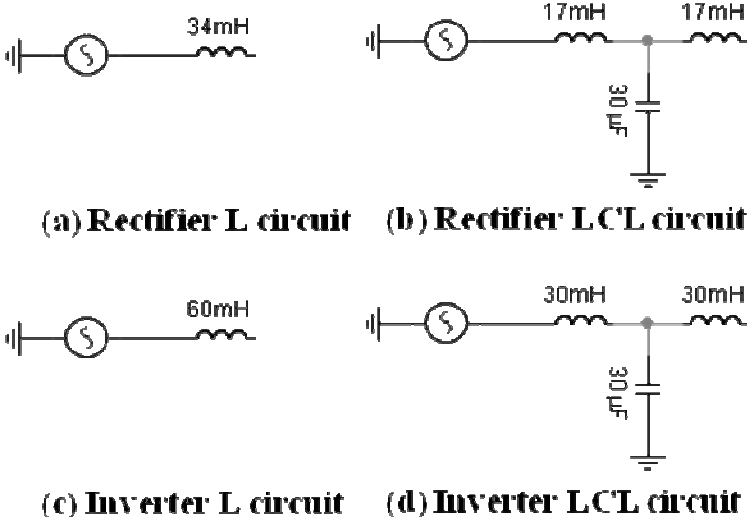
Figure 3.14: Thevenin Equivalent AC Network Representations

Fig 3.15 illustrates the corresponding impedance amplitude ($|Z|$) – frequency diagrams. Fig 3.15(a) illustrates that the dominant parallel resonant frequency rectifier ac circuit occurs around 158Hz for power inductance representation (L-circuit). By modifying the ac system impedance representation to an LCL-circuit and

while maintaining the effective short circuit level of 8, it is evident that the dominant parallel resonant frequency is shifted to around 142Hz and the impedance magnitude is significantly decreased.
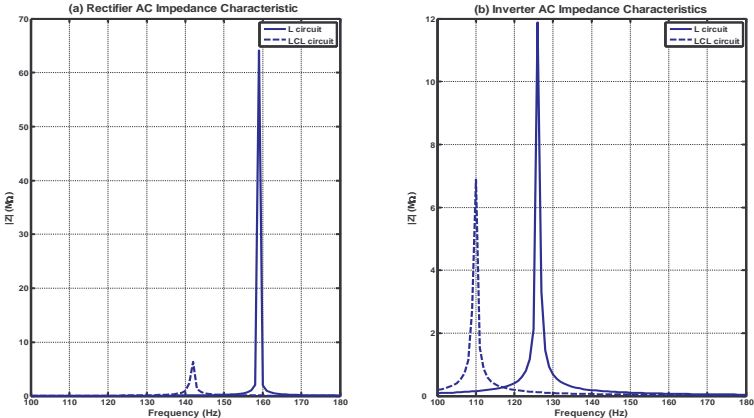
Figure 3.15: AC Impedance Characteristics for

Rectifier ESCR=8 and Inverter ESCR=8

Fig 3.15(b) illustrates that the dominant parallel resonant frequency of the inverter ac circuit occurs around 127Hz for power inductance representation (L-circuit). By modifying the ac system impedance representation to an LCL-circuit and while maintaining the effective short circuit level of 8, it is evident that the dominant parallel resonant frequency is shifted to around 110Hz and the impedance magnitude is decreased.

To analyse the impact of Thevenin's equivalent circuit representation on the HSR equations the following cases were investigated while the ESCR at both converters were maintained at 8:

Case	Rectifier AC System Representation	Inverter AC System Representation
1	L-circuit	L-circuit
2	LCL-circuit	L-circuit
3	LCL-circuit	LCL-circuit
4	L-circuit	LCL-circuit

Table 3.1: Case Studies for HSR equation sensitivity to Thevenin's equivalent circuit

representations

Rectifier Current HVDC Step Response (HSR)

The following process was used to evaluate the sensitivity of the rectifier current HSR equation for varying Thevenin's equivalent circuit representations:

1. Model the LCC HVDC system, shown in Fig. 3.1, in PSCAD/EMTDC.
2. For each of the cases stipulated in Table 3.1, model the ac system impedances according to the values in Fig. 3.14.
3. For each of the cases stipulated in Table 3.1, simulate the LCC HVDC system in PSCAD/EMTDC to reach steady-state.
4. Maintain the inverter firing angle constant.
5. Apply a 5° step increase in the rectifier firing angle α_r and measure the dc current response.

The results of this analysis are illustrated in Fig. 3.16, below.
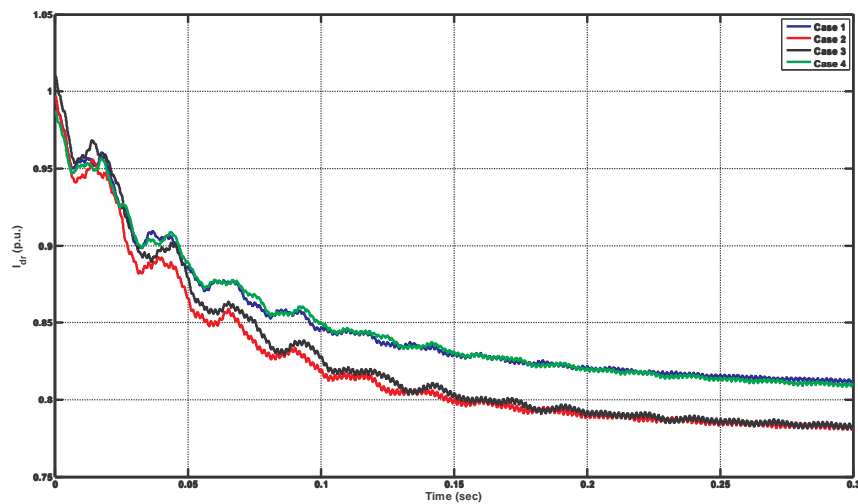
Figure 3.16: Rectifier Current HSR

Fig. 3.16 clearly illustrates that the shape of the Rectifier Current HSR curve does not significantly deviate from Case 1 with respect to the results for the other three cases listed in Table 3.1 therefore the Current HSR equation is still applicable. It should however be noted that the gain in the current response to a change in the rectifier firing angle does increase. The magnitude for gain difference will be considered as an area for further research and will be not be treated any further in this thesis.

Inverter Current HVDC Step Response (HSR)

The following process was used to evaluate the sensitivity of the inverter current HSR equation for varying Thevenin's equivalent circuit representations:

1. Model the LCC HVDC system, shown in Fig. 3.1, in PSCAD/EMTDC.
2. For each of the cases stipulated in Table 3.1, model the ac system impedances according to the values in Fig. 3.14.
3. For each of the cases stipulated in Table 3.1, simulate the LCC HVDC system in PSCAD/EMTDC to reach steady-state.
4. Maintain the rectifier firing angle constant.
5. Apply a 5° step decrease in the inverter firing angle α_i and measure the dc current response.

The results of this analysis are illustrated in Fig. 3.17, below.
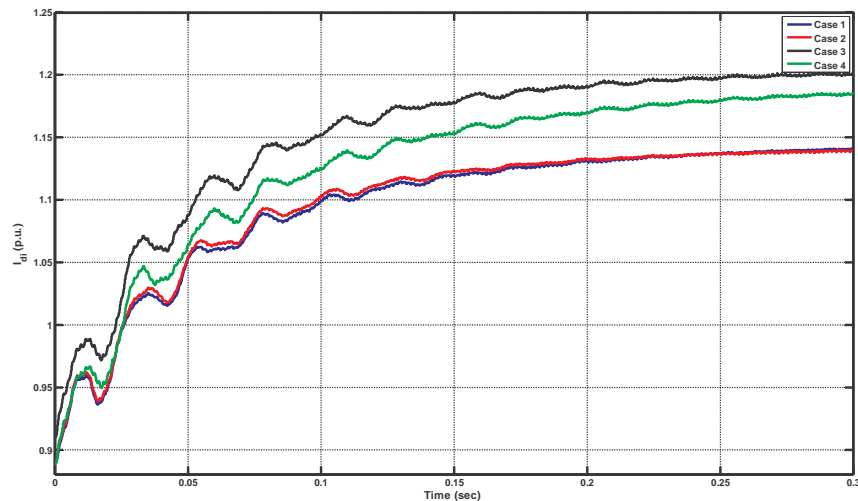
Figure 3.17: Inverter Current HSR

Fig. 3.17 clearly illustrates that the shape of the Inverter Current HSR curve does not significantly deviate from Case 1 with respect to the results for the other three cases listed in Table 3.1 therefore the Current HSR equation is still applicable. It should however be noted that the gain in the current response to a change in the rectifier firing angle does increase. The magnitude for gain difference will be considered as an area for further research and will be not be treated any further in this thesis.

Rectifier Voltage HVDC Step Response (HSR)

The following process was used to evaluate the sensitivity of the rectifier voltage HSR equation for varying Thevenin's equivalent circuit representations:

1. Model the LCC HVDC system, shown in Fig. 3.7, in PSCAD/EMTDC.

2. For each of the cases stipulated in Table 3.2, below, model the ac system impedances according to the values in Fig. 3.14.

Case	Rectifier AC System Representation
1	L-circuit
2	LCL-circuit

Table 3.2: Case Studies for Rectifier Voltage HSR equation sensitivity

to Thevenin's equivalent circuit representations

3. For each of the cases stipulated in Table 3.2, simulate the LCC HVDC system in PSCAD/EMTDC to reach steady-state.

4. Apply a 5° step increase in the rectifier firing angle α_r and measure the dc voltage response V_{dr}.

The results of this analysis are illustrated in Fig. 3.18, below.
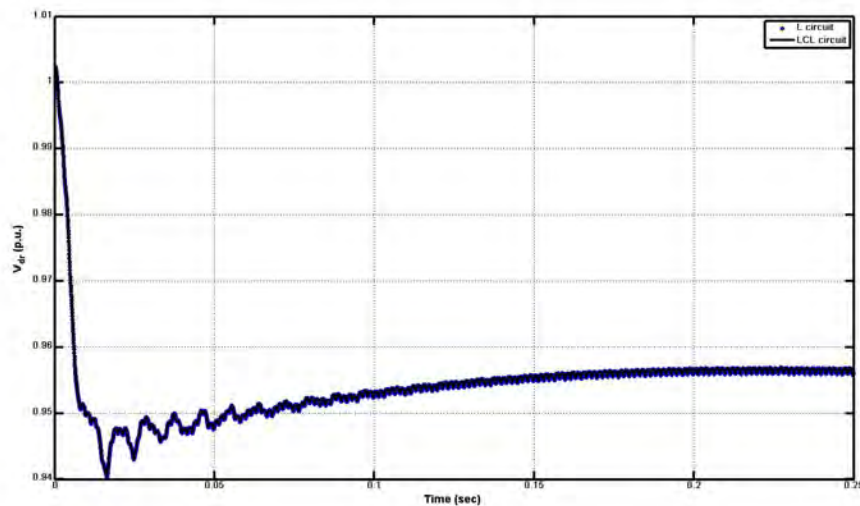
Figure 3.18: Rectifier Voltage HSR

Fig. 3.18 clearly illustrates that the shape of the Rectifier Voltage HSR curve does not deviate from L-circuit with respect to the results for the LCL-circuit therefore the Rectifier Voltage HSR equation is applicable.

Inverter Voltage HVDC Step Response (HSR)

The following process was used to evaluate the sensitivity of the inverter voltage HSR equation for varying Thevenin's equivalent circuit representations:

1. Model the LCC HVDC system, shown in Fig. 3.8, in PSCAD/EMTDC.
2. For each of the cases stipulated in Table 3.3, below, model the ac system impedances according to the values in Fig. 3.14.

Case	Inverter AC System Representation
1	L-circuit
2	LCL-circuit

Table 3.3: Case Studies for Inverter Voltage HSR equation sensitivity to Thevenin's equivalent circuit representations

3. For each of the cases stipulated in Table 3.3, simulate the LCC HVDC system in PSCAD/EMTDC to reach steady-state.
4. Apply a 3° step decrease in the inverter firing angle α_i and measure the dc voltage response V_{di}.

The results of this analysis are illustrated in Fig. 3.19.
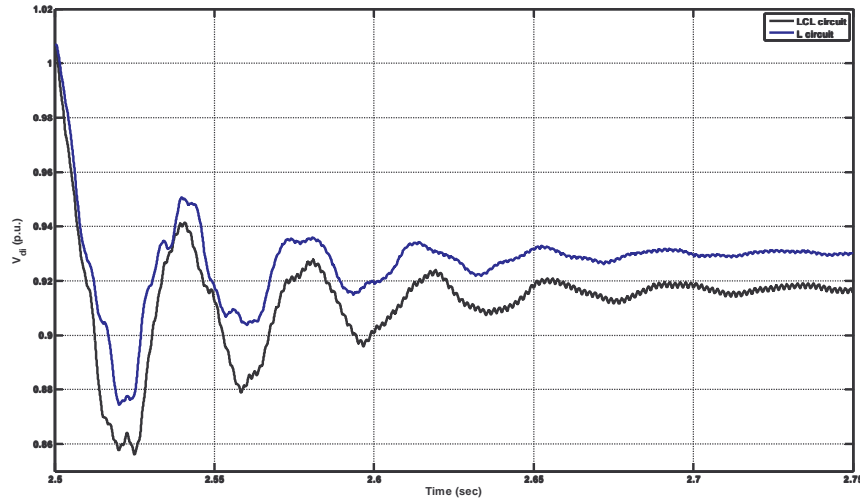
Figure 3.19: Inverter Voltage HSR

Fig. 3.19 clearly illustrates that the shape of the Inverter Voltage HSR curve does not deviate from L-circuit with respect to the results for the LCL-circuit therefore the Inverter Voltage HSR equation is applicable. It should however be noted that the gain in the current response to a change in the rectifier firing angle does increase. The magnitude for gain difference will be considered as an area for further research and will be not be treated any further in this thesis.

3.5 Sensitivity to Initial Conditions (I.C.)

Consider the inductive modelling block diagram illustrated in Fig. 3.20.
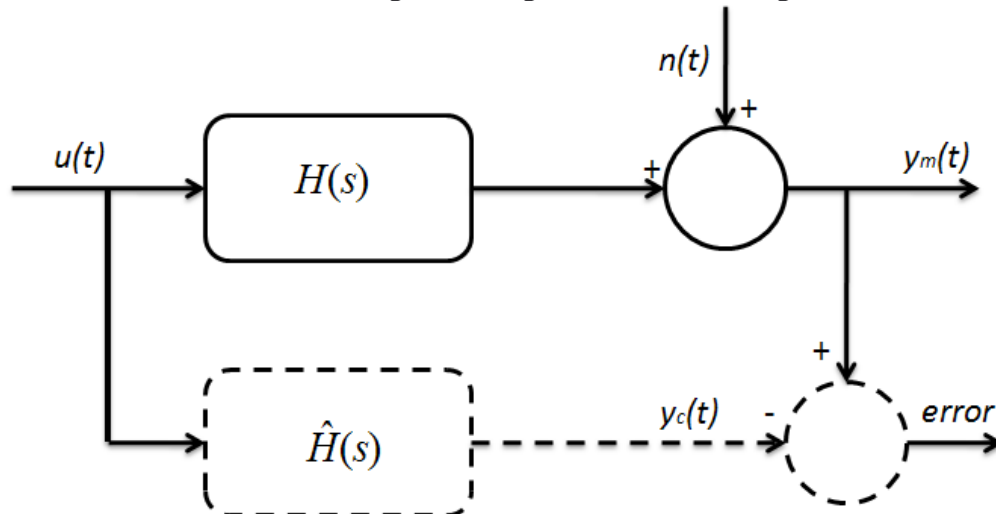
Figure 3.20: Inductive Modelling Block Diagram

Rake [20] states that the measured process output response $y_m(t)$, will consist of the uncorrupted process output plus additional process noise and/ or measurement noise $n(t)$. The inductively modelled system response will be:

$$\hat{H}(s) = H(s) + \frac{N(s)}{U(s)} \qquad (3.6.1)$$

Therefore inductive modelling methods may be sensitive to noise. High-order derivative terms of the process signals give rise to initial values in the measured output response [20].

Due to the inherent dependency of the measured output response on the initial conditions of the system, this section of the thesis investigates the sensitivity of derived HSR equations to initial conditions (I.C.).

Rectifier Current HVDC Step Response (HSR)

The following process was used to evaluate the sensitivity of the rectifier current HSR equation for varying initial conditions:

1. Model the LCC HVDC system, shown in Fig. 3.1, in PSCAD/EMTDC. The rectifier's ac system's effective short circuit ratio with reference to the transmitted dc power was chosen to be 8. The inverter's ac system's effective short circuit ratio with reference to the transmitted dc power was chosen to be 8.

2. Simulate the LCC HVDC system in PSCAD/EMTDC so that it reaches steady-state of 1 p.u. dc current from the rectifier station.

3. Maintain the inverter firing angle constant.

4. Apply a 10° step increase in the rectifier firing angle α_r and measure the dc current response.

5. Approximate the step response I_{dr}, with characteristic time domain functions.

6. Plot the characterized dc current response in MATLAB and calculate error between PSCAD/EMTDC results and MATLAB results.

7. Simulate the LCC HVDC system so that it reaches steady-state of 1.02 p.u dc current from the rectifier station.

8. Maintain the inverter firing angle constant.

9. Apply a 10° step increase in the rectifier firing angle α_r and measure the dc current response.

10. Calculate error between PSCAD/EMTDC results and original characterised MATLAB results.

11. Simulate the LCC HVDC system so that it reaches steady-state of 0.98 p.u dc current from the rectifier station.

12. Maintain the inverter firing angle constant.

13. Apply a 10° step increase in the rectifier firing angle α_r and measure the dc current response.

14. Calculate error between PSCAD/EMTDC results and original characterised MATLAB results.

The results of this analysis are illustrated in Fig. 3.21, below.
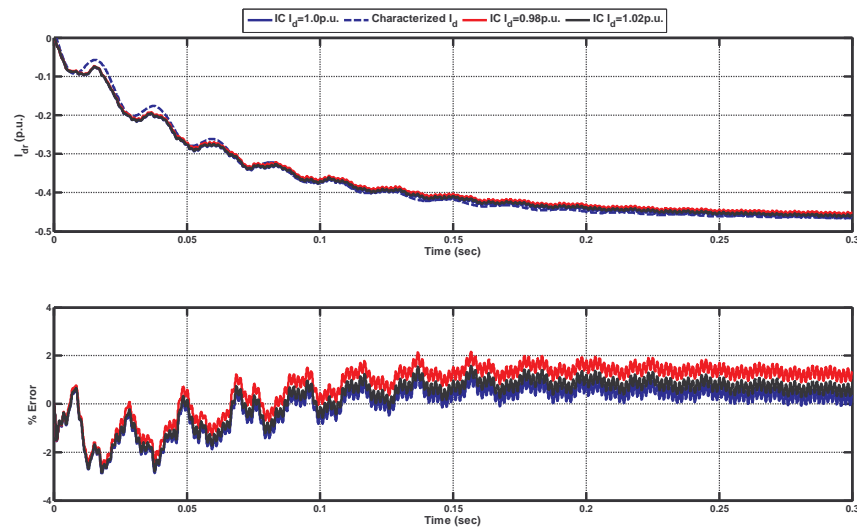
Figure 3.21: Sensitivity of Rectifier Current HSR to Initial Conditions

Fig. 3.21 clearly illustrates that original characterised Rectifier Current HSR is not sensitive to initial conditions since the error for all three initial conditions remains small (less than 2.5%). For larger variations in the dc current set point it may be possible that error increases significantly. However it should be noted that a significant change in dc current will correspond to a change in the effective short circuit ratio at the converter station. Therefore Chapter 4 investigates the change in HSR equation parameters for variations in effective short circuit ratios.

Inverter Current HVDC Step Response (HSR)

The following process was used to evaluate the sensitivity of the inverter current HSR equation for varying initial conditions:

1. Model the LCC HVDC system, shown in Fig. 3.1, in PSCAD/EMTDC. The rectifier's ac system's effective short circuit ratio with reference to the transmitted dc power was chosen to be 8. The inverter's ac system's effective short circuit ratio with reference to the transmitted dc power was chosen to be 8.

2. Simulate the LCC HVDC system in PSCAD/EMTDC so that it reaches steady-state of 0.9 p.u. dc current to the inverter station.

3. Maintain the rectifier firing angle constant.

4. Apply a 10° step decrease in the inverter firing angle α_i and measure the dc current response.

5. Approximate the step response I_{di}, with characteristic time domain functions.

6. Plot the characterized dc current response in MATLAB and calculate error between PSCAD/EMTDC results and MATLAB results.

7. Simulate the LCC HVDC system so that it reaches steady-state of 0.92 p.u dc current to the inverter station.

8. Maintain the rectifier firing angle constant.

9. Apply a 10° step increase in the inverter firing angle α_i and measure the dc current response.

10. Calculate error between PSCAD/EMTDC results and original characterised MATLAB results.

11. Simulate the LCC HVDC system so that it reaches steady-state of 0.88 p.u dc current to the inverter station.

12. Maintain the rectifier firing angle constant.

13. Apply a 10° step increase in the inverter firing angle α_i and measure the dc current response.

14. Calculate error between PSCAD/EMTDC results and original characterised MATLAB results.

Fig. 3.22 clearly illustrates that original characterised Inverter Current HSR is not sensitive to initial conditions since the error for all three initial conditions remains small (less than 4%).
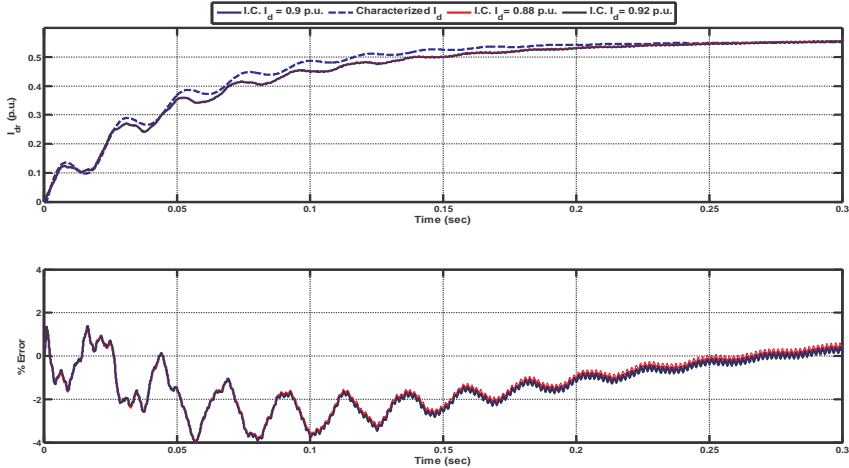
Figure 3.22: Sensitivity of Inverter Current HSR to Initial Conditions

For larger variations in the dc current set point it may be possible that error increases significantly. However it should be noted that a significant change in dc current will correspond to a change in the effective short circuit ratio at the converter station. Therefore, Chapter 4 investigates the change in HSR equation parameters for variations in effective short circuit ratios.

Rectifier Voltage HVDC Step Response (HSR)

The following process was used to evaluate the sensitivity of the rectifier voltage HSR equation for varying initial conditions:

1. Model the LCC HVDC system, shown in Fig. 3.7, in PSCAD/EMTDC.
2. Simulate the LCC HVDC system in PSCAD/EMTDC so that it reaches steady-state of 1.0 p.u. dc voltage at the retifier station.
3. Apply a 10° step increase in the rectifier firing angle α_r and measure the dc voltage response V_{dr}.
4. Approximate the step response V_{dr}, with characteristic time domain functions.
5. Plot the characterized dc voltage response in MATLAB and calculate error between PSCAD/EMTDC results and MATLAB results.

6. Simulate the LCC HVDC system in PSCAD/EMTDC so that it reaches steady-state of 0.98 p.u. dc voltage at the rectifier station.

7. Apply a 10° step increase in the rectifier firing angle α_r and measure the dc voltage response V_{dr}.

8. Approximate the step response V_{dr}, with characteristic time domain functions.

9. Calculate error between PSCAD/EMTDC results and original characterised MATLAB results.

10. Simulate the LCC HVDC system in PSCAD/EMTDC so that it reaches steady-state of 1.02 p.u. dc voltage at the rectifier station.

11. Apply a 10° step increase in the rectifier firing angle α_r and measure the dc voltage response V_{dr}.

12. Approximate the step response V_{dr}, with characteristic time domain functions.

13. Calculate error between PSCAD/EMTDC results and original characterised MATLAB results.

Fig. 3.23 clearly illustrates that original characterised Rectifier Voltage HSR is not sensitive to initial conditions.
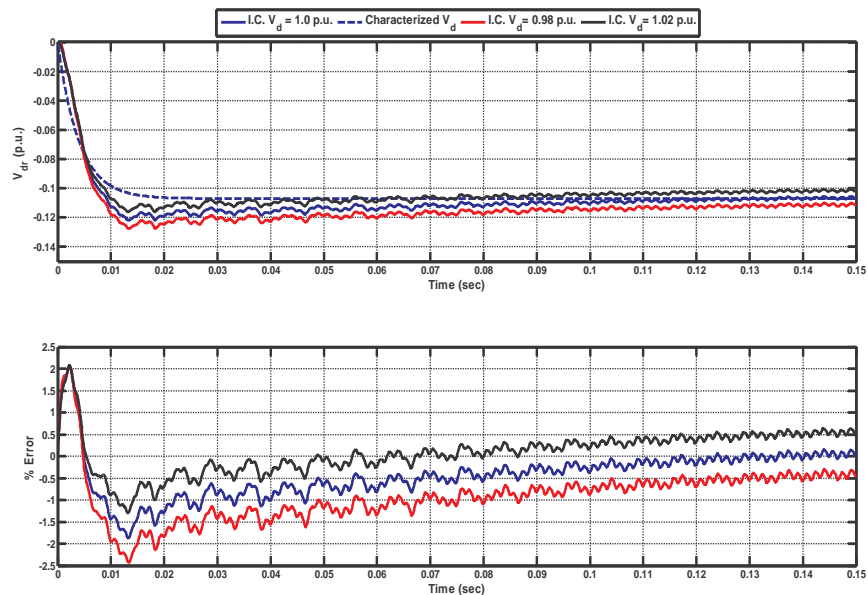
Figure 3.23: Sensitivity of Rectifier Voltage HSR to Initial Conditions

Since the error for all three initial conditions remains small (less than 2.5%). It is optimal practice to operate the LCC HVDC scheme at near maximum rated dc voltage (1p.u.). For larger variations in the dc voltage set point, it should be noted that a significant change in dc voltage will correspond to a change in the effective short circuit ratio at the converter station. Therefore Chapter 4 investigates the change in HSR equation parameters for variations in effective short circuit ratios.

Inverter Voltage HVDC Step Response (HSR)

The following process was used to evaluate the sensitivity of the inverter voltage HSR equation for varying initial conditions:

1. Model the LCC HVDC system, shown in Fig. 3.8, in PSCAD/EMTDC.
2. Simulate the LCC HVDC system in PSCAD/EMTDC so that it reaches steady-state of 1.0 p.u. dc voltage at the inverter station.
3. Apply a 5° step decrease in the inverter firing angle α_i and measure the dc voltage response V_{di}.
4. Approximate the step response V_{di}, with characteristic time domain functions.
5. Plot the characterized dc voltage response in MATLAB and calculate error between PSCAD/EMTDC results and MATLAB results.
6. Simulate the LCC HVDC system in PSCAD/EMTDC so that it reaches steady-state of 0.98 p.u. dc voltage at the inverter station.
7. Apply a 5° step decrease in the inverter firing angle α_i and measure the dc voltage response V_{di}.
8. Approximate the step response V_{di}, with characteristic time domain functions.
9. Calculate error between PSCAD/EMTDC results and original characterised MATLAB results.
10. Simulate the LCC HVDC system in PSCAD/EMTDC so that it reaches steady-state of 1.02p.u. dc voltage at the inverter station.
11. Apply a 5° step decrease in the inverter firing angle α_i and measure the dc voltage response V_{di}.

12. Approximate the step response V_{di}, with characteristic time domain functions.

13. Calculate error between PSCAD/EMTDC results and original characterised MATLAB results.

Fig. 3.24 clearly illustrates that original characterised Inverter Voltage HSR is not sensitive to initial conditions since the error for all three initial conditions remains small (less than 8.5%).
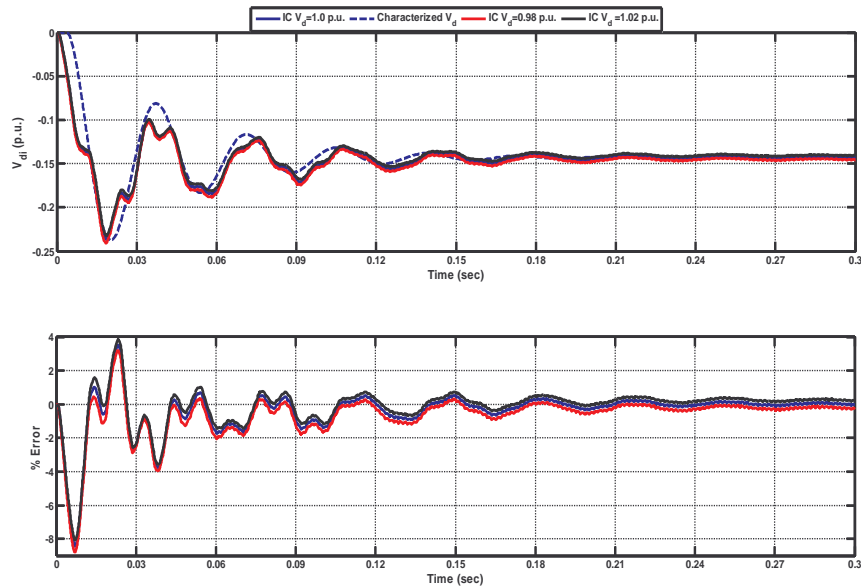
Figure 3.24: Sensitivity of Inverter Voltage HSR to Initial Conditions

It is optimal practice to operate the LCC HVDC scheme at near maximum rated dc voltage (1p.u.). For larger variations in the dc voltage set point, it should be noted that a significant change in dc voltage will correspond to a change in the effective short circuit ratio at the converter station. Therefore, Chapter 4 investigates the change in HSR equation parameters for variations in effective short circuit ratios.

3.6 Conclusions

Novel HVDC Step Response (HSR) equations were derived for LCC HVDC systems. These equations were derived based on the PSCAD/EMTDC application of "Jacobian Linearization". The shape of the HSR curves were illustrated to not be very sensitive to the Thevenin equivalent representation for the ac system impedances. The derived HSR equations were proven to not be very sensitive to initial conditions. Based on the derived characterised time domain responses, the following **HVDC Plant Transfer Functions** were calculated:

1. Rectifier Current Control plant transfer function:

$$P_{cr}(s) = \frac{\Delta I_d}{\Delta \alpha} . e^{-s.T_o} \left(\frac{s^3 + (3a-1)s^2 + (3a^2 - 2a + w^2 + k|\Delta I_d|w)s + (a^3 - a^2 + aw^2 - w^2 + k|\Delta I_d|aw)}{(s+a)(s^2 + 2as + a^2 + w^2)} \right)$$

2. Inverter Current Control plant transfer function:

$$P_{ci}(s) = \frac{\Delta I_d}{\Delta \alpha} . e^{-s.T_o} \left(\frac{s^3 + (3a-1)s^2 + (3a^2 - 2a + w^2 + k|\Delta I_d|w)s + (a^3 - a^2 + aw^2 - w^2 + k|\Delta I_d|aw)}{(s+a)(s^2 + 2as + a^2 + w^2)} \right)$$

3. Rectifier Voltage Control plant transfer function:

$$P_{vr}(s) = \frac{\Delta V_d}{\Delta \alpha} \frac{1}{s+a}$$

4. Inverter Voltage Control plant transfer function:

$$P_{vi}(s) = \frac{\Delta V_d}{\Delta \alpha} \frac{w}{(s+a)^2 + w^2} e^{-s.T_o}.$$

Due to the uncertain nature of the state of power systems, the parameters that define the above transfer functions vary. The variation range of the parameters of the HSR equations for variations in effective short circuit ratios are presented in the next chapter.

Chapter 4

LCC HVDC Plant Uncertainty

4.1 Introduction

The state of power systems changes with sudden disturbances in the power system. These sudden disturbances will change the short circuit capacity of ac busbars in the power system. The factors defining the quantitative change in short circuit capacity are loss of generation, restoration of generation, loss of transmission, loss of demand and loss of reactive compensation.

Due to the diverse nature of the factors affecting the quantitative change in short circuit capacity of an ac busbar, the short circuit capacity at a given HVDC converter ac busbar will vary within a range. Therefore, combined with the varying amount of dc power, (change dc current operating point), that will be transmitted on the HVDC transmission system, the effective short circuit ratio for a given HVDC converter station will vary within a certain range.

Due to the uncertain nature of the effective short circuit ratio of rectifier and inverter stations, the plant transfer functions developed in the previous chapter will have a range of uncertainty. The objective of this chapter will be to determine the plant transfer function parametric ranges for varying short circuit ratios.

The method used to calculate the parametric variations in the plant transfer functions were exactly the same as the methods developed in the previous chapter, with the only exception being that the effective short circuit ratios were varied.

4.2 AC Network Representations for Varying ESCRs

Hingorani et. al. [33] have suggested that it is important to simulate ac network impedance correctly at various frequencies due to distortions of ac voltages at the converter. Section 3.5 illustrated that the shapes of the HSR curves were not very sensitive to the Thevenin's equivalent representation for the ac system impedances.

In this thesis, the Thevenin's equivalent network impedance were represented using a pure inductance. This implies that the network resistance is assumed to be zero and the "damping angle" was taken as 90°.

4.3 Rectifier Current Control

The rectifier's current control transfer function was defined by:

$$P_{cr}(s) = \frac{\Delta I_d}{\Delta \alpha} . e^{-sT_o} \left(\frac{s^3 + (3a-1)s^2 + (3a^2 - 2a + w^2 + c|\Delta I_d|w)s + (a^3 - a^2 + aw^2 - w^2 + c|\Delta I_d|aw)}{(s+a)(s^2 + 2as + a^2 + w^2)} \right)$$

(4.3.1)

In the above equation the key output parametric variables are:

T_o is the time delay (sec)

ΔI_d is the change in the dc current (p.u.)

$a = \dfrac{1}{T_1}$ T_1 is defined as the time (sec) it takes the decaying waveform to reach e^{-1} of its final value.

$w = \dfrac{2\pi}{T_2}$ T_2 is defined as the period (sec) of the superimposed ac waveform.

$\Delta \alpha$ is the change in the rectifier firing angle (^{o})

c is a constant $= 0.25$

Kundur [28] states that the dynamic performance of a current controller is dependent on the strength of both the rectifier and inverter ac systems. Therefore, the variations in the above listed parameters were calculated according to the method presented in Section 3.3.1, when the rectifier converter station's and the inverter converter station's effective short circuit ratios were varied. The results of the calculations are illustrated in Table 4.1.

Inverter	Rectifier					
ESCR	**ESCR**	ΔI_d	a	w	T_o	$\Delta \alpha$
7.96	7.96	-0.22	14.95	290.89	0.70	5.00
7.96	6.24	-0.20	20.54	285.60	0.80	5.00
7.96	4.50	-0.17	31.51	279.25	1.00	5.00
7.96	2.77	-0.13	44.23	239.82	1.65	5.00
5.97	8.03	-0.23	12.38	278.02	0.63	5.00
5.97	6.30	-0.22	14.73	285.60	0.81	5.00
5.97	4.54	-0.21	21.39	272.00	1.08	5.00
5.97	2.79	-0.13	43.20	240.74	1.65	5.00
3.93	8.18	-0.29	7.12	265.11	0.60	5.00
3.93	6.43	-0.27	8.40	262.89	0.76	5.00
3.93	4.64	-0.23	13.62	254.38	0.99	5.00
3.93	2.83	-0.14	35.71	216.66	1.59	5.00

Table 4.1: Parametric Variations of Rectifier Current Control
Plant Transfer Function for Varying ESCRs

Table 4.1 clearly illustrates that when the rectifier converter station's ESCR varies from 2.83 to 7.96 and the inverter converter station's ESCR varies from 3.93 to 7.96, the rectifier current control plant transfer function parameters vary in the following respective ranges:

$$\Delta I_d \in \left[-0.29, -0.13\right] \quad \text{(p.u.)}$$

$$a \in \left[7.12, 44.23\right] \quad \text{(1/sec)}$$

$$w \in \left[216.66, 290.89\right] \quad \text{(rad/s)}$$

$$T_o \in \left[0.60, 1.65\right] \quad \text{(msec)}$$

4.4 Inverter Current Control

The inverter's current control transfer function is defined by:

$$P_{ci}(s) = \frac{\Delta I_d}{\Delta \alpha} . e^{-sT_o} \left(\frac{s^3 + (3a-1)s^2 + (3a^2 - 2a + w^2 + k|\Delta I_d|w)s + (a^3 - a^2 + aw^2 - w^2 + k|\Delta I_d|aw)}{(s+a)(s^2 + 2as + a^2 + w^2)} \right)$$

(4.4.1)

In the above equation the key output parametric variables are T_o, ΔI_{di}, a, w and $\Delta \alpha_i$. The variations in the above parameters were calculated for different rectifier converter station's and the inverter converter station's effective short circuit ratios. The results of the calculations are illustrated in Table 4.2.

Inverter ESCR	Rectifier ESCR	ΔI_d	a	w	T_d	$\Delta \alpha$
7.96	8	0.27	15.19	280.50	0.06	-5.00
8.4335	6	0.23	21.12	278.02	0.89	-5.00
9.29	4	0.18	23.80	276.79	0.86	-5.00
11.8	2	0.10	41.63	248.35	0.24	-5.00
5.97	8	0.30	14.27	280.50	0.81	-5.00
6.34	6	0.26	19.31	275.58	0.78	-5.00
6.99	4	0.20	22.16	268.51	0.73	-5.00
8.87	2	0.11	39.62	248.35	0.00	-5.00
3.94	8	0.42	8.31	279.25	0.51	-5.00
4.2112	6	0.35	10.67	280.50	0.46	-5.00
4.69	4	0.26	19.16	279.25	0.45	-5.00

Table 4.2: Parametric Variations of Inverter Current Control
Plant Transfer Function for Varying ESCRs

Table 4.2 clearly illustrates that when the rectifier converter station's ESCR varies from 4 to 8 and the inverter converter station's ESCR varies from 3.94 to 8.87, the inverter current control plant transfer function parameters vary in the following respective ranges:

$$\Delta I_d \in [0.1, 0.42] \quad \text{(p.u.)}$$

$$a \in [10.67, 41.63] \quad \text{(1/sec)}$$

$$w \in [248.35, 280.50] \quad \text{(rad/s)}$$

$$T_o \in [0.06, 0.89] \quad \text{(msec)}$$

4.5 Rectifier Voltage Control

The rectifier's voltage control transfer function is defined by:

$$P_{vr}(s) = \frac{\Delta V_d}{\Delta \alpha} \frac{1}{s+a}$$

(4.5.1)

In the above equation the key output parametric variables are

ΔV_d is the change in the dc voltage (p.u.)

$a = \dfrac{1}{T_1}$ T_1 is defined as the time (sec) it takes the decaying waveform

to reach e^{-1} of its final value.

The variations in the above parameters were calculated for different rectifier converter station's effective short circuit ratios. The results of the calculations are illustrated in Table 4.3.

Rectifier ESCR	ΔV_d	a	$\Delta \alpha$
8	-0.042	192.68	5.00
6	-0.043	195.31	5.00
4	-0.045	192.31	5.00
2	-0.046	165.29	5.00

Table 4.3: Parametric Variations of Rectifier Voltage Control
Plant Transfer Function for Varying ESCRs

Table 4.3 clearly illustrates that when the rectifier converter station's ESCR varies from 2 to 8, the rectifier voltage control plant transfer function parameters vary in the following ranges:

$$a \in [165.29, 195.31] \qquad (1/\text{sec})$$

$$\Delta V_d \in [-0.046, -0.042] \qquad (\text{p.u.})$$

4.6 Inverter Voltage Control

The inverter's voltage control transfer function is defined by:

$$P_{vi}(s) = \frac{\Delta V_d}{\Delta \alpha} \frac{1}{(s+a)^2 + w^2} e^{-sT_o}$$
(4.6.1)

In the above equation the key output parametric variables are

T_o is the time delay (sec)

ΔV_d is the change in the dc current (p.u.)

$a = \dfrac{1}{T_1}$ T_1 is defined as the time (sec) it takes the decaying waveform

                       to reach e^{-1} of its final value.

$w = \dfrac{2\pi}{T_2}$ T_2 is defined as the period (sec) of the superimposed as ac

                       waveform.

The variations in the above parameters were calculated for different inverter converter station's effective short circuit ratios. The results of the calculations are illustrated in Table 4.4.

Inverter ESCR	ΔV_d	a	w	T_o	$\Delta \alpha$
8	-0.148	29.95	175.18	0.78	-5.00
6	-0.152	27.38	171.50	0.78	-5.00
4	-0.162	25.31	165.06	0.58	-5.00

Table 4.4: Parametric Variations of Inverter Voltage Control
Plant Transfer Function for Varying ESCRs

Table 4.4 clearly illustrates that when the inverter converter station's ESCR varies from 4 to 8, the following inverter voltage control plant transfer function parameters varies in the following respective ranges:

$$a \in [25.31, 29.95] \quad (1/\text{sec})$$

$$T_o \in [0.58, 0.78] \quad (\text{msec})$$

$$V_d \in [-0.162, -0.148] \ (\text{p.u.})$$

$$w \in [165.06, 175.18] \quad (\text{rad/s})$$

4.7 Conclusions

Due to the uncertain nature of the state of power systems, the parameters of the plant transfer functions that define the LCC HVDC systems vary. In this chapter, the range of plant transfer function parametric variation, was determined as a function of ac systems effective short circuit ratio. Therefore, if the range of the ac system's effective short circuit ratio is known, the range of parametric uncertainty of the LCC HVDC plant transfer functions can be obtained from Table 4.1 to Table 4.4.

Based on the determined range of LCC HVDC plant parametric uncertainty, the next chapter uses Quantitative Feedback Theory [31] to design the parameters of the LCC HVDC control system.

Chapter 5

Design of LCC HVDC Control Systems

5.1 Quantitative Feedback Theory

Quantitative feedback theory (QFT) was developed by Horowitz [34], to provide an effective approach for the design of control systems for uncertain plants and/or disturbances. Quantitative feedback theory is a frequency-domain technique utilising the Nichols chart, Fig. 5.1, in order to achieve a robust design over a specified region of uncertainty.
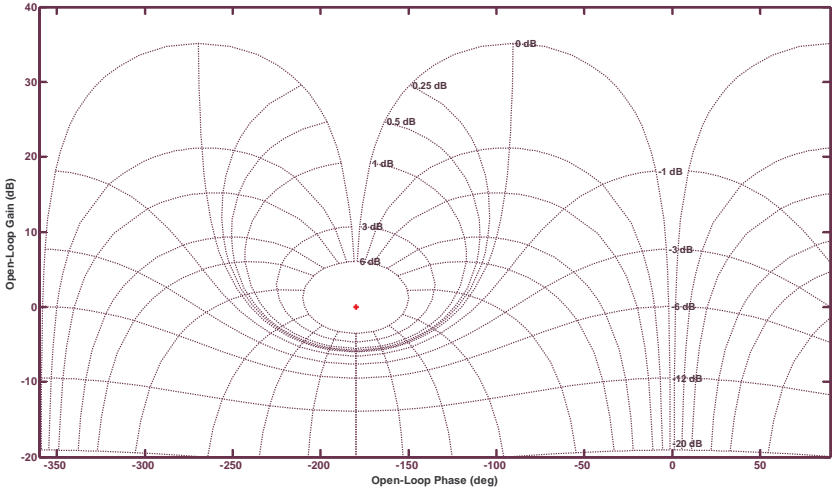
Figure 5.1: Nichols Chart

The QFT design philosophy was chosen to design the LCC HVDC control system parameters due to the fact that LCC HVDC systems are naturally uncertain. The reasons for the uncertain nature of LCC HVDC systems studied in this thesis are as follows:

1. AC systems' effective short circuit ratios are variable in nature as discussed in Chapter 4.

2. The LCC HVDC plant transfer functions were developed from simulations thus introducing, errors even though minor, which can be considered/treated as plant uncertainty.

3. Linear LCC HVDC plant transfer functions were derived from nonlinear HVDC dynamics thus introducing, errors even though minor, which can be considered/treated as plant uncertainty.

The controller should meet the performance specifications in spite of the variations of the parameters of the LCC HVDC plant models. QFT works directly with such uncertainties and does not require any particular representation.

A key element of QFT is embedding the performance specifications at the onset of the design process. These specifications include:

- Percentage overshoot
- Settling time (t_s) which is defined as the time required by the step response to settle within $\pm\delta\%$ of the final value, where δ is defined.

Figure 5.2: Control System Performance Specifications

These specifications establish design goals that enhance and expedite the achievement of a successful design.

One of the fundamental aspects in control design is the use of an accurate description of the plant dynamics. QFT involves frequency-domain arithmetic, therefore, the plant dynamics must be defined in terms of its frequency response. The term "template" is used to denote the collection of an uncertain plant's frequency responses at given frequencies. Samples of plant templates at different frequencies are illustrated in Fig. 5.3. The use of templates alleviates the need to develop any particular plant model representation.
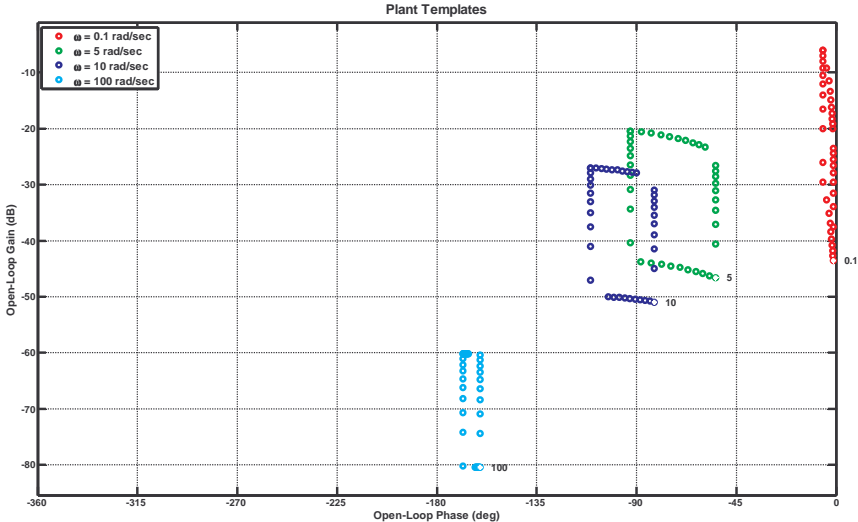
Figure 5.3: Plant Templates for various frequencies

Once the plant templates are developed, QFT converts closed-loop magnitude specifications into magnitude and phase constraints on a nominal open-loop function. These constraints are called *QFT bounds* (illustrated in Fig. 5.4).
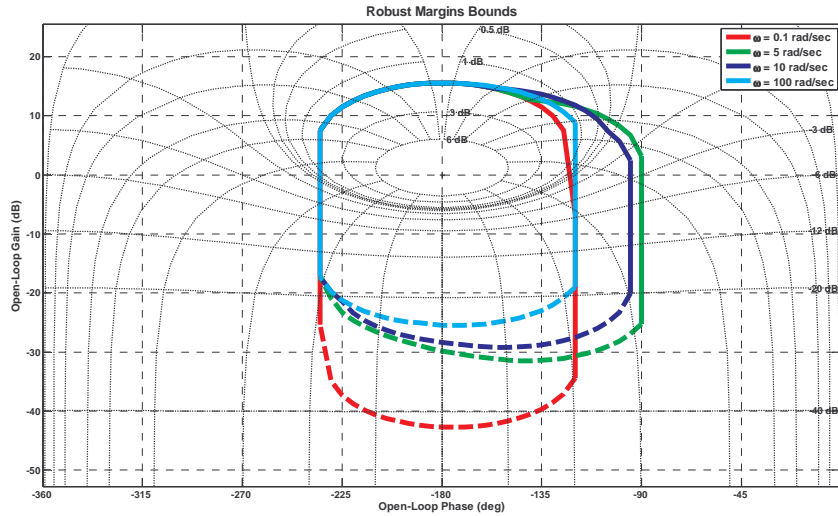
Figure 5.4: QFT Bounds at various frequencies

A detailed discussion on the method used to plot templates on the stability margin based on plant parameter uncertainty can be found in [34]. The size of the templates indicates whether or not a robust design is achievable. If a robust design is not possible, then the templates can be used as a metric in the reformation of the control design problem. Another aspect of the QFT design process is the ability to concurrently analyze frequency responses of the plant transfer functions that represent the non-linear dynamical system through its operating environment. This gives the designer insight into the behaviour of the system. The designer can use this insight for such things as picking out the key frequencies to use during the design process, as an indicator of potential problems such as non-minimum phase behaviour, and as a tool to compare the nonlinear system with the desired performance boundaries.

Non-minimum phase behaviour occurs when the loop transfer function has real poles and zeros in the right half plane or even consists of dead-time. The non-minimum phase behaviour will restrict the maximum gain cross-over frequency and will therefore affect the achievement of the specifications.

The plotting of the loop transfer functions on Nichols Chart gives the designer a first look at any areas of the design that may present problems during simulation and

implementation. To obtain a successful control design, the controlled system must meet all of the requirements during simulation. If the controlled system fails any of the simulation tests, using the design elements of QFT, the designer can trace that failure back through the design process and make necessary adjustments to the design.

5.2 HVDC Control System Design

Erikson et. al [1]. stated that there is a distinct need for quantitative methods for stability analysis. Based on a computer program developed by Persson [8] that calculated the rectifier current control transfer function of the uncompensated control loop, Erikkson [1] et. al. used Nyquist plots to analyse the stability of the LCC HVDC rectifier current control loop. Erikson et. al. [1] also used Bode plots and Nyquist plots to design a PI controller for a certain parametric rectifier current control plant.

Freris et. al. [9] used Nyquist plot to analyze the stability of the compensated certain parametric rectifier current control loop of a dc transmission system connected between a rectifier with short circuit ratio 3.75 and inverter with an infinite short circuit ratio.

Jovcic et. al. [13] used root locus diagrams to analyse the effect of phase locked loop gains on the stability of a certain parametric rectifier current control plant. Jovcic et. al. [21] also used root locus diagrams to analyse the difference of the direct current feedback control loop and the fast power feedback control loop for a certain parametric HVDC system.

From the above analysis, it is evident that although LCC control theory has been superficially investigated to design control systems, parametric plant uncertainty has not been investigated. Therefore, this chapter designs robust LCC HVDC control system parameters using quantitative feedback theory to accommodate parametric plant uncertainty.

5.2.1 Performance Specifications and Control Problem Definition

An HVDC system consists of uncertain plants. These uncertainties are result of changes/disturbances in the ac networks or in the HVDC system itself. Further uncertainties can be introduced due to simplified system modelling techniques. Therefore, negative feedback control (as described in Chapter 2) is used to limit the effect of these uncertainties in the HVDC system operation.

Erikson et. al [1] specifies that a minimum phase margin of 40° from the Nyquist point should be maintained for all frequencies. On the Nichols chart, the 40° phase margin specification corresponds to the 6dB M-circle.

It has been decided that the LCC HVDC control system should achieve the following performance specifications:

Overshoot $< 5\%$

Settling Time (t_s) < 15 times the largest time constant

Steady state error (δ) $< 2\%$

The control problem is defined as:

"For LCC HVDC plant transfer functions (P_{cr}, P_{ci}, P_{vr}, P_{vi}) defined in Section 3.3, whose parameters vary according to Table 4.1 to 4.4, design the fastest possible control system. The control system should be designed for the following operating conditions: the rectifier's ESCR varies from 6 to 8 and the inverter's ESCR varies from 6 to 8 with the nominal operating condition being rectifier's ESCR equal to 8 and inverter's ESCR equal to 8. The HVDC control system should be designed so as to maintain the 6dB stability margin for all frequencies."

5.2.2 Plant Templates and QFT Bounds

A fundamental element of the QFT design method is the generation of parametric uncertainty templates and the integration of these templates into the stability margin design bounds.

Fig. 5.5 illustrates the chosen templates (with regard to the parameter variations illustrated in Table 4.1) for the rectifier current control plant transfer function.
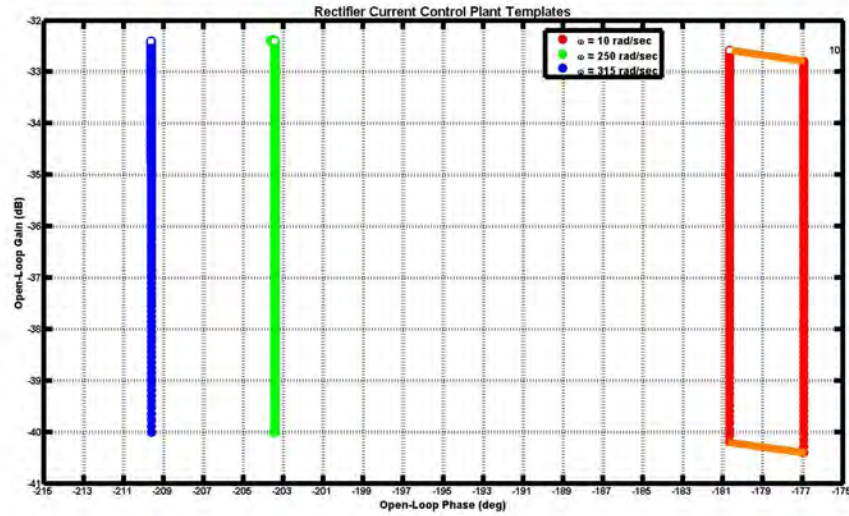
Figure 5.5: Rectifier Current Control Plant Templates

Fig. 5.6 illustrates how the stability margin is modified for nominal rectifier current control plant transfer function, according to parameter variations illustrated in Table 4.1.
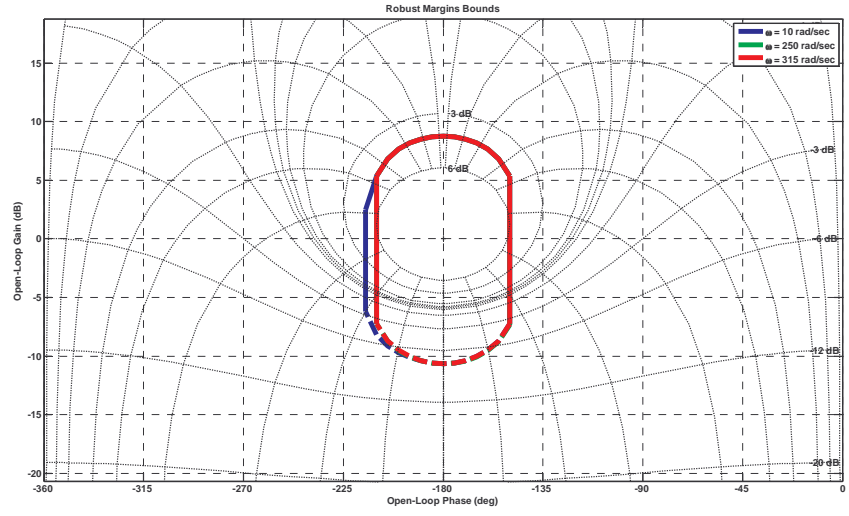
Figure 5.6: Rectifier Current Control QFT Bounds

Fig. 5.7 illustrates the chosen templates (with regard to the parameter variations illustrated in Table 4.2) for the inverter current control plant transfer function.
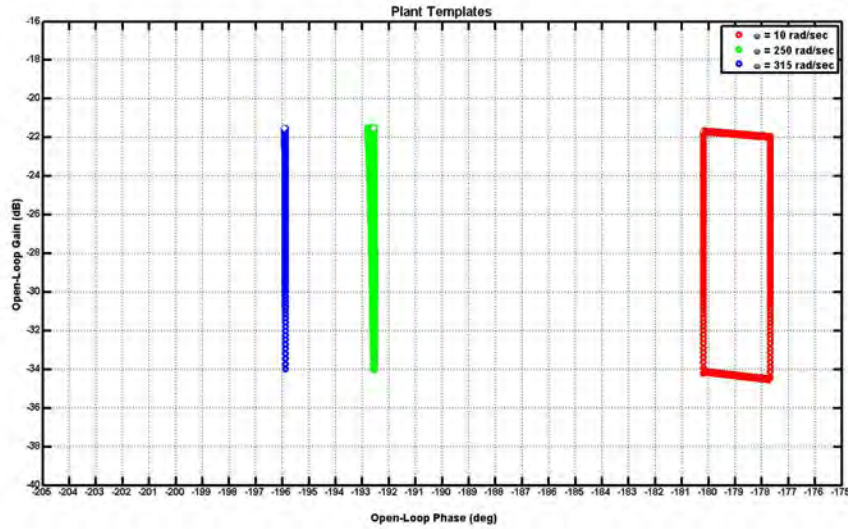
Figure 5.7: Inverter Current Control Plant Templates

Fig. 5.8 illustrates how the stability margin is modified for nominal inverter current control plant transfer function, according to parameter variations illustrated in Table 4.2.
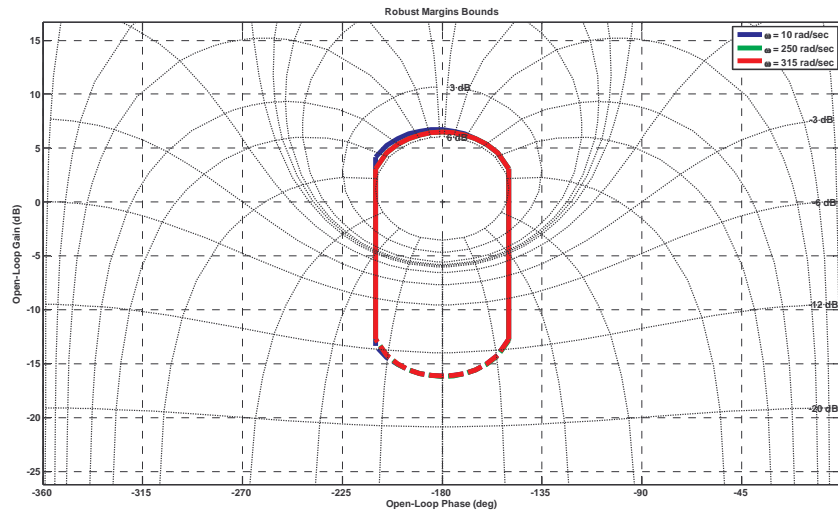
Figure 5.8: Inverter Current Control QFT Bounds

Fig. 5.9 illustrates the chosen templates (with regard to the parameter variations illustrated in Table 4.3) for the rectifier voltage control plant transfer function.
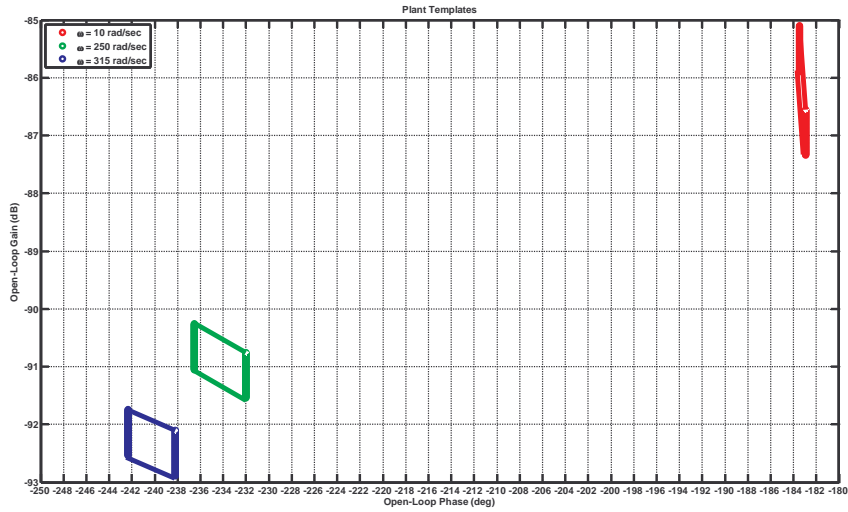
Figure 5.9: Rectifier Voltage Control Plant Templates

Fig. 5.10 illustrates how the stability margin is modified for nominal inverter current control plant transfer function, according to parameter variations illustrated in Table 4.3.
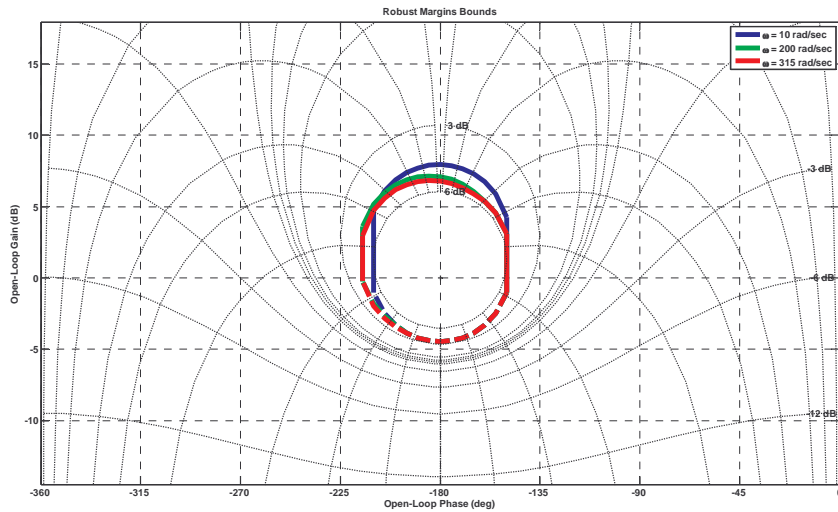
Figure 5.10: Rectifier Voltage Control QFT Bounds

The chosen templates (with regard to the parameter variations illustrated in Table 4.4) for the inverter voltage control plant transfer function were developed.

Fig. 5.11 illustrates how the stability margin is modified for nominal inverter current control plant transfer function, according to parameter variations illustrated in Table 4.4.
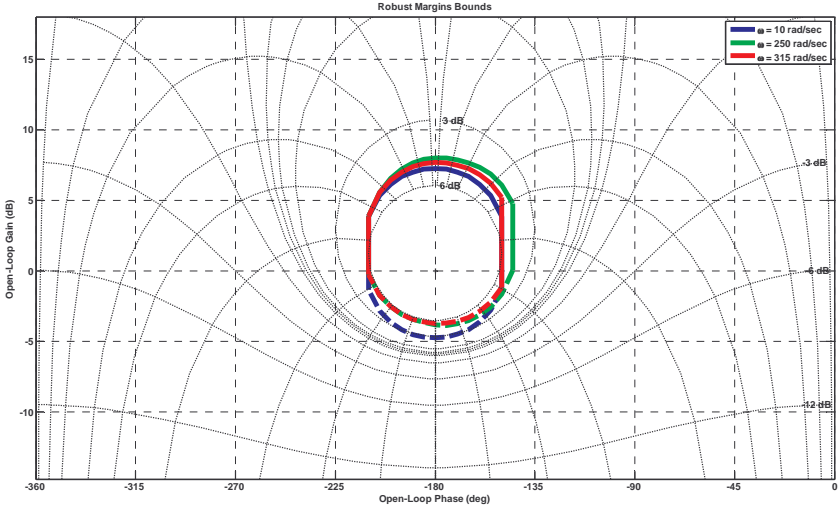
Figure 5.11: Inverter Voltage Control QFT Bounds

5.2.3 QFT Design of the HVDC Control System Parameters

Since the stability design bounds have been derived, the parameters of the LCC HVDC control system can be designed. The following high-to-low frequency QFT design method was used:

1. The maximum possible gain cross-over frequency ω_{gc} was determined from the non-minimum phase-lag properties of the plant. This gain cross-over frequency will be attempted to be achieved by applying a proportional gain.

2. Then the magnitude of the loop transfer function will be increased, for ω approaching zero, as fast as possible. This will be achieved by applying a first-order integral term.

Rectifier Current Controller Design

Analysis of Table 4.1, reveals that the largest time constant is 1.65msec, therefore the specifications for the Rectifier Current Controller are:

Overshoot $< 5\%$

Settling Time (t_s) < 24.75msec

Steady state error (δ) $< 2\%$

Gain Margin   < 6dB

The nominal rectifier current control plant is defined as:

$$P_{cr}(s) = e^{-1.65 \times 10^{-3} s} \left(\frac{-0.026s^3 - 3.424s^2 - 2351s - 9.732 \times 10^4}{s^3 + 132.7s^2 + 9.049 \times 10^4 s + 3.829 \times 10^6} \right)$$ (5.3.1)

The negative of this plant transfer function is plotted on Nichols Chart with the modified stability margin as shown in Fig. 5.12.
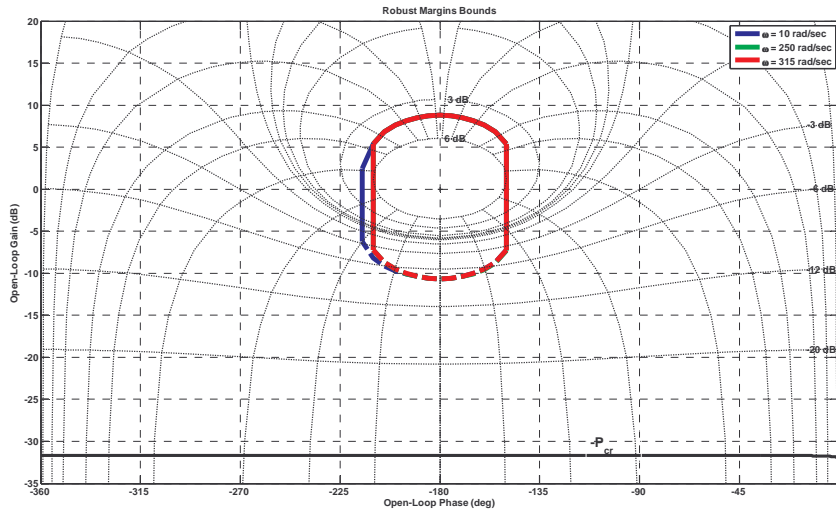
Figure 5.12: Nichols Plot of $-P_{cr}(s)$

To achieve the maximum possible gain cross-over frequency, the gain of the controller was increased, ie k=6.3. To further improve the low frequency performance, a low frequency modifying controller term $(1+\omega_c/s)$ was be used, with ω_c=1750 rad/s. The gain and the low-order controller term define the parameters of the PI controller:

$$G(s) = -6.3\left(1 + \frac{1750}{s}\right)$$ (5.3.2)

Equation (2.5.1) describes the actual controller parameters as:

$$G(s) = -\left(k_i.k_p + \frac{k_i}{s.T_i}\right)$$ (5.3.3)

Equating (5.3.2) and (5.3.3) gives:

$$\frac{k_i}{T_i} = 11025 \tag{5.3.4}$$
$$k_p . k_i = 6.3$$

Let T_i=1msec, this results in:

$$k_i = 11.025$$
$$k_p = 0.57 \tag{5.3.5}$$

The effect of the controller is displayed in Fig. 5.13, with the plot labelled G.P$_{cr}$.
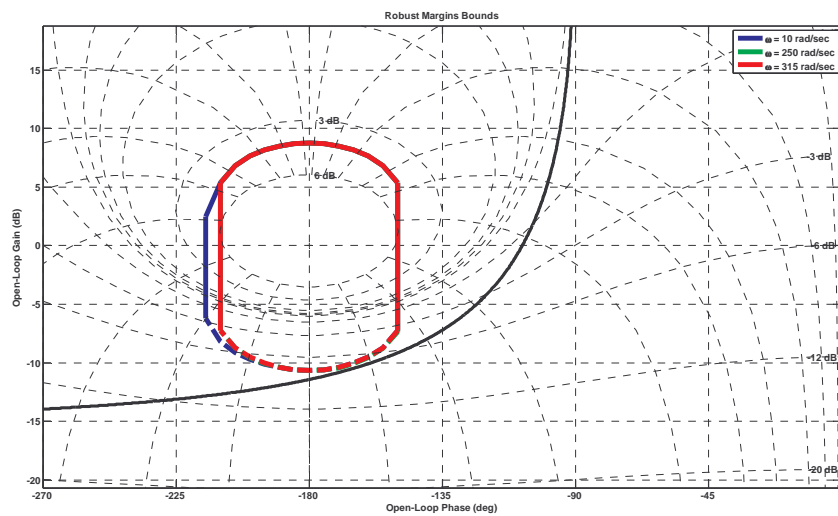
Figure 5.13: Influence of the designed PI controller on P$_{cr}$(s)

To verify the performance of the control system, the following scenario was simulated in PSCAD/EMTDC:

- The rectifier's ESCR was equal to 8
- The inverter's ESCR was equal to 8
- The HVDC system was configured so that the rectifier was in current control mode and the inverter was in voltage control mode.
- The inverter's firing angle was held constant at 138 degrees
- The rectifier's current controller's parameters were set according to equation (5.3.5)
- After the HVDC system is run to steady state, the dc current order was decreased by 5%.

The plant output response to the small signal transient is illustrated in Fig. 5.14.
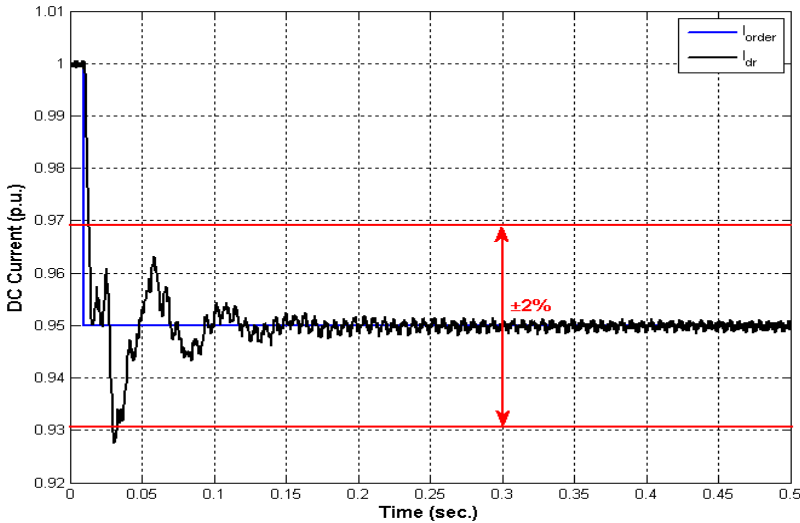
Figure 5.13: Rectifier DC Current Response

The control system performance is evaluated in Table 5.1, below :

Performance Criterion	Expected	Actual
Overshoot	5%	2.1%
Settling Time (t_s)	24.75msec	23msec
Steady state error (δ)	<2%	<0.1%
Gain Margin	<6dB	<6dB

Table 5.1: Rectifier Current Controller Performance Assessment

Table 5.1 clearly illustrates that the rectifier controller design did meet the specified performance requirements.

Inverter Current Controller Design

Analysis of Table 4.2, reveals that the largest time constant is 0.89msec. It should be noted that there exists a 1msec communication time delay with regard to the current order being processed at the rectifier station and then transmitted to the inverter station. Therefore the specifications for the Inverter Current Controller are:

Overshoot   < 5%

Settling Time (t_s)   < 28.35msec

Steady state error (δ) $< 2\%$

Gain Margin $< 6\text{dB}$

The nominal rectifier current control plant is defined as:

$$P_{ci}(s) = e^{-0.89 \times 10^{-3} s} \left(\frac{-0.02s^3 - 2.478s^2 - 1676s - 6.535 \times 10^4}{s^3 + 124.9s^2 + 8.388 \times 10^4 s + 3.348 \times 10^6} \right)$$

(5.3.6)

The negative of this plant transfer function is plotted on Nichols Chart with the modified stability margin as shown in Fig. 5.15.
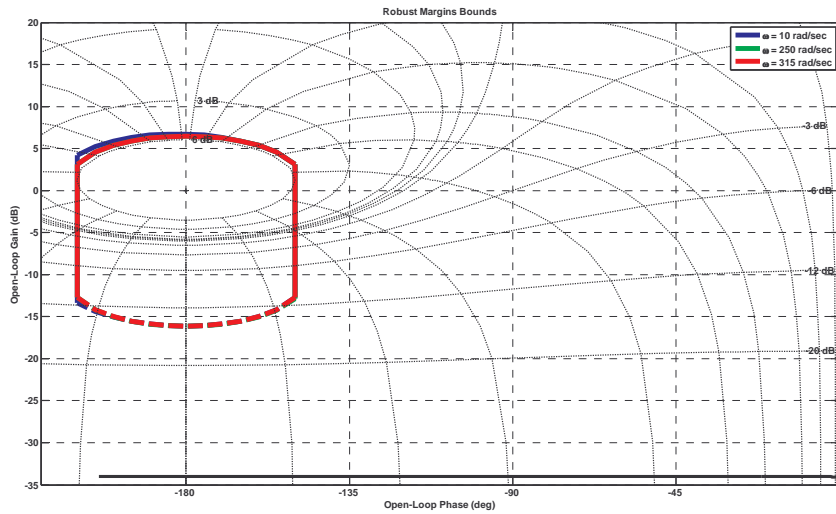
Figure 5.15: Nichols Plot of –P$_{ci}$(s)

To achieve the maximum possible gain cross-over frequency, the gain of the controller was increased, ie k=5.62. To further improve the low frequency performance, a low frequency modifying controller term $(1+\omega_c/s)$ was be used, with ω_c=2400 rad/s. The gain and the low-order controller term define the parameters of the PI controller:

$$G(s) = -5.62\left(1 + \frac{2400}{s}\right)$$

(5.3.7)

Equation (2.5.1) describes the actual controller parameters as:

$$G(s) = -\left(k_i.k_p + \frac{k_i}{s.T_i} \right)$$

(5.3.8)

Equating (5.3.7) and (5.3.8) gives:

$$\frac{k_i}{T_i} = 13488$$

$$k_p.k_i = 5.62$$

(5.3.9)

Let T_i=1msec, this results in:

$$k_i = 13.5$$

$$k_p = 0.417$$

(5.3.10)

The effect of the controller is displayed in Fig. 5.16, with the plot labelled G.P$_{ci}$.
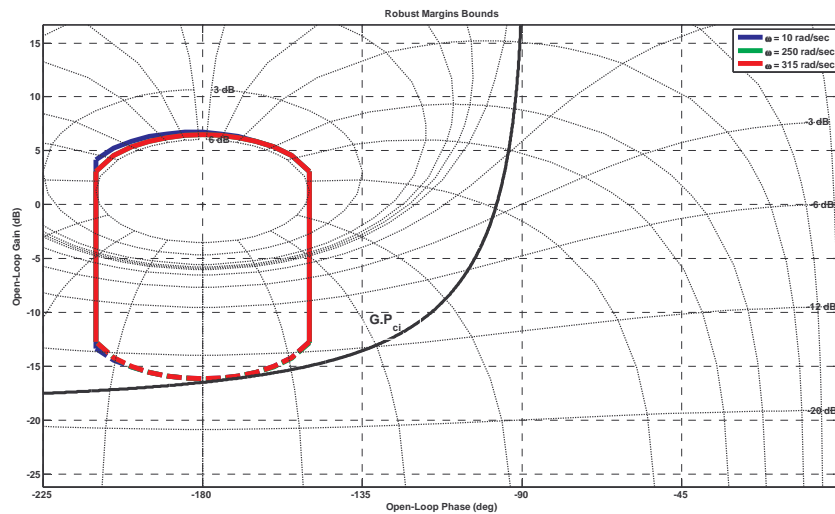
Figure 5.16: Influence of the designed PI controller on P$_{ci}$(s)

To verify the performance of the control system, the following scenario was simulated in PSCAD/EMTDC:

- The rectifier's ESCR was equal to 8
- The inverter's ESCR was equal to 8
- The HVDC system was configured so that the inverter was in current control mode and the rectifier was in voltage control mode.
- The rectifier's firing angle was held constant at 27 degrees
- The inverter's current controller's parameters were set according to equation (5.3.10)

- After the HVDC system is run to steady state, the dc current order was decreased by 5%.

The plant output response to the small signal transient is illustrated in Fig. 5.17.
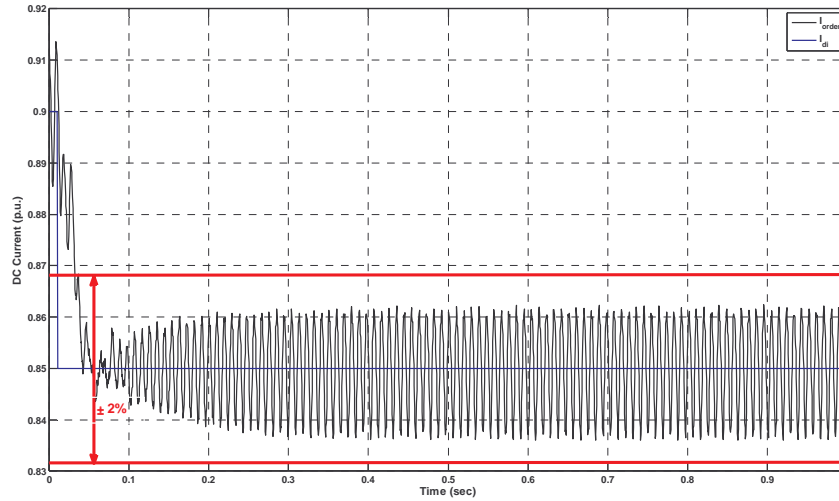
Figure 5.17: Inverter DC Current Response

The control system performance is evaluated in Table 5.2, below :

Performance Criterion	Expected	Actual
Overshoot	5%	1.3%
Settling Time (t_s)	28.35msec	23msec
Steady state error (δ)	<2%	<1.3%
Gain Margin	<6dB	<6dB

Table 5.2: Inverter Current Controller Performance Assessment

Table 5.2 clearly illustrates that the rectifier controller design does meet the specified performance requirements.

Rectifier Voltage Controller Design

The nominal rectifier voltage control plant is defined as:

$$P_{vr}(s) = \frac{-0.0084}{s+165.3} \qquad (5.3.11)$$

This plant transfer function is plotted on Nichols Chart with the modified stability margin as shown in Fig. 5.18.
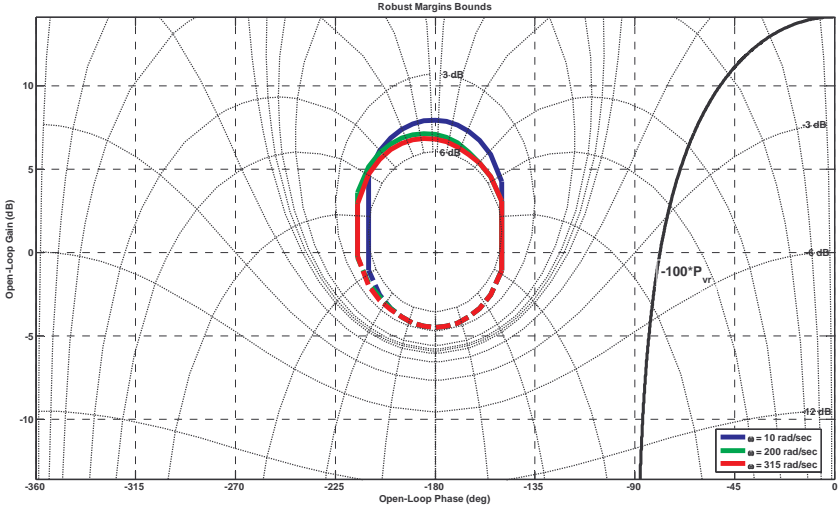
Figure 5.18: Nichols Plot of -100*P$_{vr}$(s)

Please note that plant transfer function was multiplied by -100 purely to improve the perspective of the illustration and does not indicate the controller that was designed. Analysis of Section 2.5 reveals that the control implementation does not facilitate the inclusion of a controller function. Therefore no controller was designed for this plant transfer function.

Inverter Voltage Controller Design

The nominal inverter voltage control plant is defined as:

$$P_{vi}(s) = \frac{-0.0324}{s^2 + 59.9s + 3.159 \times 10^4} e^{-.78 \times 10^{-3}.s} \qquad (5.3.12)$$

This plant transfer function is plotted on Nichols Chart with the modified stability margin as shown in Fig. 5.19.
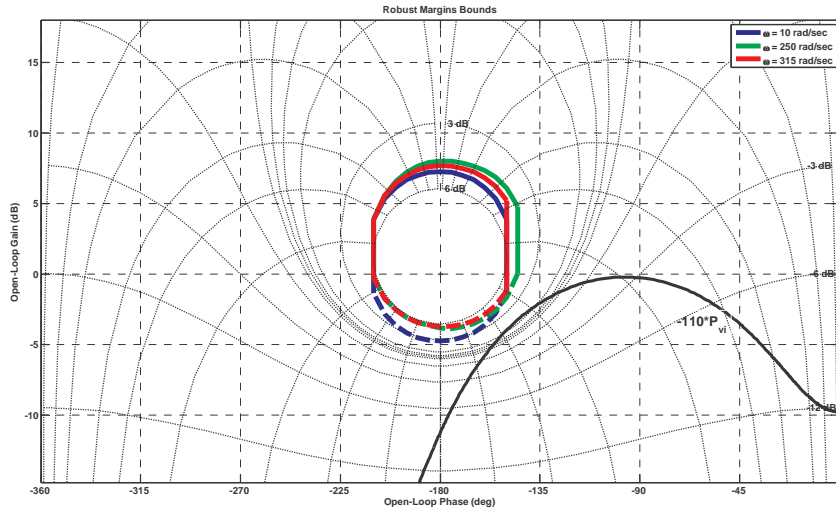
Figure 5.19: Nichols Plot of -110*P_{vi}(s)

Please note that plant transfer function was multiplied by -110 purely to improve the perspective of the illustration and does not indicate the controller that was designed. Analysis of Section 2.5 reveals that the control implementation does not include a controller function. Therefore no controller was designed for this plant transfer function.

5.3 Validation of HVDC Control System Design

The design of the HVDC control system has been sectionalized into separate design and analysis of four control systems that constitute the LCC HVDC control system. The design and analysis of the complete LCC HVDC control system was validated by integrating the four control systems as illustrated in Fig. 5.20.
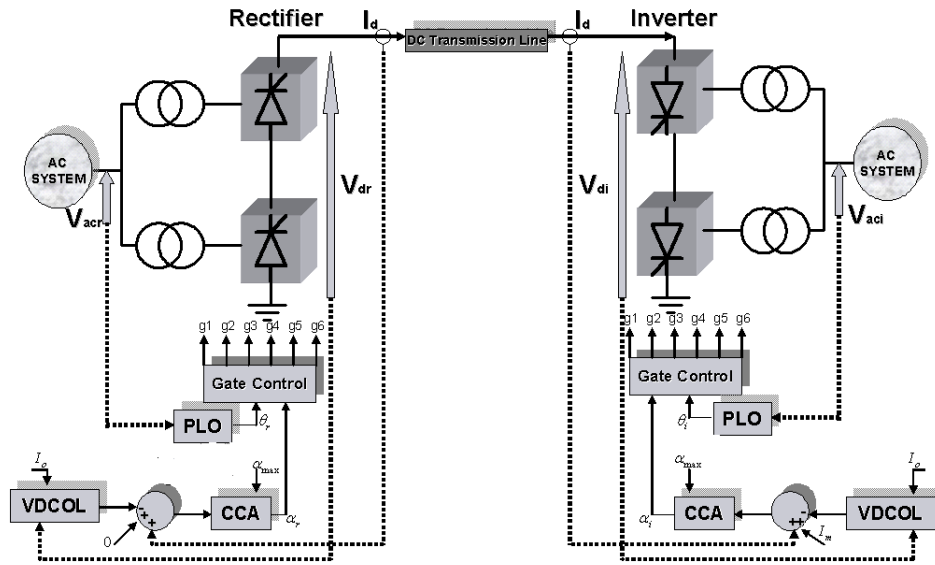
Figure 5.20: LCC HVDC Control System

The stability of the integrated LCC HVDC system was verified by simulating the following scenario in PSCAD/EMTDC:

- The rectifier's ESCR was equal to 8
- The inverter's ESCR was equal to 8
- The firing angle of the inverter station is deblock first at $t_o = 10ms$.
- The rectifier's firing angle is then deblocked at $t_1 = 50ms$ and then ramped up
- The rectifier's current controller's parameters were set according to equation (5.3.5)
- The inverter's current controller's parameters were set according to equation (5.3.10)

The start-up response of the integrated LCC HVDC system is illustrated in Fig. 5.21.
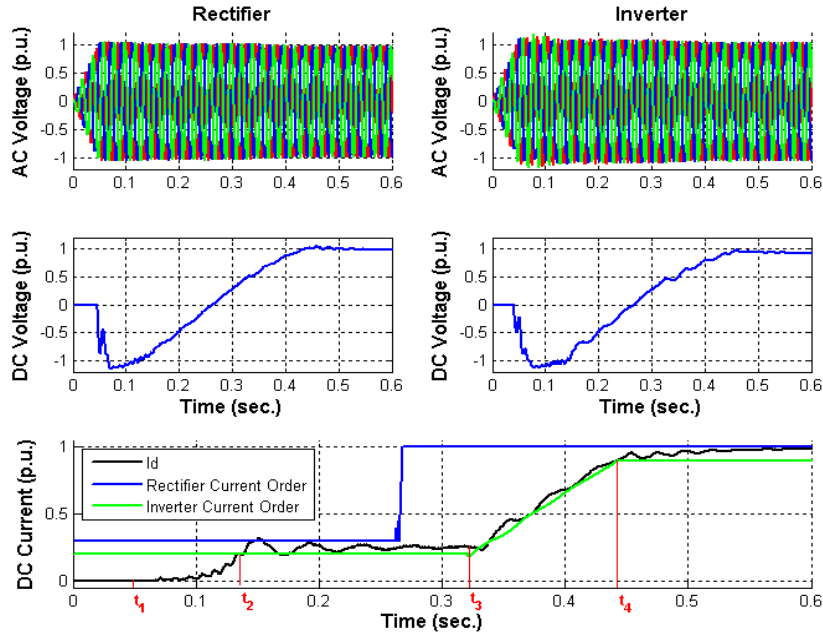
Figure 5.21: Start-up Response of the LCC HVDC System

Analysis of start-up response reveals that the dc current increases after t_1. Between time t_3 and t_2, the dc voltage has not increased above the minimum required dc voltage (0.2 p.u.) as specified by the VDCOL, therefore the current order is constrained to the minimum current order (Rectifier – 0.3 p.u. and Inverter – 0.2 p.u.) as defined by the VDCOL. During this period of time, the designed LCC HVDC control system ensures that LCC HVDC system operates stably and according to the requirements of the VDCOL.

Between time t_4 and t_3, the dc voltage increases above the minimum required dc voltage and the current order is determined by the inverter VDCOL. During this period of time, the designed LCC HVDC control system ensures that LCC HVDC system operates stably and according to the requirements of the inverter VDCOL.

After time t_4, the inverter receives more current than is ordered therefore the current control moves to the rectifier station. During this current control transitional period, the designed LCC HVDC control system ensures that the LCC HVDC system operates stably and according to the requirements of the rectifier current control amplifier.

5.4 Conclusions

A LCC HVDC control system design method based on Quantitative Feedback Theory (QFT) has been presented. This control system design method was used to design the rectifier and inverter current controllers for the LCC HVDC system whose parameters are defined by Table 4.1 to Table 4.4. The designed current controllers individually achieved the specified performance specifications.

The stability of the integrated LCC HVDC control system was verified by simulating the start-up of a LCC HVDC system with the rectifier ac system's ESCR=8 and the inverter ac system's ESCR=8. The results revealed that the designed LCC HVDC control system does ensure a stable start-up process, thus preliminarily validating the design method.

Due to the uncertain nature of the state of power systems, the conditions defining the operating point of the LCC HVDC system vary. The ability of the designed LCC HVDC control system to remain stable during these operating condition variations is categorized as the "Transient Stability of the LCC HVDC System". This topic is covered in detail in the next chapter.

Chapter 6

Transient Analysis of LCC HVDC Control Systems

6.1 Introduction

In the previous chapter, the LCC HVDC control system parameters were designed. During the design process, consideration was given to plant transfer function parameter variations and the performance specifications. In this chapter, the transient stability of the designed LCC HVDC system, illustrated in Fig. 6.1, is evaluated for varying operating conditions. Transient analysis of an HVDC system provides insight into the interactions between the ac and dc systems.
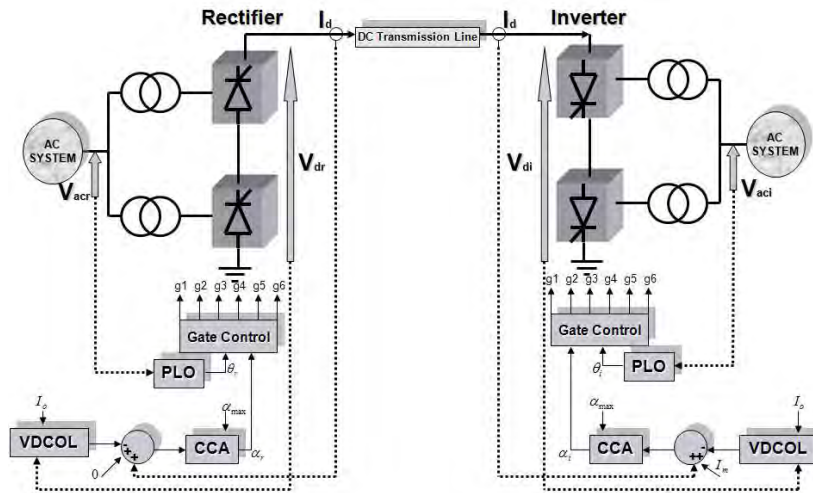
Figure 6.1: Designed LCC HVDC Control System

During the transient stability analysis, the rectifier and inverter ac systems' effective short circuit ratios were varied and the LCC HVDC system responses for the following small disturbances were analysed:

- Start-up response
- Step decrease (5%) in the rectifier ac system voltage
- Step increase (5%) in the rectifier ac system voltage
- Step decrease (5%) in the inverter ac system voltage
- Step increase (5%) in the inverter ac system voltage

6.2 Start-Up Response

To evaluate the start-up responses for varying ac system operating conditions, the LCC HVDC system, shown in Fig. 6.1, was simulated the following scenarios in PSCAD/EMTDC:

- The rectifier's ESCR was varied from 8 to 6
- The inverter's ESCR was varied from 8 to 6
- The firing angle of the inverter station is deblock first at $t_o = 10ms$.
- The rectifier's firing angle is then deblocked at $t_1 = 50ms$ and then ramped up
- The rectifier's current controller's parameters were set according to equation (5.3.5)
- The inverter's current controller's parameters were set according to equation (5.3.10)

A sample of the LCC HVDC system start-up response is illustrated in Fig. 6.2, for the rectifier ac system ESCR=8 and the inverter ac system ESCR=6.
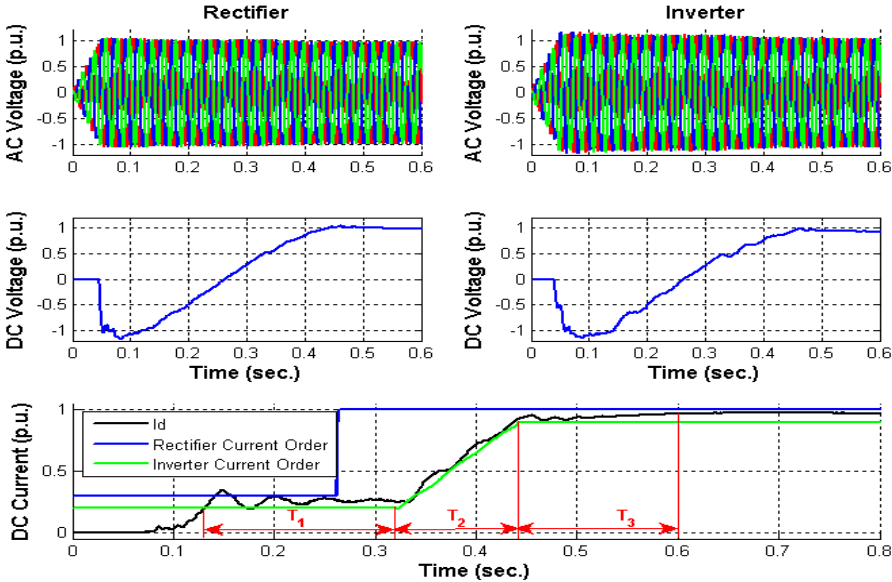
Figure 6.2: Sample of LCC HVDC System Start-up Response

The detailed summary of the LCC HVDC system start-up responses for varying ac system conditions is illustrated in Table 6.1.

Rectifier	Inverter	Characteristics			
ESCR	ESCR	O.S[1] (%)	t_s[2] (msec)	Error[3](%)	Stable
8	8	184	122	1.18	Yes
6	8	181	121	1.20	Yes
8	6	190	123	1.23	Yes
6	6	187	122	1.25	Yes

Table 6.1: Analytical Summary of LCC HVDC System Start-Up Responses

Analysis of start-up responses reveals that the designed LCC HVDC control system ensures that LCC HVDC system is operates stably for varying ac system conditions.

6.3 Stepped Decrease in Rectifier AC Voltage

To evaluate the LCC HVDC system responses to a 5% stepped decrease in the rectifier ac system voltage, for varying ac system operating conditions, the LCC HVDC system, shown in Fig. 6.1, was simulated the following scenarios in PSCAD/EMTDC:

- The rectifier's ESCR was varied from 8 to 6
- The inverter's ESCR was varied from 8 to 6
- The rectifier's current controller's parameters were set according to equation (5.3.5)
- The inverter's current controller's parameters were set according to equation (5.3.10)
- After the LCC HVDC system is run to steady state, at $t_1 = 10ms$, the rectifier's ac system voltage is decreased by 5%.
- At $t_2 = 0.3\sec$, the current order is decreased by 5%.

A sample of the LCC HVDC system response to a stepped decrease in the rectifier ac system's voltage is illustrated in Fig. 6.3, for the rectifier ac system ESCR=8 and the inverter ac system ESCR=6.

---

[1] Overshoot
[2] Settling Time
[3] Steady State Error
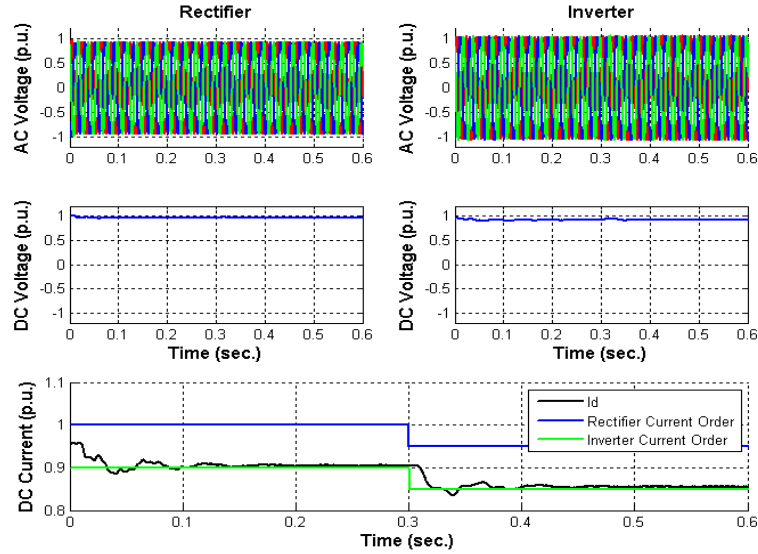
Figure 6.3: Sample of LCC HVDC System Response to a stepped decrease in the rectifier ac system's voltage

The detailed summary of the LCC HVDC system responses to a stepped decrease in the rectifier ac system's voltage for varying ac system conditions is illustrated in Table 6.2.

Constant Current Order					
Rectifier ESCR	Inverter ESCR	Characteristics			
		O.S (%)	t_s (msec)	Error (%)	Stable
8	8	1.2	43	0.6	Yes
6	8	1.3	22	0.5	Yes
8	6	2.1	49	0.4	Yes
6	6	2.0	28	0.5	Yes
5% Step Decrease in Current Order					
Rectifier ESCR	Inverter ESCR	Characteristics			
		O.S (%)	t_s (msec)	Error (%)	Stable
8	8	1.6	21	0.5	Yes
6	8	1.6	19	0.6	Yes
8	6	1.9	16	0.6	Yes
6	6	1.9	15	0.6	Yes

Table 6.2: Analytical Summary of LCC HVDC System Responses to stepped a decrease in the rectifier ac system's voltage

Analysis of LCC HVDC system responses reveals that the designed LCC HVDC control system ensures that LCC HVDC system operates stably for varying ac system conditions.

6.4 Stepped Increase in Rectifier AC Voltage

To evaluate the LCC HVDC system responses to a 5% stepped increase in the rectifier ac system voltage, for varying ac system operating conditions, the LCC HVDC system, shown in Fig. 6.1, was simulated the following scenarios in PSCAD/EMTDC:

- The rectifier's ESCR was varied from 8 to 6
- The inverter's ESCR was varied from 8 to 6
- The rectifier's current controller's parameters were set according to equation (5.3.5)
- The inverter's current controller's parameters were set according to equation (5.3.10)
- After the LCC HVDC system is run to steady state, at $t_1 = 10ms$, the rectifier's ac system voltage is increased by 5%.
- At $t_2 = 0.3\sec$, the current order is decreased by 5%.

A sample of the LCC HVDC system response to a stepped increase in the rectifier ac system's voltage is illustrated in Fig. 6.4, for the rectifier ac system ESCR=8 and the inverter ac system ESCR=6.
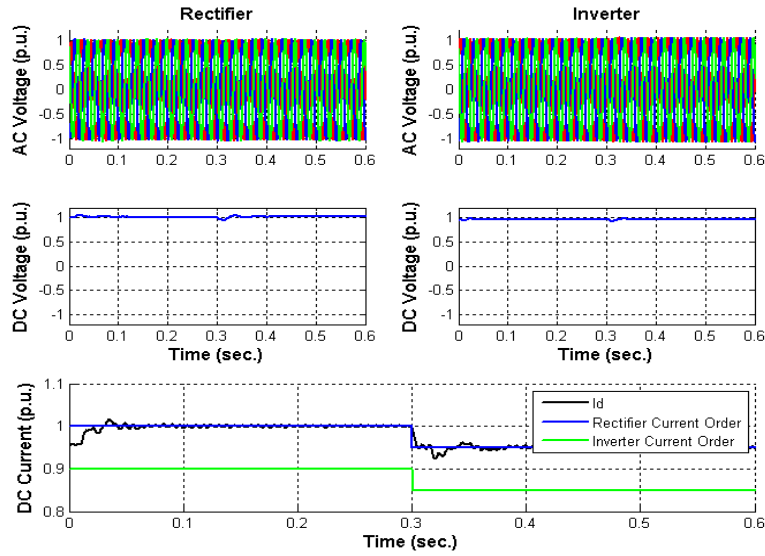
Figure 6.4: Sample of LCC HVDC System Response to a stepped increase in the rectifier ac system's voltage

The detailed summary of the LCC HVDC system responses to a stepped increase in the rectifier ac system's voltage for varying ac system conditions is illustrated in Table 6.3.

Constant Current Order					
Rectifier	**Inverter**	**Characteristics**			
ESCR	**ESCR**	**O.S (%)**	**t_s (msec)**	**Error (%)**	**Stable**
8	8	1.8	20	0.3	Yes
6	8	1.8	32	3.5	Yes
8	6	1.6	25	0.3	Yes
6	6	1.2	29	1.7	Yes
5% Step Decrease in Current Order					
Rectifier	**Inverter**	**Characteristics**			
ESCR	**ESCR**	**O.S (%)**	**t_s (msec)**	**Error (%)**	**Stable**
8	8	3.1	23	0.2	Yes
6	8	5.1	29	4.0	Yes
8	6	2.9	23	0.3	Yes
6	6	3.2	29	2.2	Yes

Table 6.3: Analytical Summary of LCC HVDC System Responses to stepped increase in the rectifier ac system's voltage

Analysis of LCC HVDC system responses reveals that the designed LCC HVDC control system ensures that LCC HVDC system operates stably for varying ac system conditions.

6.5 Stepped Decrease in Inverter AC Voltage

To evaluate the LCC HVDC system responses to a 5% stepped decrease in the inverter ac system voltage, for varying ac system operating conditions, the LCC HVDC system, shown in Fig. 6.1, was simulated the following scenarios in PSCAD/EMTDC:

- The rectifier's ESCR was varied from 8 to 6
- The inverter's ESCR was varied from 8 to 6
- The rectifier's current controller's parameters were set according to equation (5.3.5)
- The inverter's current controller's parameters were set according to equation (5.3.10)
- After the LCC HVDC system is run to steady state, at $t_1 = 10ms$, the inverter's ac system voltage is decreased by 5%.
- At $t_2 = 0.3\sec$, the current order is decreased by 5%.

A sample of the LCC HVDC system response to a stepped decrease in the inverter ac system's voltage is illustrated in Fig. 6.5, for the rectifier ac system ESCR=8 and the inverter ac system ESCR=6.
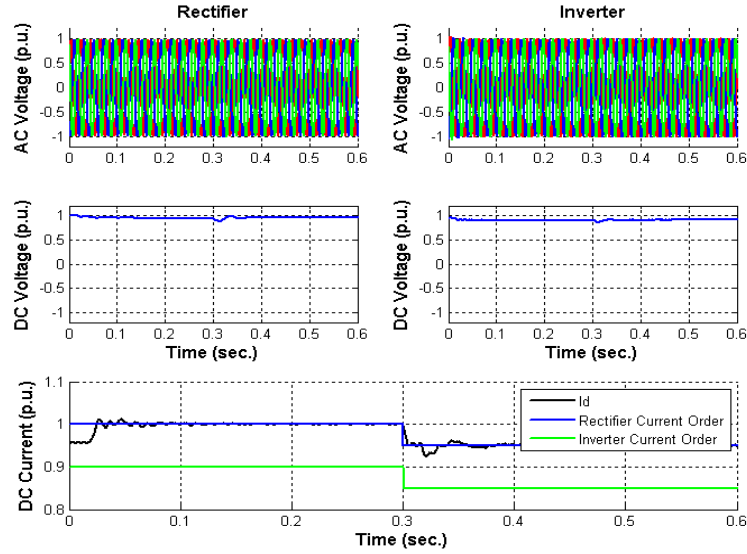
Figure 6.5: Sample of LCC HVDC System Response to a stepped decrease in the
inverter ac system's voltage

The detailed summary of the LCC HVDC system responses to a stepped decrease in
the inverter ac system's voltage for varying ac system conditions is illustrated in
Table 6.4.

Constant Current Order					
Rectifier	**Inverter**	**Characteristics**			
ESCR	**ESCR**	**O.S (%)**	**t_s (msec)**	**Error (%)**	**Stable**
8	8	2.7	27	0.1	Yes
6	8	1.8	26	0.8	Yes
8	6	1.3	37	0.1	Yes
6	6	1.8	38	0.5	Yes
5% Step Decrease in Current Order					
Rectifier	**Inverter**	**Characteristics**			
ESCR	**ESCR**	**O.S (%)**	**t_s (msec)**	**Error (%)**	**Stable**
8	8	2.7	24	0.1	Yes
6	8	3.6	25	1.7	Yes
8	6	2.7	23	0.1	Yes
6	6	4.0	31	1.5	Yes

Table 6.4: Analytical Summary of LCC HVDC System Responses to stepped a
decrease in the inverter ac system's voltage

Analysis of LCC HVDC system responses reveals that the designed LCC HVDC control system ensures that LCC HVDC system operates stably for varying ac system conditions.

6.6 Stepped Increase in Inverter AC Voltage

To evaluate the LCC HVDC system responses to a 5% stepped increase in the inverter ac system voltage, for varying ac system operating conditions, the LCC HVDC system, shown in Fig. 6.1, was simulated the following scenarios in PSCAD/EMTDC:

- The rectifier's ESCR was varied from 8 to 6
- The inverter's ESCR was varied from 8 to 6
- The rectifier's current controller's parameters were set according to equation (5.3.5)
- The inverter's current controller's parameters were set according to equation (5.3.10)
- After the LCC HVDC system is run to steady state, at $t_1 = 10ms$, the inverter's ac system voltage is increased by 5%.
- At $t_2 = 0.3\sec$, the current order is decreased by 5%.

A sample of the LCC HVDC system response to a stepped increase in the inverter ac system's voltage is illustrated in Fig. 6.6, for the rectifier ac system ESCR=8 and the inverter ac system ESCR=6.
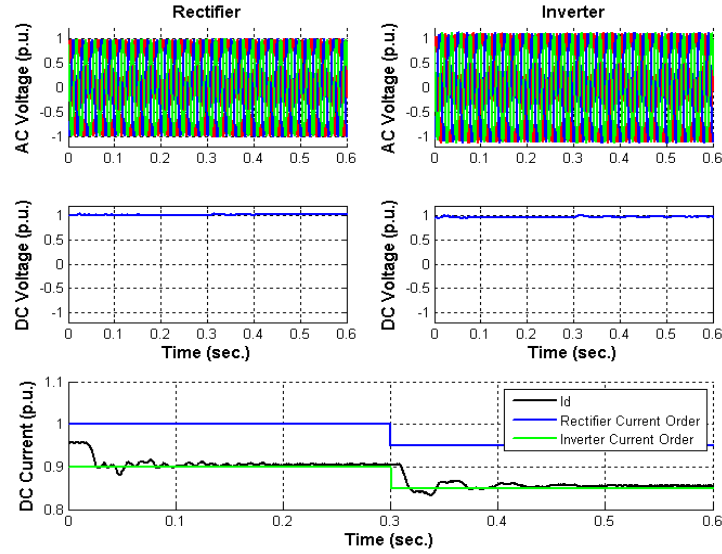
Figure 6.6: Sample of LCC HVDC System Response to a stepped increase in the
inverter ac system's voltage

The detailed summary of the LCC HVDC system responses to a stepped increase in
the inverter ac system's voltage for varying ac system conditions is illustrated in
Table 6.5.

Constant Current Order					
Rectifier	**Inverter**	**Characteristics**			
ESCR	**ESCR**	**O.S (%)**	**t_s (msec)**	**Error (%)**	**Stable**
8	8	1.7	44	0.6	Yes
6	8	2.0	67	0.6	Yes
8	6	2.0	38	0.7	Yes
6	6	2.4	68	0.6	Yes
5% Step Decrease in Current Order					
Rectifier	**Inverter**	**Characteristics**			
ESCR	**ESCR**	**O.S (%)**	**t_s (msec)**	**Error (%)**	**Stable**
8	8	1.7	21	0.6	Yes
6	8	1.8	18	0.7	Yes
8	6	2.1	15	0.8	Yes
6	6	2.0	37	0.7	Yes

Table 6.5: Analytical Summary of LCC HVDC System Responses to stepped
increase in the inverter ac system's voltage

Analysis of LCC HVDC system responses reveals that the designed LCC HVDC control system ensures that LCC HVDC system operates stably for varying ac system conditions.

6.7 Small Signal Stability Analysis

Small signal stability is defined as the ability of the LCC HVDC system to maintain stability following a small disturbance. The small signal stability behaviour of the designed closed loop LCC HVDC control system was obtained by applying a small step output disturbance using MATLAB Control Systems Toolbox. To valid these results, the designed closed loop LCC HVDC system illustrated in Fig. 6.7 was simulated in PSCAD/EMTDC.
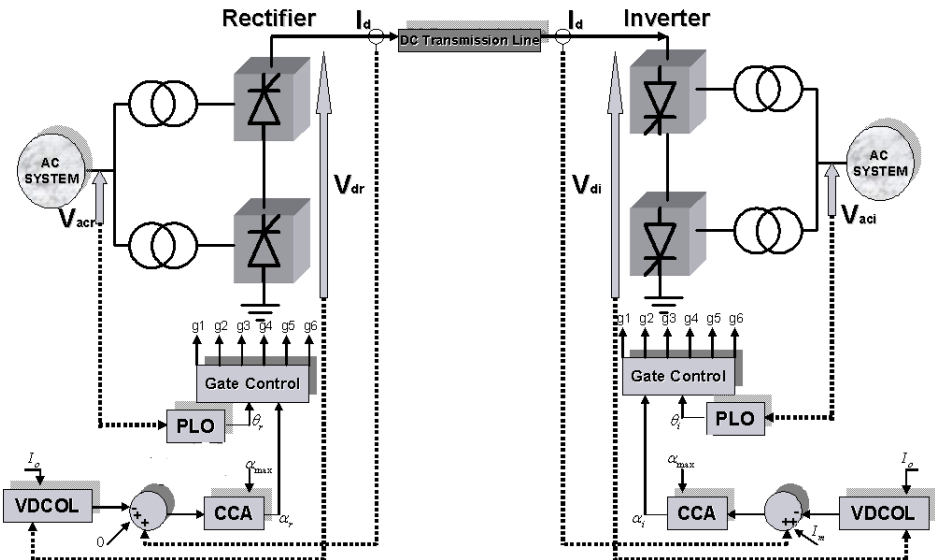
Figure 6.7: Designed Closed Loop LCC HVDC System

Section 2.4 illustrated that there are 2 definitive modes of operation of the LCC HVDC system. These definitive operational modes are explicitly described as:

1. Rectifier in Current Control and the Inverter in Voltage Control
2. Rectifier in Voltage Control and the Inverter in Current Control

Therefore the small signal stability behaviour of the designed closed loop LCC HVDC control system was analysed for the above two scenarios. The rectifier effective short circuit ratio was chosen to be 4 and the inverter effective short circuit ratio was chosen to be 6.

Scenario 1: Rectifier in Current Control and Inverter in Voltage Control

For this scenario, the control system illustrated in Fig. 6.8, determines the small signal behaviour of the dc current. The parameters for the rectifier current control plant transfer function (equation 4.3.1) were obtained Table 4.1.
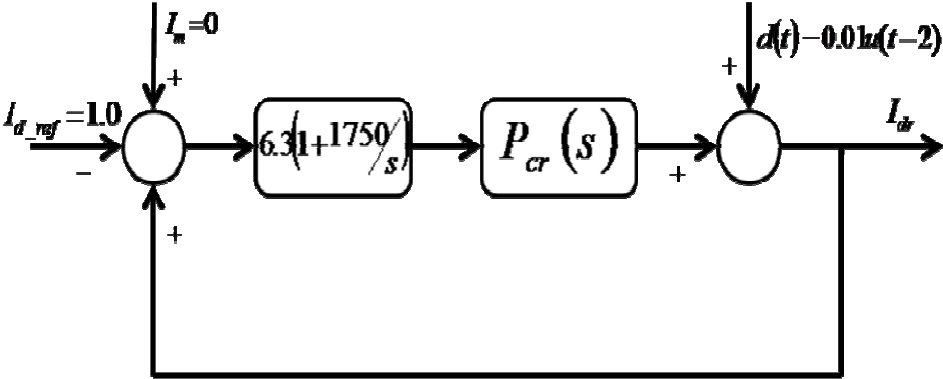
Figure 6.8: Rectifier Current Control Loop

The solution for the roots of the closed loop system is illustrated in Table 6.6. Table 6.6 show that all the closed loop poles reside in the left hand s-plane, thereby illustrating the unconditional stability of the LCC HVDC system. The lightly damped complex conjugate pole pair at -21.4±273i indicates the response will contain approximately a 43Hz oscillation.

Eigenvalue	Frequency (Hz)
-20.3	-
-21.40 + 273i	43.45
-21.40 - 273i	43.45
-205	-

Table 6.6: Eigenvalue Analysis for Rectifier Current Control Closed Loop System

The small signal stability behaviour of the designed rectifier current control loop (Fig. 6.8) was obtained by applying a small (1%) step output disturbance at t = 2.0 seconds using MATLAB Control Systems Toolbox. The same scenario was simulated in PSCAD/EMTDC. The small signal stability behaviour results are illustrated in Fig. 6.9. The results clearly that the MATLAB model results and PSCAD/EMTDC simulation results both concur that the LCC HVDC system is stable which is in agreement with the results and analysis of Table 6.6.
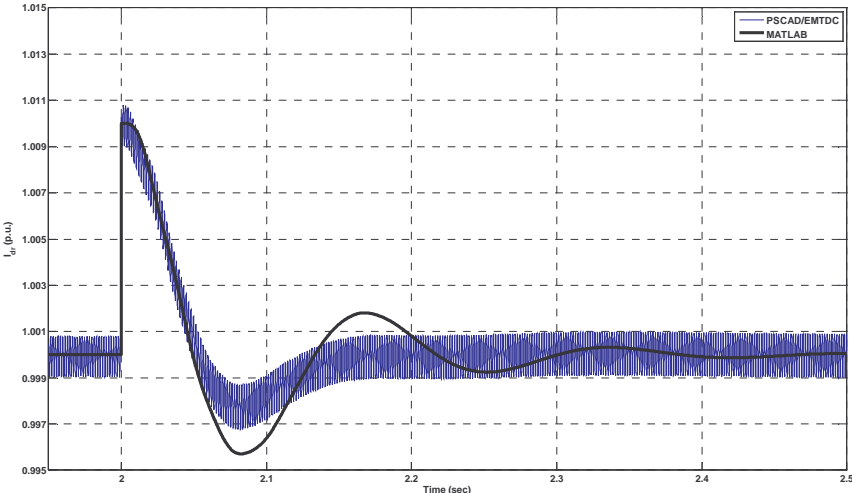
Figure 6.9: Rectifier DC Current Small Signal Behaviour

The small signal results compare favourably two each other with the approximate 43Hz frequency effect apparent in both the MATLAB model and the PSCAD/EMTDC simulation. The PSCAD/EMTDC simulation results do illustrate increased damping as compared the MATLAB model. The origin and reasons for the increased damping will be considered as an area for further research and will not be treated any further in this study.

Scenario 2: Inverter in Current Control and Rectifier in Voltage Control

For this scenario, the control system illustrated in Fig. 6.10, determines the small signal behaviour of the dc current. The parameters for the inverter current control plant transfer function (equation 4.4.1) were obtained Table 4.2.
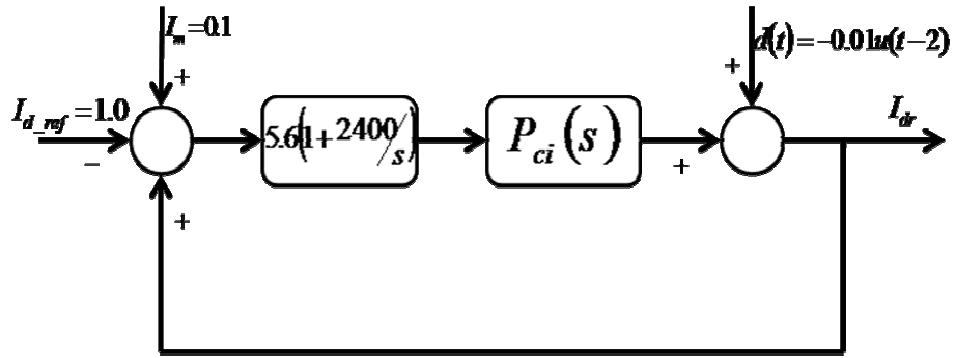
Figure 6.10: Inverter Current Control Loop

The solution for the roots of the closed loop system is illustrated in Table 6.7. Table 6.7 show that all the closed loop poles reside in the left hand s-plane, thereby illustrating the unconditional stability of the LCC HVDC system. The lightly damped complex conjugate pole pair at -22+268i indicates the response will contain approximately a 43Hz oscillation.

Eigenvalue	Frequency (Hz)
-21.1	-
-22.10 + 268i	42.8
-22.10 - 268i	42.8
-244	-

Table 6.7: Eigenvalue Analysis for Inverter Current Control Closed Loop System

The small signal stability behaviour of the designed rectifier current control loop (Fig. 6.10) was obtained by applying a small (1%) step output disturbance at t = 2.0 seconds using MATLAB Control Systems Toolbox. The same scenario was simulated in PSCAD/EMTDC. The small signal stability behaviour results are illustrated in Fig. 6.11. The results clearly that the MATLAB model results and PSCAD/EMTDC simulation results both concur that the LCC HVDC system is stable which is in agreement with the results and analysis of Table 6.7.
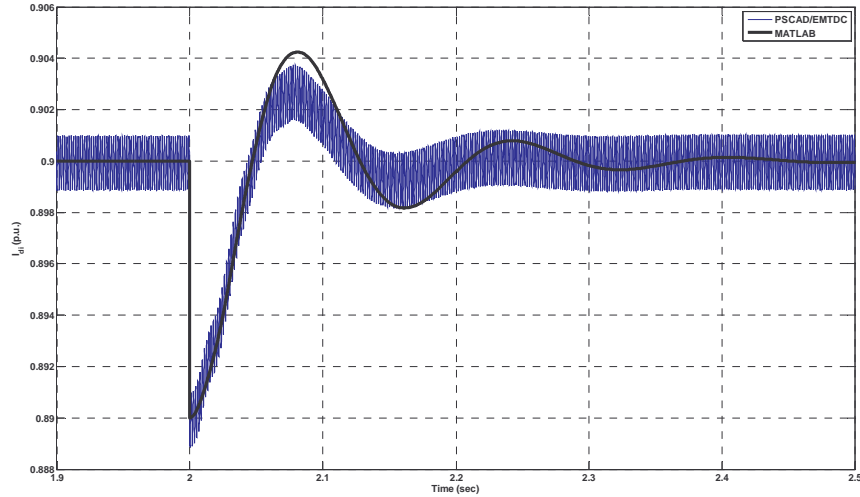
Figure 6.11: Inverter DC Current Small Signal Behaviour

The small signal results compare favourably two each other with the approximate 43Hz frequency effect apparent in both the MATLAB model and the PSCAD/EMTDC simulation. The PSCAD/EMTDC simulation results do illustrate increased damping as compared the MATLAB model. The origin and reasons for the increased damping will be considered as an area for further research and will not be treated any further in this study.

6.8 Conclusions

In the previous chapter, the QFT control system design method was used to design the rectifier and inverter current controllers for the LCC HVDC system whose parameters are defined by Table 4.1 to Table 4.2. In this chapter, the stability of the integrated LCC HVDC control system was verified by simulating the start-up and step responses of the LCC HVDC system with the rectifier ac system's ESCR varying from 8 to 6 and the inverter ac system's ESCR varying from 8 to 6.

The stable start-up and step responses of the LCC HVDC system, for varying ac system conditions, and the prediction of small signal stability conclusively validate the novel derived HSR equations and the QFT design method.

Chapter 7

Conclusions

7.1 Conclusions

This thesis illustrated that classical control theory can be used design the LCC HVDC control system.

Chapter 2 presented a detailed overview of the LCC HVDC control systems. The different fundamental topologies of LCC HVDC transmission systems were illustrated. From the illustrations, it is evident that only monopolar LCC HVDC systems need to be investigated for control system studies. A mathematical analysis of the converter operation and the associated LCC HVDC control system was also described. Chapter 2 concluded by illustrating the practical implementation of the mathematical concepts that describe the LCC HVDC control system.

In Chapter 3, novel HVDC step response (HSR) equation were developed for LCC HVDC systems. The inductive modeling technique used to derive the HSR equations was based on the PSCAD/EMTDC application of "Jacobian Linearization". Subsequently the time domain characterised equations were derived to describe the step responses of the LCC HVDC system. Based on the derived characterised time domain responses, the following plant transfer functions were calculated:

1. Rectifier Current Control plant transfer function:

$$P_{cr}(s) = \frac{\Delta I_d}{\Delta \alpha} . e^{-s.T_o} \left(\frac{s^3 + (3a-1)s^2 + \left(3a^2 - 2a + w^2 + k|\Delta I_d|w\right)s + \left(a^3 - a^2 + aw^2 - w^2 + k|\Delta I_d|aw\right)}{(s+a)\left(s^2 + 2as + a^2 + w^2\right)} \right)$$

2. Inverter Current Control plant transfer function:

$$P_{ci}(s) = \frac{\Delta I_d}{\Delta \alpha} . e^{-s.T_o} \left(\frac{s^3 + (3a-1)s^2 + \left(3a^2 - 2a + w^2 + k|\Delta I_d|w\right)s + \left(a^3 - a^2 + aw^2 - w^2 + k|\Delta I_d|aw\right)}{(s+a)\left(s^2 + 2as + a^2 + w^2\right)} \right)$$

3. Rectifier Voltage Control plant transfer function:

$$P_{vr}(s) = \frac{\Delta V_d}{\Delta \alpha} \frac{1}{s+a}$$

4. Inverter Voltage Control plant transfer function:

$$P_{vi}(s) = \frac{\Delta V_d}{\Delta \alpha} \frac{w}{(s+a)^2 + w^2} e^{-s.T_o.}$$

Due to the uncertain nature of the state of power systems, the parameters of the plant transfer functions that define the LCC HVDC systems vary. In Chapter 4, the range of plant transfer function parametric variation, was determined as a function of ac systems effective short circuit ratio. Therefore if the range of the ac system's effective short circuit ratio is known, the range of parametric uncertainty of the LCC HVDC plant transfer functions can be obtained from Table 4.1 to Table 4.4.

A LCC HVDC control system design method based on Quantitative Feedback Theory (QFT) was presented Chapter 5. The QFT design method was used to design the rectifier and inverter current controllers for the LCC HVDC system whose parameters are defined by Table 4.1 to Table 4.2. The designed current controllers individually achieved the specified performance specifications. The stability of the integrated LCC HVDC control system was verified by simulating the start-up of a LCC HVDC system with the rectifier ac system's ESCR=8 and the inverter ac system's ESCR=8. The results revealed that the designed LCC HVDC control system does ensure a stable start-up process, thus preliminarily validating the design method.

Due to the uncertain nature of the state of power systems, the conditions defining the operating point of the LCC HVDC system vary. The ability of the designed LCC HVDC control system to remain stable during these operating condition variations is categorized as the "Transient Stability of the LCC HVDC System".

In Chapter 6, the stability of the integrated LCC HVDC control system was verified by simulating the start-up and step responses of the LCC HVDC system with the rectifier ac system's ESCR varying from 8 to 6 and the inverter ac system's ESCR varying from 8 to 6. The stable start-up and step responses of the LCC HVDC

system, for varying ac system conditions, conclusively validates the novel derived HSR equations and the QFT design method of the LCC HVDC control system parameters.

7.2 Recommendations for Future Research

The controller investigated thus far has been proportional-integral (PI) type. Control literature suggests that the addition of a differential component i.e. PID controller can improve the settling time of the system response. Therefore the design and implementation of PID into the LCC HVDC control system is recommended for further research.

Section 2.5 illustrated that the voltage control loop does not include a controller function, therefore the viability of including a controller in the voltage control loop is recommended for further research.

It has been noticed that designing of stable LCC HVDC control system when the LCC HVDC system is interconnected to weak systems has been a challenge. The challenges are with regard to the unstable nature of the weak ac system voltages. The static compensator (STATCOM) has been reported to provide voltage support similar to a synchronous condenser. Therefore it is recommended that QFT design of LCC HVDC control systems when the HVDC system is interconnecting weak ac systems should be researched, especially with regard to using the STATCOM to provide voltage support to the ac system.

References

[1]   AINSWORTH J.D.: 'Harmonic instability between controlled static converters and ac networks'. *Proc. IEE*, 1967, **114**, (7), PP.949-957

[2]   YACAMINI R., DE OLIVEIRA J.C.: 'Instability in hvdc schemes at low order integer harmonics'. *Proc. IEE*, 1980, **127**, (3), pp. 179-188

[3]   LARSEN E.V., BAKER D.H., McIVER J.C.: 'Low order harmonic interaction on ac/dc systems'. *IEEE Trans. Power Deliv.*, 1989, **4**, (1), pp.493-501

[4]   WOOD A.R., ARRILLAGA J.: 'HVDC converter waveform distortion: a frequency domain analysis'. *IEE Proc.*, **142**, (1), 1995, pp.88-96

[5]   WOOD A.R., ARRILLAGA J.: 'The frequency dependent impedance of an HVDC converter'. *IEEE Trans. on Power Deliv.*, **10**, (3), 1995, pp.1635-1641

[6]   WOOD A.R., ARRILLAGA J.: 'Composite resonance; a circuit approach to the waveform distortion dynamics of an HVDC converter'. *IEEE Trans. on Power Deliv.*, **10**, (4), 1995, pp.1882-1888

[7]   JIANG X., GOLE A.M.: 'A frequency scanning method for the identification of harmonic instabilities in HVDC systems'. *IEEE Trans. on Power Deliv.*, **10**, (4), 1995, pp.1875-1881

[8]   BURTON R.S. et. al.: 'Prediction of core saturation instability at an HVDC converter'. *IEEE Trans. on Power Deliv.*, **11**, (4), 1996, pp.1961-1969

[9]   PERSSON E.V.: 'Calculation of transfer functions in grid-controlled converter systems, with special reference to HVDC transmissions'. *Proc. IEE*, 1970, **117**, (5), PP.989-997

[10]   ERIKSSON K., LISS G., PERSSON E.V.: 'Stability Analysis of the HVDC Control System Transmission Using Theoretically Calculated Nyquist Diagrams'. *IEEE Trans. on Power App. Sys.*, **89**, (5/6), 1970, pp.733-740.

[11]   SUCENA-PAIVA J.P., FRESIS L.L: 'Stability of a dc transmission link between weak ac systems'. *IEE Proc.*, **121**, (6), 1974, pp.508-515

[12]   TODD S., WOOD A.R., BODGER P.S.: 'An s-domain model of an HVdc converter'. *IEEE Trans. on Power Deliv.*, **12**, (4), 1997, pp.1723-1729

[13]   JOVCIC D., PAHALAWATHTHA N., ZAVAHIR M.: 'Analytical modelling of HVDC-HVAC systems'. *IEEE Trans. on Power. Deliv.*, **14**, (2), 1998, pp. 506-511

[14]   JOVCIC D., PAHALAWATHTHA N., ZAVAHIR M.: 'Stability analysis of HVDC control loops'. *IEE Proc. Gener. Transm. Distrib.*, **146**, (2), 1998, pp.143-147

[15]   JOVCIC D., PAHALAWATHTHA N., ZAVAHIR M.: 'Small signal analysis of HVDC-HVAC interactions'. *IEEE Trans. on Power. Deliv.*, **14**, (2), 1999, pp. 525-530

[16]   OSAUSKAS C.M., HUME D.J., WOOD A.R.: 'Small signal frequency domain model of an HVDC converter'. *IEE Proc. Gener. Transm. Distrib.*, **148**, (6), 2001, pp.573-578

[17]   DE TOLEDO P.F., ANGQUIST L., NEE H.P.: 'Frequency domain model of an HVDC link with a line-commutated current-source converter. Part I: fixed overlap'. *IET Gener. Transm. Distrib.*, **3**, (8), 2009, pp.757-770

[18]   LJUNG L.: 'System Identification - Theory for the User' (1999, edn)

[19] GROESSLER, A. et. al.: 'Inductive and Deductive System Dynamics Modelling'. International Conference of the System Dynamics Society, 29 July – 2 August 2007, ISBN: 978-0-9745329-8-1

[20] RAKE H.: 'Step response and frequency response methods'. *Automatica*, **16**, 1980, pp.519-526

[21] SZECHTMAN M., et. al.: 'CIGRE benchmark model for dc controls'. *Electra*, **135**, 1991, pp.54-73

[22] GOLE A.M., SOOD V.K.: 'A static compensator model for use with electromagnetic simulation programs'. *IEEE Trans. on Power. Deliv.*, **5**, (3), 1990, pp. 1398-1407

[23] WOODFORD D.A.: 'Validation of Digital Simulation of DC Links- Part I'. *IEEE Transactions on Power App. Sys.*, **104**, (9), 1985, pp. 2588-2596.

[24] INO T., MATHUR R.M., IRAVANI M.R., SASAKI S.: 'Validation of Digital Simulation of DC Links - Part II'. *IEEE Transactions on Power App. Sys.*, **104**, (9), 1985, pp. 2596-2602.

[25] GUSTAVSEN B., SEMLYEN A.: 'Rational Approximation of frequency domain responses by vector fitting'. *IEEE Trans. on Power. Deliv.*, **14**, (3), 1999, pp. 1052-1061

[26] COHEN G.H., et. al.: 'Theoretical consideration of retarded control'. Trans. ASME, **75**, 1953, pp. 827-834

[27] YACAMINI R., DE OLIVEIRA J.C.: 'Harmonics produced by direct current in converter transformers'. *Proc. IEE*, 1978, **125**, (9), pp. 873-878

[28] KUNDUR P.: 'Power System Stability and Control'. (1994, edn)

[29]   MOHAN N., UNDERLAND T.M., ROBBINS W.P.: 'Power Electronics'. (2003, edn)

[30]   KARLSSON J.: 'Simplified Control Model for HVDC LCC'. *MSc Thesis, Royal Institute of Technology*, 2006

[31]   HOUPIS C.H., RASMUSSEN S.T.: 'Quantitative Feedback Theory'. (1999)

[32]   PACKARD, POOLA, HOROWITZ: 'Dynamic Systems and Feedback' *Class Notes, University of California*, 2002

[33]   HINGORANI N.G., BURBERY M. F.: 'Simulation of AC System Impedance in HVDC System Studies'. *IEEE Transactions on Power App. Sys.*, **89**, (5/6), 1970, pp. 820-827.

[34]   HOROWITZ I.: 'Quantitative Feedback Design Theory'. (1993)

[35]   HAYKIN S., VAN VEEN B.: 'Signal and Systems'. (1999, edn)

Appendix A

Journal article submit to IET Generation, Transmission and Distribution, Manuscript ID: GTD-2010-0746

Development of a Parametric Model of LCC HVDC Systems

L. Chetty, N.M. Ijumba

HVDC Centre, University of KwaZulu Natal, South Africa
E-mail: chettyl2 @ukzn.ac.za

Abstract: This study presents a simple method to derive a step response model and plant transfer function of an high voltage direct current (HVDC) transmission system with line commutated converter (LCC). The step response model was determined from the HVDC process reaction curve which is the output current response obtained when the phase locked oscillator is given a sudden sustained firing angle order perturbation with the controller disconnected. The prediction of fundamental frequency component in the dc current response using the HVDC step response model and the subsequent validation of the HVDC step response model was demonstrated using the CIGRE HVDC model. In the first validation technique, the well established frequency scan method was utilized to determine the response of the rectifier dc current to sinusoidal variations in the rectifier firing angle. The results illustrate that there is good engineering agreement between the two methods especially with reference to the identification of the fundamental frequency harmonic amplification in the dc current response. The second validation technique utilized transient studies. Harmonic analysis clearly indicates that a large component close to fundamental frequency is present in the transient dc current. This result validates the HVDC step response model. Subsequently it was concluded that the derived step response model can adequately analysis and predict the behavior of LCC HVDC systems including low harmonic interactions.

1 Introduction

Line Current Commutated (LCC) HVDC systems are dynamic systems that have natural oscillatory modes [1-3]. The natural oscillatory modes of LCC HVDC systems are the result of the interactions between the dc network and the ac networks. [3-8]. The importance of developing mathematical models of LCC HVDC systems to study these oscillatory modes has been appreciated from the early days of LCC HVDC system applications. [1-17].

There are essentially two methodologies used to develop mathematical models of dynamic systems. One methodology is to define the properties of the system by the "laws of nature" and other well established relationships [18]. Basic techniques of this methodology involve describing the system processes using differential equations. This methodology is called "Deductive Modeling" [19].

The other methodology used to determine mathematical models of a dynamic system is based on experimentation [18]. Input and output signals from the original system are recorded to infer a mathematical model of the system. This methodology is known as "Inductive Modeling" [19]. Inductive models maybe described by a system's response $H(s)$, to an impulse or a frequency response function $H(j\omega)$ [20]. These functions are obtained by application of either periodic input signals or non-periodic input signals to the dynamic system. Periodic input signals are utilized in such a manner that the dynamic system is operating in steady state with the output oscillating with the same frequency as the input signal with all transients having decayed. Models determined from periodic input and output signals are usually the frequency

response type $H(j\omega)$. Frequency response models are naturally non-parametric models.

With regard to the non-periodic input signal, the dynamic system is operated until steady state operation, corresponding to zero initial conditions and then the dynamic system is perturbed by the input signal. The step function is the most commonly used non-periodic input signal and the output step response facilitates the impulse response $H(s)$. Step response models are parametric in nature.

In this paper, the states of the art of methodologies utilized to derive mathematical models of LCC HVDC systems are analyzed. The analysis is presented with reference to the mathematical modeling framework depicted in Fig. 1.
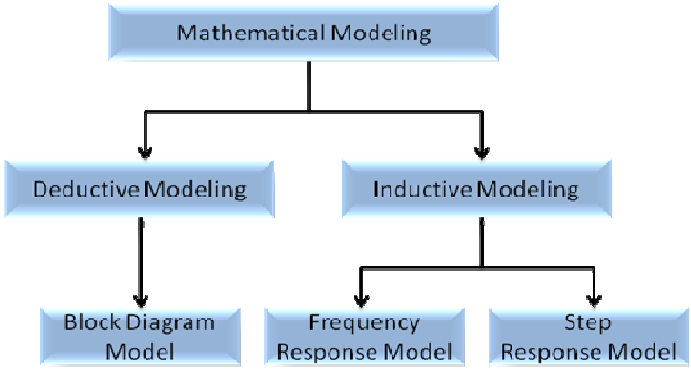
Figure 1 *Mathematical Modeling Framework*

This paper also presents a simple method to derive a step response model and plant transfer function of an LCC HVDC system. Specifically the CIGRE Benchmark HVDC Model [21] was used to derive the step response model.

The model was validated using the frequency scan method [7], transient studies and a comparative discussion with reference to original study [21]. The results of this study indicate that the derived step response model illustrates good agreement with the frequency scan method and with the original study conducted in [21]. Subsequently it can concluded that the step response model can adequately analysis and predict the behavior of LCC HVDC systems including low harmonic interactions.

2 State of the Art

Traditionally classic HVDC systems have been treated as "linear time invariant systems" [4-17]. Based on this premise, Persson [9] developed a meshed block diagram, illustrated in Figure 2, to calculate the current control loop plant transfer function. The transfer functions of each block in the meshed system were derived using the state variable approach. The transfer functions describing the ac and dc interactions were derived using describing function analysis. Persson [9] called these transfer functions "conversion functions". Toledo et. al. recently applied space vectors to the Persson's classic technique [17]. Space vector analysis was therefore proven to be a form of describing function analysis.
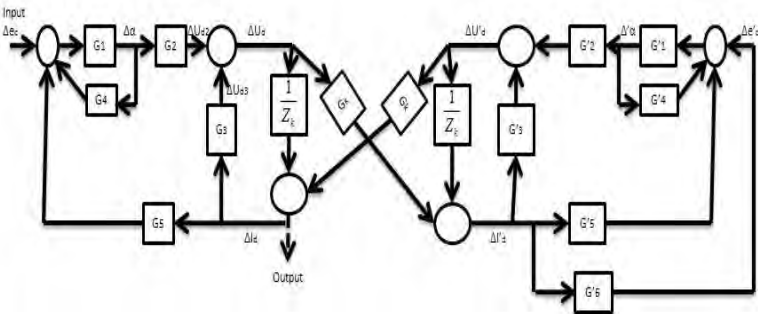
Figure 2 *Block diagram of HVDC transmission system according to Persson [9]*

Based on the assumption that the classic HVDC system is linear with regard to small variations in the firing angle, Freris et al. [11] developed a block diagram, illustrated in Figure 3, to calculate the transfer function of the rectifier current control loop. Continuous wave modulation and Fourier analysis were used to determine the transfer functions of each block in the meshed block diagram. The continuous wave modulation technique was used as a method of developing the describing functions to account for the ac/dc interactions.
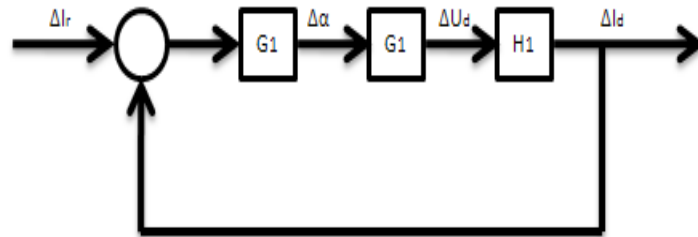
Figure 3 *Block diagram of HVDC transmission system according to Freris et. al. [11]*

From the linear time invariant system foundation, Wood et al. [4] performed Fourier analysis on the dc voltage and ac current waveforms of the converter. From these analyses, transfer functions were obtained for the dc voltage and ac currents with respect to the phase voltages and dc currents. These transfer functions accommodated variations in the firing angle and the commutation period. The subsequent transfer functions facilitated the predictions of voltage waveform distortion on the dc side of the converter, and the prediction of current waveform distortion on the ac side of the converter. Using the transfer functions derived in [4], Wood et al. [5] developed an expression for the converter dc side frequency dependent

impedance. This expression was developed using the state-variable approach. Using the state-variable approach and the frequency dependent impedance of the converter, Wood et al [6] derived the transfer function for the current control loop.

Jovcic et al. [13], assumed that classic HVDC systems are linear time invariant systems, therefore developed the plant transfer function of the current control loop using a state-variable approach and the block diagram illustrated in Figure 4. The state variables were chosen to be the instantaneous values of currents in the inductors and voltages across the capacitors. In order to represent the ac system dynamics together with the dc system dynamics in the same frequency frame, the effect of the frequency conversion through the AC-DC converter was accommodated using Park's transformation. The developed system model was linearized around the normal operating point, and all states were represented as dq components of the corresponding variables. The phase locked oscillator [22] was incorporated into the system model.
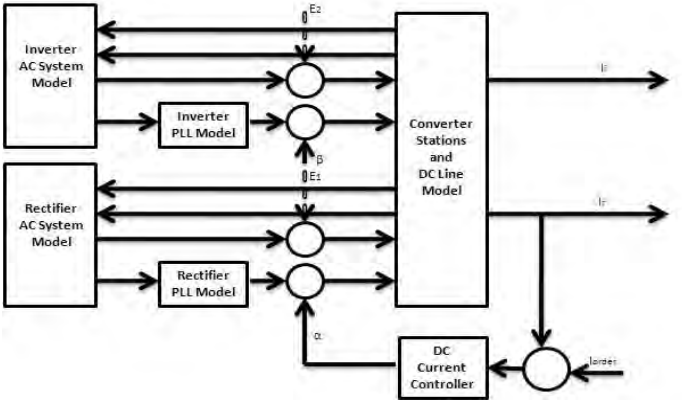
Figure 4 *Block diagram of HVDC transmission system according to Jovcic et. al. [13]*

A review of the above state of the art of modeling LCC HVDC systems clearly indicates that the techniques utilized to develop mathematical models of LCC HVDC systems have used the "Deductive Modeling" methodology. This methodology requires accurate knowledge of the ac systems and the dc systems and involves complicated mathematics.

In practice, it is nearly impossible to obtain accurate knowledge of the ac systems connected to classic HVDC systems. Also the limited time constraints imposed on HVDC control practitioners, the ac system uncertainties and the complicated mathematics have prevented the widespread practical use of the "Deductive Modeling" methodology to derive the plant transfer functions of classic HVDC systems. Therefore the objective of this study was to utilize an "Inductive Modeling" method to derive mathematical models of the classic HVDC systems.

"Inductive Modeling" is the art of building mathematical models of dynamic systems based on observed data from the systems [19]. A key concept in utilizing the inductive modeling technique is the definition of the dynamic system upon which experimentation can be conducted. Manitoba HVDC Research Centre commissioned a study to examine the validity of digitally defining the LCC HVDC system [23-24]. To examine the validity of digitally defining the LCC HVDC system, the Nelson River HVDC system was defined and simulated using the PSCAD/EMTDC program. PSCAD/EMTDC is a Fortran program and was used to represent and solve the linear and non-linear differential equations of electromagnetic systems in the time domain. A

comparison was conducted between the actual real-time system responses and the digitally derived responses. The results of the study illustrated that the digitally derived responses correlated excellently with the real system responses. The study concluded that the PSCAD/EMTDC program is a valid option for digitally defining a LCC HVDC system [23-24].

Based on this premise, Jiang et. al [7] modeled the LCC HVDC system using EMTDC, and developed a frequency response model of the LCC HVDC system. A current source was used to inject a spectrum of frequency components into an operating LCC HVDC system. The resulting harmonic voltages were observed. The frequency response model that was developed for the LCC HVDC system was non-parametric. It is possible however to develop the plant transfer function by the fitting of measured frequency domain responses with rational function approximations [25].

The next section presents a simple method to develop a parametric step response model (i.e. an inductive model) of an LCC HVDC system.

3 Step Response Method

Two principle components of a control loop are the process and the controller. The process is considered to include all parts of the installation exclusive of the controller. The actuator can also be included as part of the process [26]. The step response model can be determined from the process reaction curve which is the output response obtained when the actuator is given a sudden sustained perturbation with the controller disconnected [26].

Based on this premise the LCC HVDC system was simulated so that it reached steady-state. The inverter firing angle was then kept constant. A feed-forward step increase in the rectifier firing angle α_r, was executed and the dc current response I_{dr} was measured. The CIGRE Benchmark HVDC model [21] was chosen to develop the step response model. The HVDC control system was operated in open loop. The firing system is a dqo type phase locked loop based equidistant scheme [22]. The LCC HVDC system illustrated in Fig. 6, represents a 12-pulse 500kV dc transmission system rated at 1000MW. The rectifier and inverter short circuit ratios are both 2.5. Details of the model are described in [21]. The CIGRE Benchmark HVDC model was started up and a feed-forward step increase in the rectifier firing angle α_r, was executed at 0.9 seconds.
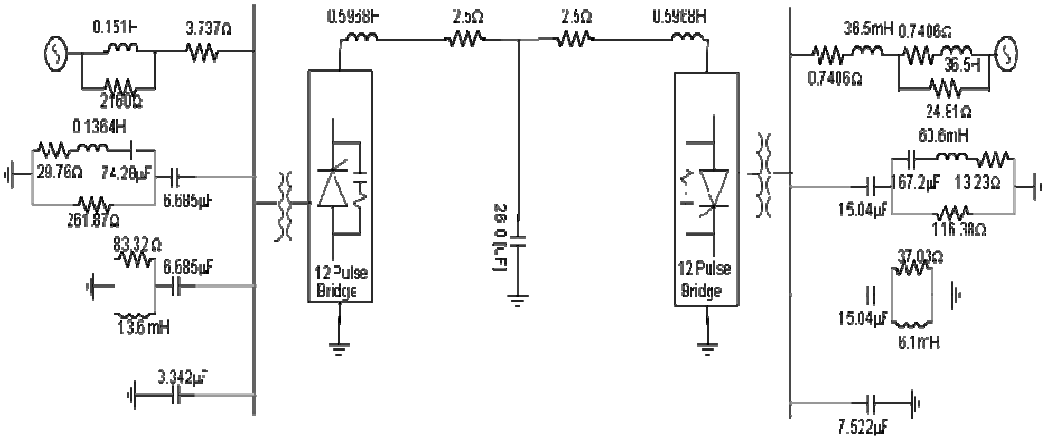
Figure 5 *CIGRE Benchmark HVDC Model*

The dc current response I_{dr} was measured. The results of the observations are illustrated Fig. 6. A magnified view of the step response is illustrated in Fig. 7.
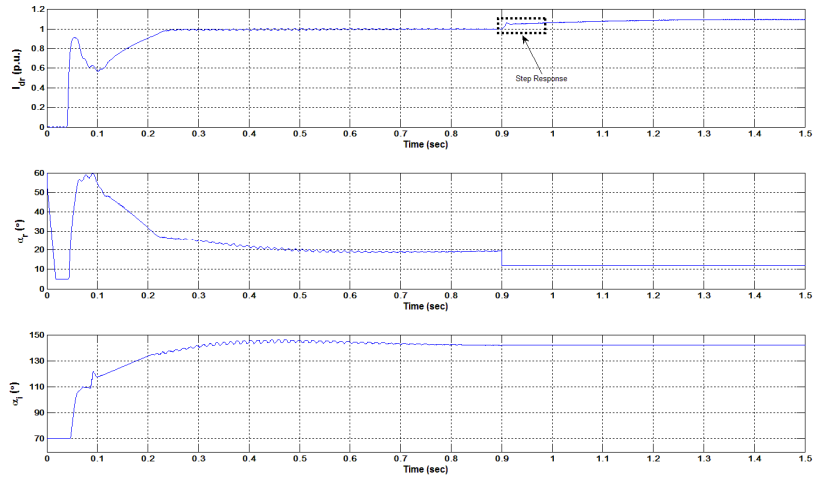
Figure 6 Startup and Step Response of *CIGRE Benchmark HVDC Model*
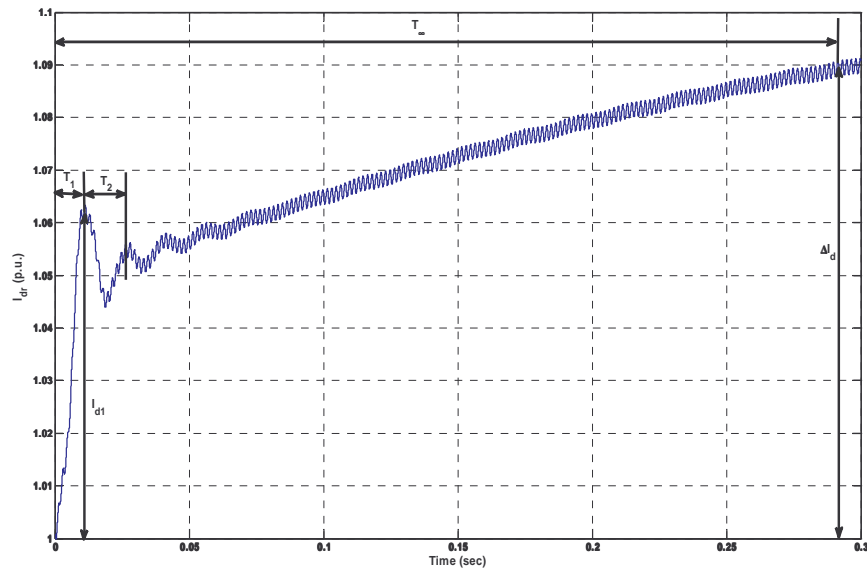
Figure 7 Step Response of *CIGRE Benchmark HVDC Model*

The measured current step response was approximated using the time domain function which is illustrated in equation (1):

$$I_{dr}(t) = \begin{cases} 1.1.(\Delta I_d - I_{d1})(1 - e^{-bt}) & 0 < t < T_o \\ 1.1.(\Delta I_d - I_{d1})(1 - e^{-bt}) + I_{d1}.(1 - k.e^{-a.t} + k.e^{-a.t}.(\sin(\alpha t) - \cos(\alpha t))) & t \geq T_o \end{cases} \quad (1)$$

Where ΔI_d Defined final value of the dc current (p.u.)

I_{d1} is the first peak of the oscillating component of the dc current

(p.u.)

$a = \dfrac{1}{T_1}$ T₁ is defined as the time (sec) of the first peak of the dc current

(p.u.)

$\omega = \dfrac{2\pi}{T_2}$ T₂ is defined as the first period (sec) of the oscillating

component of the dc current.

k is constant ($0 < k \leq 1$); chosen to be 0.5

T_∞ Defined final value of time (sec.)

$$b = \frac{\log\left(\dfrac{1}{11}\right) - \log\left(1 - \dfrac{10.I_{d1}\left(1 - e^{-1}\right)}{11.\Delta I_d}\right)}{-T_\infty}$$

T_o Time delay (sec) illustrated and defined in Fig. 8. This time

delay is introduced to avoids the formation of very high order

models.
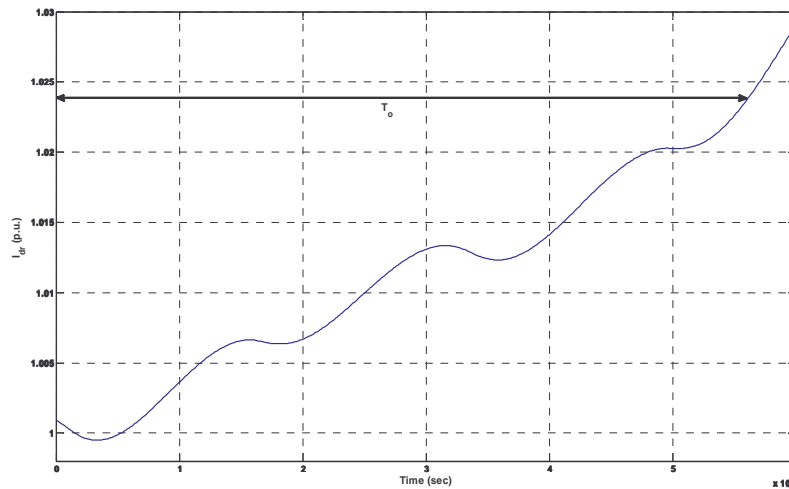
Figure 8 Time Delay Definition

The function described by equation (1) is called the *HVDC Step Response (HSR) equation* and was simulated using MATLAB. The characterized time domain response is illustrated in Fig. 9.
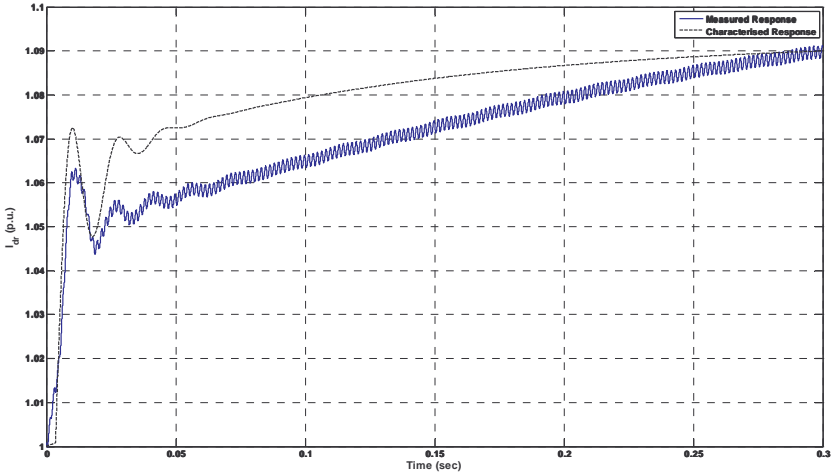
Figure 9 Characterized Step Response of *CIGRE Benchmark HVDC Model*

Fig. 9 clearly illustrates that the HSR Equation adequately approximates the dc current response to a step change in the rectifier's firing angle.

4 Prediction of Fundamental Frequency DC Current Response

Low-order harmonic instability occurs when a fundamental harmonic component is evident in dc current [27]. Due to converter coupling between the dc system and the ac system, second harmonic positive-sequence currents and dc currents are generated on the ac system [27]. The dc currents cause saturation of the converter transformers, resulting in the magnetizing current having second harmonic positive-sequence components [27]. The ac commutation voltages would consist of significant second harmonic positive-sequence components should the ac system present a

large second harmonic impedance to the ac commutation busbar [22]. This process reiteratively produces relatively large fundamental frequency components in the dc system voltage and current thus resulting in low-order harmonic instability [22].

The prediction of fundamental frequency component in the dc current response using the HSR equation and subsequent validation of the HSR equation was demonstrated using the CIGRE HVDC model. In the first validation technique, the frequency scan method [7] was utilized to determine the response of the rectifier dc current to sinusoidal variations in the rectifier firing angle. The resulting frequency scan results are illustrated in Fig. 11. The impulse response, also illustrated from Fig. 11, was calculated from equation (2). Comparison of these two plots clearly indicates that there is good engineering agreement between the plots especially with reference to the identification of the 50Hz (fundamental frequency) harmonic amplification in the dc current response.

$$P(s) = \frac{L\{I_{dr}(t)\}}{\Delta\alpha_r/s} = \frac{L\left\{\begin{matrix} 1.1.(\Delta I_d - I_{d1}).(1-e^{-bt}) & 0 < t < T_o \\ 1.1.(\Delta I_d - I_{d1})(1-e^{-bt}) + I_{d1}.(1-k.e^{-at} + k.e^{-at}.(\sin(\alpha t) - \cos(\alpha t)) & t \geq T_o \end{matrix}\right\}}{\Delta\alpha_r/s} \quad (2)$$

Where $L\{\ \}$ Laplace Transform

$\Delta\alpha_r$ rectifier firing angle step input (^{o})
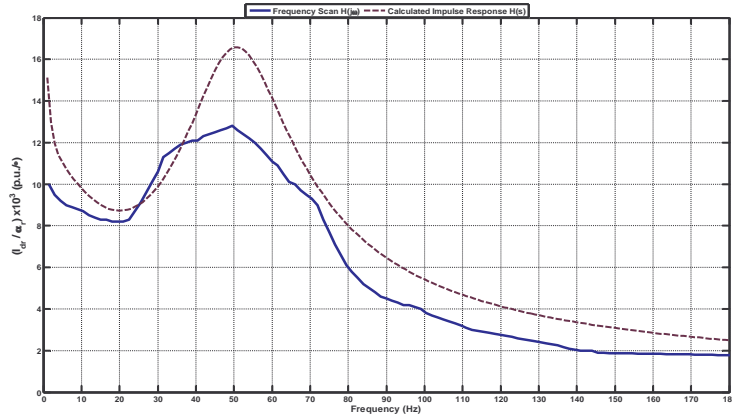
Figure 11 Comparison between frequency scan and calculated impulse

response of *CIGRE HVDC Model*

The second validation technique utilized transient studies. A three phase 4 cycle fault was applied to the rectifier ac busbar. Fig. 12(a) illustrates the rectifier dc current during the fault recovery. Harmonic analysis of the rectifier dc current at t=0.8 seconds is illustrated in Fig. 12(b). The harmonic analysis clearly indicates that a large component close to 50Hz (fundamental frequency) is present in the transient dc current. This result validates the calculated impulse response results (Fig. 12) and consequently validates the HSR equation. These transient study results are also confirmed by the original CIGRE Benchmark HVDC Model studies [21]. The original study clearly illustrated that a fault on the rectifier ac busbar would produce a fundamental frequency (50Hz) current in the dc system.
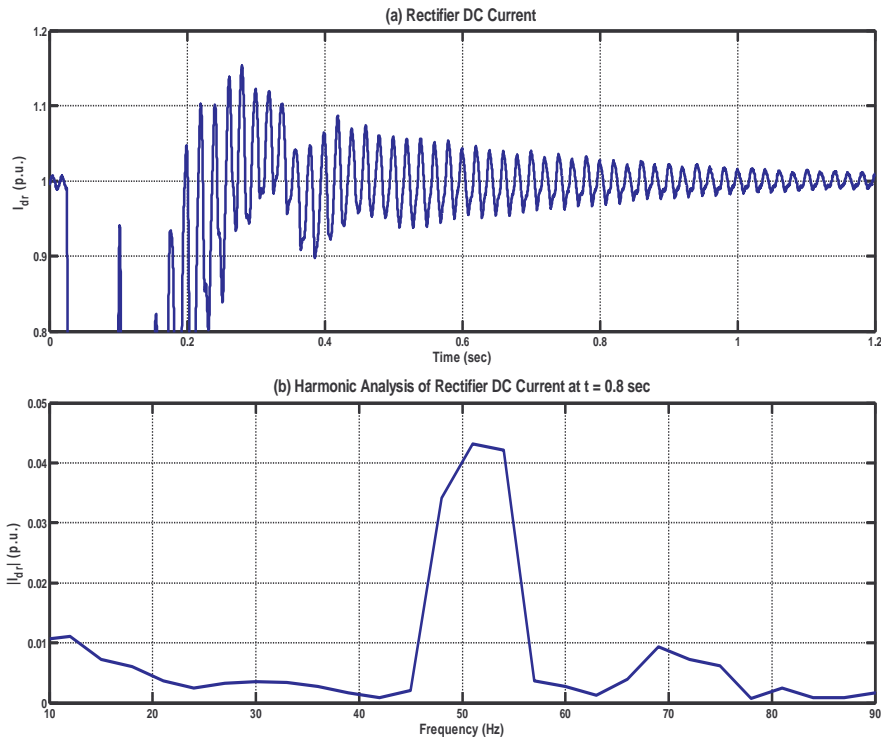
Figure 12 Fault Recovery Analysis of *CIGRE HVDC Model*

5 Conclusion

A simple inductive modeling method has presented to calculate the transfer function of an LCC HVDC system. The method involves the application of a step increase/decrease to converter firing and measuring the dc current response. The dc current response was subsequently characterized using time domain functions. The general equation defining the characterized current response was defined as HVDC Step Response (HSR) equation. The HSR was validated against the frequency scan method [7] and the transient analysis of the CIGRE HVDC model [21]. The results of the validation process illustrated that there is good engineering agreement between the HSR model, frequency scan method and the transient analysis of the HVDC

system especially with regard to identifying fundamental frequency component in the dc current response.

6 References

[1]   AINSWORTH J.D.: 'Harmonic instability between controlled static converters and ac networks'. *Proc. IEE*, 1967, **114**, (7), PP.949-957

[2]   YACAMINI R., DE OLIVEIRA J.C.: 'Instability in hvdc schemes at low order integer harmonics'. *Proc. IEE*, 1980, **127**, (3), pp. 179-188

[3]   LARSEN E.V., BAKER D.H., McIVER J.C.: 'Low order harmonic interaction on ac/dc systems'. *IEEE Trans. Power Deliv.*, 1989, **4**, (1), pp.493-501

[4]   WOOD A.R., ARRILLAGA J.: 'HVDC converter waveform distortion: a frequency domain analysis'. *IEE Proc.*, **142**, (1), 1995, pp.88-96

[5]   WOOD A.R., ARRILLAGA J.: 'The frequency dependent impedance of an HVDC converter'. *IEEE Trans. on Power Deliv.*, **10**, (3), 1995, pp.1635-1641

[6]   WOOD A.R., ARRILLAGA J.: 'Composite resonance; a circuit approach to the waveform distortion dynamics of an HVDC converter'. *IEEE Trans. on Power Deliv.*, **10**, (4), 1995, pp.1882-1888

[7]   JIANG X., GOLE A.M.: 'A frequency scanning method for the identification of harmonic instabilities in HVDC systems'. *IEEE Trans. on Power Deliv.*, **10**, (4), 1995, pp.1875-1881

[8]   BURTON R.S. et. al.: 'Prediction of core saturation instability at an HVDC converter'. *IEEE Trans. on Power Deliv.*, **11**, (4), 1996, pp.1961-1969

[9]   PERSSON E.V.: 'Calculation of transfer functions in grid-controlled converter systems, with special reference to HVDC transmissions'. *Proc. IEE*, 1970, **117**, (5), PP.989-997

[10]   ERIKSSON K., LISS G., PERSSON E.V.: 'Stability Analysis of the HVDC Control System Transmission Using Theoretically Calculated Nyquist Diagrams'. *IEEE Trans. on Power App. Sys.*, **89**, (5/6), 1970, pp.733-740.

[11]   SUCENA-PAIVA J.P., FRESIS L.L: 'Stability of a dc transmission link between weak ac systems'. *IEE Proc.*, **121**, (6), 1974, pp.508-515

[12]   TODD S., WOOD A.R., BODGER P.S.: 'An s-domain model of an HVdc converter'. *IEEE Trans. on Power Deliv.*, **12**, (4), 1997, pp.1723-1729
[13]   JOVCIC D., PAHALAWATHTHA N., ZAVAHIR M.: 'Analytical modelling of HVDC-HVAC systems'. *IEEE Trans. on Power. Deliv.*, **14**, (2), 1998, pp. 506-511

[14]   JOVCIC D., PAHALAWATHTHA N., ZAVAHIR M.: 'Stability analysis of HVDC control loops'. *IEE Proc. Gener. Transm. Distrib.*, **146**, (2), 1998, pp.143-147

[15]   JOVCIC D., PAHALAWATHTHA N., ZAVAHIR M.: 'Small signal analysis of HVDC-HVAC interactions'. *IEEE Trans. on Power. Deliv.*, **14**, (2), 1999, pp. 525-530

[16]   OSAUSKAS C.M., HUME D.J., WOOD A.R.: 'Small signal frequency domain model of an HVDC converter'. *IEE Proc. Gener. Transm. Distrib.*, **148**, (6), 2001, pp.573-578

[17]   DE TOLEDO P.F., ANGQUIST L., NEE H.P.: 'Frequency domain model of an HVDC link with a line-commutated current-source converter. Part I: fixed overlap'. *IET Gener. Transm. Distrib.*, **3**, (8), 2009, pp.757-770

[18]   LJUNG L.: 'System Identification - Theory for the User' (1999, edn)

[19]   GROESSLER, A. et. al.: 'Inductive and Deductive System Dynamics Modelling'. International Conference of the System Dynamics Society, 29 July – 2 August 2007, ISBN: 978-0-9745329-8-1

[20]   RAKE H.: 'Step response and frequency response methods'. *Automatica*, **16**, 1980, pp.519-526

[21]   SZECHTMAN M., et. al.: 'CIGRE benchmark model for dc controls'. *Electra*, **135**, 1991, pp.54-73

[22]   GOLE A.M., SOOD V.K.: 'A static compensator model for use with electromagnetic simulation programs'. *IEEE Trans. on Power. Deliv.*, **5**, (3), 1990, pp. 1398-1407

[23]   WOODFORD D.A.: 'Validation of Digital Simulation of DC Links. *IEEE Transactions on Power App. Sys.*, **104**, (9), 1985, pp. 2588-2596.

[24]   INO T., MATHUR R.M., IRAVANI M.R., SASAKI S.: 'Validation of Digital Simulation of DC Links - Part II'. *IEEE Transactions on Power App. Sys.*, **104**, (9), 1985, pp. 2596-2602.

[25]   GUSTAVSEN B., SEMLYEN A.: 'Rational Approximation of frequency domain responses by vector fitting'. *IEEE Trans. on Power. Deliv.*, **14**, (3), 1999, pp. 1052-1061

[26]   COHEN G.H., et. al.: 'Theoretical consideration of retarded control'. Trans. ASME, **75**, 1953, pp. 827-834

[27]   YACAMINI R., DE OLIVEIRA J.C.: 'Harmonics produced by direct current in converter transformers'. *Proc. IEE*, 1978, **125**, (9), pp. 873-878